Model Based Solutions for Structural Coupling in Flight Control Systems

By

Scott Anthony Halsey

A Doctoral Thesis submitted in partial fulfilment of the
requirements for the award of

Doctor of Philosophy

of Loughborough University

September 2002

Synopsis

Structural Coupling is the interaction between an aircraft's Flight Control System (FCS) and its structural and aero-dynamics These interactions have the potential to cause significant problems to the aircraft, possibly through structural fatigue failure, or by corruption of sensor readings leading to degradation of the FCS loop

Presently notch filters are used to attenuate the sensor signals at the structural mode frequencies which cause significant problems However, each of these notch filters adds a small amount of phase lag to the control loop which limits the performance of the FCS.

This research has looked at using Kalman filters to provide an alternative approach to overcoming the structural coupling problem. The Kalman filters are used to provide an estimate of the rigid component of the sensor signals Simple, but representative, models have been used, starting with a basic model with a single flexible mode, moving to a model of a flexible beam with 2 flexible modes An aircraft model has also been used, allowing a more complex model, with up to 40 flexible modes, to be examined

The flexible beam model has been developed into an experimental rig, which allows a comparison between the results obtained from the theoretical model with those gained from practical assessment

Results are included comparing the Kalman and notch filter approaches, primarily in the frequency domain in line with the aerospace industry

Acknowledgements

Publications

Kalman Filters for Reducing the Effects of Structural Coupling; Pearson JT, Halsey SA, Goodall RM, Caldwell BD, *Control 2000, September 2000* (included in Appendix A)

Reducing Structural Coupling on a Flexible Beam Using Kalman Filters, Halsey SA, Pearson JT, Goodall RM, Caldwell BD, *15th IFAC World Congress; July 2002* (included in Appendix B)

Table of Contents

Table of Figures

Abbreviations

ACA	Agile Combat Aircraft
ADC	Analogue to Digital Converter
ASE	AeroServoElasticity
COG	Centre Of Gravity
DAC	Digital to Analogue Converter
DSP	Digital Signal Processor
FCS	Flight Control System
GM	Gain Margin
MIMO	Multiple Input Multiple Output
PM	Phase Margin
TI	Texas Instruments

List of Symbols

A,B,C,D	state space matrices
A_a	aircraft model inertia matrix
A_f,B_f,C_f,D_f	flexible mode state space matrices
$A_{fr},B_{fr},C_{fr},D_{fr}$	r^{th} flexible mode state space matrices
A_i,B_i	state space matrices for beam spring damper connection
A_r,B_r,C_r,D_r	rigid beam state space matrices
A_1,B_1	first flexible mode state space matrices
A_2,B_2	second flexible mode state space matrices
A_{beam}	cross sectional area of beam
a_i	spring input force scaling factor
a_{xh}	beam receptance
B_a	aircraft model aerodynamic damping matrix
C_a	aircraft model aerodynamic stiffness matrix
C_{out}	rigid estimate state space output matrix
c	damping constant
D_a	aircraft model structural damping matrix
d	distance from input force to beam cog
E_a	aircraft model structural stiffness matrix
F	input force
F_c	force at damper
F_k	force at spring
G	process noise matrix
K	Kalman filter gain matrix

k	spring constant
l	distance between springs
l_b	length of beam
l_1	distance from spring 1 to beam cog
l_2	distance from spring 2 to beam cog
M	discrete Kalman filter innovations matrix
m	mass of beam
m_1	weight of large mass
m_2	weight of small mass
n	linear transformation factor
Q	process noise co-variance matrix
q	generalised co-ordinates
$\ddot{q}_r$	acceleration of rth flexible mode generalised co-ordinates
R	sensor noise co-variance matrix
X_1	State vector of beam spring damper connection
X_r	rigid mode state vector
X_1	first flexible mode state vector
X_2	second flexible mode state vector
x_1	position of large mass
x_2	position of small mass
$\dot{x}_1$	velocity of large mass
$\dot{x}_2$	velocity of small mass
$\ddot{x}_1$	acceleration of large mass
$\ddot{x}_2$	acceleration of small mass
$\hat{x}_1$	estimate of large mass position

Z	aircraft model sensor output matrix
z	position of spring beam junction
$\dot{z}$	velocity of spring beam junction
$\ddot{z}$	acceleration of spring beam junction
z'	position of spring damper junction
$\dot{z}'$	velocity of spring damper junction
z_r	vertical displacement of rth mode
$\ddot{z}_r$	acceleration of rth flexible mode
z_1	position of beam at spring 1
z_2	position of beam at spring 2
$\dot{z}_1$	velocity of beam at spring 1
$\dot{z}_2$	velocity of beam at spring 2
ω	notch frequency
ω_r	frequency of rth flexible mode
ζ	notch damping ration
ζ_n	notch numerator damping ration
ζ_d	notch denominator damping ration
$\dot{\theta}$	angular velocity
θ_r	angular displacement of rth flexible mode
$\dot{\theta}_r$	angular velocity of rth flexible mode
ρ	density of beam
Φ_r	r^{th} characteristic function

1 Introduction

The stability of the flight control system has been a key part of the design of aircraft systems for many years, and the problems relating to structural coupling have grown more important with time

Structural coupling is a term used to describe the interactions of the aircraft system, and can, if left unconsidered, introduce undesirable harmonics, which could reduce the life time of the airframe through fatigue, or cause other more significant stability effects

Currently structural coupling engineers use notch filters to attenuate feedback signals at the airframe flexible mode frequencies, in order to minimise the undesirable effects of those frequencies   However, these notch filters introduce phase lag at low frequencies which reduces the stability margins

The designers of military aircraft are being pushed to develop lighter more agile aircraft, specified to operate in a multi role capacity   The lighter airframe leads to lower flexible mode frequencies, bringing the first mode closer to the 'rigid' mode which the designers wish to control   In addition the desire for more agile aircraft leads to the need for higher bandwidth systems, and tighter stability margins   This leaves less space for the notch filters required to overcome the flexibility effects

This thesis presents a novel technique to overcome the problems associated with structural coupling   The primary focus of the work has been to examine the potential for estimation techniques to be used in place of the notch filters, to estimate the rigid body movements of the airframe rather than filter out the flexible body effects

The thesis is organised into seven chapters which introduce the problem, and develop techniques on models of increasing complexity   The chapters are organised as follows

Chapter 2 looks at the background to the project, provides some history behind structural coupling, and discusses the literature available in this field A brief discussion of the scope of the research is also provided

Chapter 3 studies the potential of the proposed solution on a basic model, which has a single flexible mode   The developed solution will be compared to the notch filter approach, and the results will be discussed   The effects of small changes to the frequency of the flexible mode will also be discussed

Chapter 4 develops the novel solution for a system with a second flexible mode and compares this with a notch filter solution will be made   The system will be developed to provide a better representation of an aircraft control system, and the effects of unexpected changes to the flexible modes will be examined in more depth

Chapter 5 develops the model used in chapter 4 into an experimental rig   This will be used to verify the model, and will allow novel solutions to be assessed on a real system.

Chapter 6 will use a model of an Agile Combat Aircraft (ACA) to examine the performance of the new approach, on a more complicated and more realistic system Refinements to the techniques will be made, and the results of these discussed

Chapter 7 will draw conclusions from the work completed, and will also discuss the potential for future work

2 Background

This chapter discusses the motivation for this research It includes some history behind the structural coupling problem and looks at the current solution A discussion of the available literature is also provided

2.1 Literature Review

This section discusses previously published work on the structural coupling topic, and also other areas of interest to this research The section is split up into logical topic areas

2 1.1 Structural Coupling

Research into structural coupling (or aeroservoelasticity (ASE) as it is also known) can be split into a two different areas research which looks at the causes of the problem, and research which looks at solutions to the problem

2 1 1 1 Causes

[Felt et al – 1979][1] covers many aspects of the problem, providing a brief discussion of what SC is, along with some of the analysis techniques used and the type of testing which is carried out to assess the likelihood of problems The paper also provides some examples of where ASE has occurred, both those which were predicted by analysis and some where the problem was not predicted

[Taylor et al – 1996][2] looks at the effects of signal propagation through a digital FCS on a flexible aircraft It also examines the impact of the introduction of digital implementation (e g zero order hold) Another paper [Taylor et al – 1996][3] by the same authors looked at the effects of actuator non-linearities (e g actuator limits) on the ASE problem The paper also looks at the effect of both low and high frequency structural modes on the performance of the actuators

Some of the significant effects concerning the design of an FCS were discussed by [Pratt et al – 1994][4]. The paper discusses the development of a finite element model of the flexible aircraft and briefly mentions the inclusion of the dynamics of the other parts of the system (control surface, rigid body and actuator dynamics) as well as the effects of a digital system

[Evans & Beele – 1968][5] compared 3 sets of predicted problems with the actual characteristics seen on the aircraft, and discussed some different ways of obtaining frequency response data (both on ground testing and flight testing methods). The paper discusses the differences between the actual results and those predicted, and makes some recommendations for the improvement of the both the model and the testing procedures

2.1 1 2 Solutions

An alternative approach to the clearance of ASE problems was discussed by [Taylor et al – 1996][6]. The paper discusses non-linearities of actuators and presents the results from some basic tests. The prediction of limit cycles is also described, and how this could be used to allow a reduction in the attenuation requirements of filters

Most of the assessment of ASE problems at the early stage of the design process is done in the frequency domain. [Cutchins et al – 1983][7] developed a non-linear time domain based method for assessing the stability of high performace aircraft. The paper uses some early F-16 problems as a test case to check the quality of the method

A combined methodology for the analysis of ASE problems is presented by [Noll et al – 1986][8]. The methodology takes a number of different analysis techniques (including unsteady aerodynamics, MIMO controls, and structural dynamics) and combines them into a single interactive tool. The paper discusses the need for an integrated development process in order to avoid ASE problems. The conversion of the equations of motion into a state-space form is also presented

A summary of the evolving techniques is provided by [Caldwell – 1996][9] The paper briefly describes the elements of the structural coupling system, the formulation of a solution and the existence of a trade off between attenuation and low frequency phase lag A number of examples are described, showing how the complexity of the structural coupling problem and solution has increased over the last 25 years

2 1 2   Modelling

The research discussed here looks at the modelling of mechanical systems, in particular relating to the modelling of a beam

The first two papers in this section look at the effect on vibration control of small modifications to the structure of the system, using a flexible beam as part of the testing of ideas   [Haftka et al – 1985][10] looked at whether small changes to the structure of the beam (e g by adding small weights) can significantly affect the vibration control system   The second paper [Haftka et al – 1987][11] developed the work further, and looked at the sensitivity of the control system performance   This was applied to a cruciform beam structure (much like the basic shape of an aircraft) These papers provide some insight into how the mode shapes of the flexible beam can be altered in order to see the effects of changes in the frequency response of the control system

The next three references develop a method of modelling the dynamic response of a beam structure to a harmonic input (force or torque)   [Bishop, Johnson – 1960][12] develops the basis of flexible models of a number of different structures, including a chapter on beam structures   The model can be developed for either force or torque input (at any point on the beam), and can provide an angular or linear output   The formulation of the model will depend upon the end conditions of the beam (e g free, clamped, or pinned), and [Milne – 1989][13] derives a general solution for the dynamic response of a beam with any type of end condition   [Milne – 1991][14] extends the previous paper to include the rotational receptance functions

It is important that any model used provides a good representation of an aircraft structure [Lee][15] described such a model, producing the equivalent beam model of a composite skinned aircraft wing This is performed by companng the reduced stiffness and mass matrices of a wing segment with those of a finite element analysis of a beam-rod model The model provides most equivalent structural properties, including couplings between bending, torsional and transverse shear deformations. The paper provides evaluation of the model through free vibration and aeroelastic analysis, and results have been compared to other wing models

[Dovel – 1989][16] discusses the use of modal analysis in the identification of the dynamic properties of a structure The paper describes the concepts behind modal analysis, and provides information relating to preparation for testing the structure in question It also discusses the measurement of data, and the identification of modes

2 1 3   Kalman filtering

The aim of this research is to look at the use of model based estimation techniques as a replacement for notch filters in the FCS These papers look at the development of the Kalman filter.

The Kalman filter can be developed in both discrete and continuous form [Kalman – 1960][17] develops the discrete form [Kalman & Bucy – 1961][18] combines the work of Kalman and Bucy, to produce the continuous form of the filter Both papers derive the equations which set up the filter, and provide a number of examples of varying complexity

[Hutchinson – 1984][19] discusses the application of the Kalman filter in the aerospace industry A summary of the types of application where the Kalman filter was first used is provided, along with a discussion on how the Kalman filter has been enhanced as a result of its use in the aerospace industry

There are many sources available containing the derivation of the Kalman filter [Chui and Chen][20] explains the Kalman filter and [Brammer and Siffling][21] describes

the Kalman Bucy filter   These books also provide a number of examples of applications of the filters

It should be noted here that no references are available which examine the use of Kalman filters in research looking at Structural Coupling issues

2 1 4   Electro-magnetism

The experiment rig has used electromagnetism to provide damping which was required   These papers discuss the use of electromagnetism for this purpose

A good introduction to electro-magnetics can be found in [Christopoulos – 1995][22] The book introduces the topics of electric and magnetic fields in a progressive manner, without resorting to complicated mathematics until the later stages of the book.

The forces caused by the interaction of a magnetic field and a conducting sheet have been discussed by a number of papers   [Reitz – 1970][23] looked at the forces on a magnet moving past a fixed conducting sheet   The effects of different types of magnet were examined

[Weinberger – 1977][24] derives analytical formula to calculate the damping forces The formula is intended for use in real design problems, so where many papers provide calculations based upon infinite sized conducting sheets, this paper also includes calculations for sheets of finite size

[Perry – 1984][25] examined the uses of an array alternating magnetic poles with a conducting sheet   The paper discusses how eddy current braking occurs, and looks at the effect on the magnetic field distribution in a conducting sheet of high and low magnetic permeability   The results are compared for sheets of different thickness

The braking effect of a conducting sheet passing between two poles is discussed in [Schieber – 1972][26]   The magnetic poles used are d c excited electro magnets, and

the conducting sheet is of finite thickness   The work of the paper is expanded on by [Schieber – 1975][27]   This paper develops a cost function used to calculate the optimal dimensions of the core of an electromagnetic damper

2.2   Structural Coupling

The term 'structural coupling' is used to describe the interactions between an aircraft's structural dynamics, aerodynamics, and the FCS   These interactions, shown in Figure 2-1, if left unchecked can lead to instabilities in the FCS loop
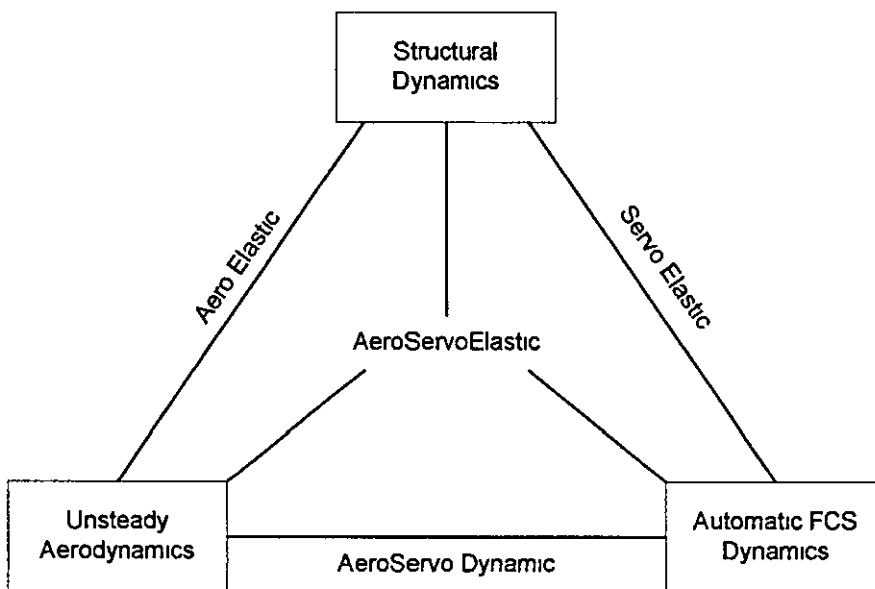
Figure 2-1. Aircraft Interactions

2 2 1   History

Since the late 1940s, the issues related to structural coupling have become more significant, as the FCS has become a more significant part of the design of an aircraft One of the earliest instances of the problem arose when the sensors on a B-36 picked up the bending motion of the aircraft [Felt et al – 1979][1]   The solution to the problem in this case turned out to simply to move the sensor package to a position where the bending motion was less significant

The incorrect analysis of an aircraft has frequently missed problems, a large bomber showed instability during ground FCS trials, which had not been shown up during

analysis, since the aircraft supports during the analysis tests significantly altered the structural dynamics Early flight tests on the YF-16 showed 2 unpredicted instabilities at high subsonic speeds [Felt et al – 1979][1], the analysis had only been carried out at high supersonic speeds Further analysis showed the instabilities

Modelling only works to a certain point, because local structural vibrations can be too detailed to include in a structural dynamics model, the movement of a crew member on a B-52 was enough to excite the local structure around an accelerometer [Felt et al – 1979][1]. Changing the mounting was enough to attenuate the effects

More recently with the introduction of more advanced FCS, it has become increasingly difficult to overcome any instability by adjusting the position or mounting of a sensor. The Jaguar aircraft (and the F-4) both required a small amount of filtering (1 or 2 notch filters only), as shown in the block diagram of Figure 2-2, whereas Tornado required filtering on each axis (pitch, roll, and yaw) [Caldwell – 1996][9]
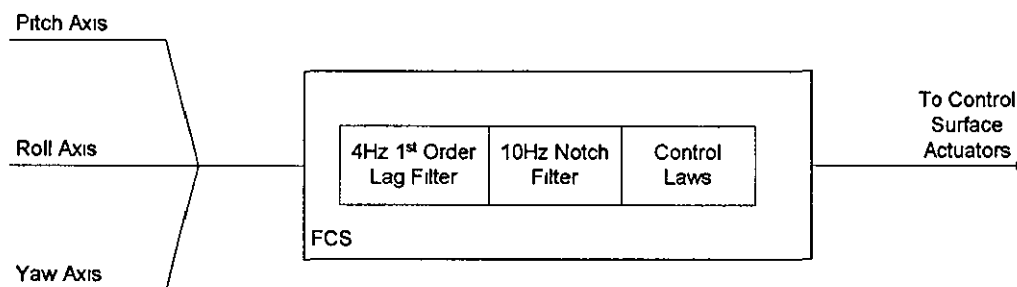
Figure 2-2. Jaguar Filter Design

However these were simple designs compared to the design for the Experimental Aircraft Programme (EAP) This design required 7 filters in the pitch rate feedback path alone [Caldwell – 1996][9]. Figure 2-3 shows the arrangement for EAP
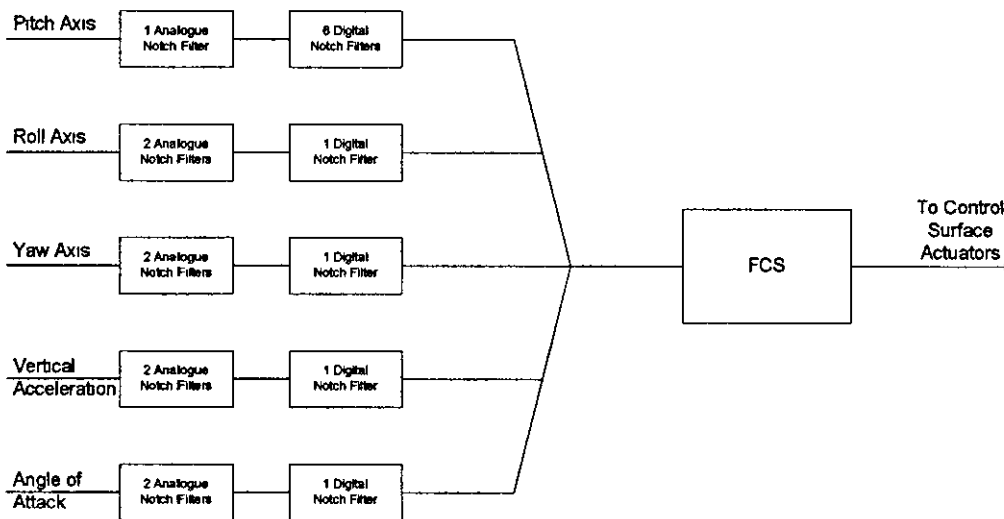
Figure 2-3. EAP Filter Design

Comparison of Figure 2-2 and Figure 2-3 clearly shows the increase in complexity from the late 1960s to the 1990s   This has resulted from the requirement for higher bandwidth FCS and the use of inherently unstable aircraft   This is in addition to the lower resonant mode frequencies which have resulted from the use of lighter materials and advanced structural design

2 2 2   Types of Solution

As discussed in the previous section, there are a number of solutions that can be used to overcome a structural coupling instability, though not all work in any situation One of the simplest ways is to move the sensor from the position where a flexible mode is significant to one where it is not   Figure 2-4 shows the frequency response of an Agile Combat Aircraft (ACA) when the position of the main sensor package is moved over a distance of 5m along the length of the aircraft   This data has been developed using the model which will be discussed in Chapter 6
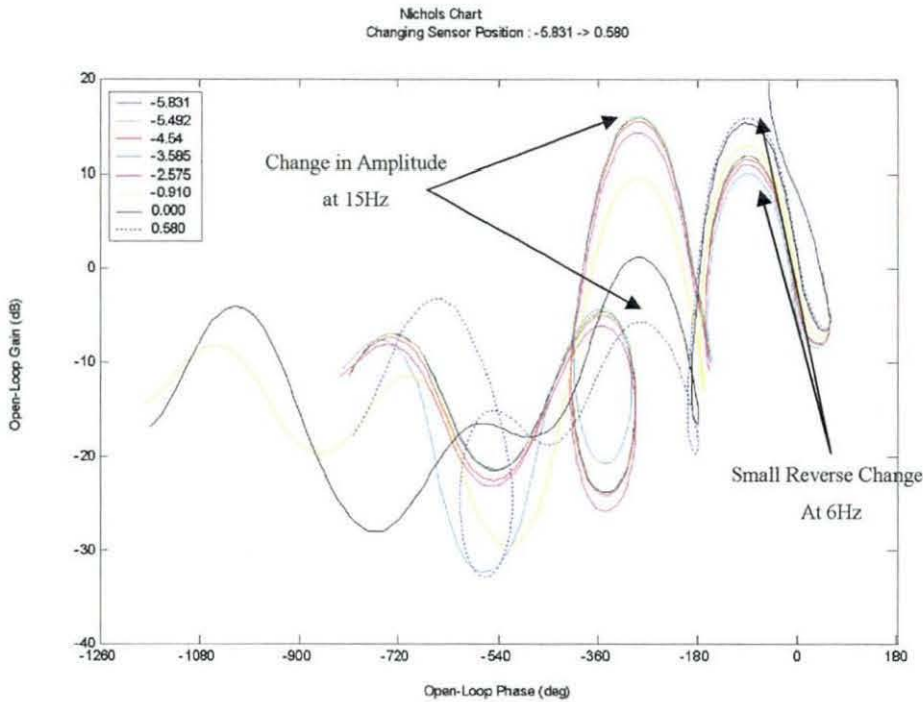
Figure 2-4. Frequency Response of Changing Sensor Position

As the response shows, the action of changing the position of the sensor may have an effect on some flexible modes, and not others. In Figure 2-4, one mode at approximately 10Hz is attenuated by approximately 25 dB as the sensor is moved from -5.9m to 0.5m, but for another mode at 6Hz the effect is reversed.

An alternative method of overcoming a potential instability is to alter the control loop gain; although this may not be possible if strict requirements have been laid down for the performance of the aircraft.

A third way, and at the present the most common method, is to attenuate the signal at the flexible mode frequency using notch filters. This method is known to work reliably, but can introduce problems of its own if the solution involves a large number of notch filters, and the stability margins of the rigid aircraft and FCS are tight. Each notch filter will add an amount of phase lag at low frequencies, and the summation of these phase lags reduces the stability margin; this results in the need for a trade off between attenuation and phase lag.

2.2.3   System Response

Whether there will be a problem with a particular aircraft is generally predicted on the basis of the results of a number of tests.   If the results indicate the existence of a potential instability, then correcting action can be taken.

Early aircraft relied on the results of testing carried out on a physical system, either the aircraft itself, or on a wind tunnel scale model of the aircraft.   The results from tests on the aircraft are often gathered in response to stimuli applied to the control surfaces of the aircraft.   These signals are then measured as they pass through the aircraft, and through the FCS.

More recently, the development of new techniques, combined with the availability of computers which can cope with complex mathematics, has allowed the aircraft system to be modelled.   From these models, frequency responses can be plotted, which can be used to predict potential problems.

2.2.4   Preventing Potential Instabilities

If the results gained from system tests and models show that there is a potential problem, then corrective action can be taken, using the solutions outlined in Section 2.2.2.

If notch filters are required, then the gathered frequency response data can be used to help develop a solution which satisfies the requirement to both sufficiently attenuate the flexible modes, and also meet the required low frequency stability margins.   This process may take several iterations to achieve a satisfactory result.

Since the frequency response is likely to vary between different flight configurations, it is important to use data on as many configurations as is practical.   It is also important to use a combination of both model and test data, since there can often be significant inaccuracies in the model.   Figure 2-5, which shows a comparison of ground test data and model data, when stimulation is applied to the outboard flap control surfaces, highlights this difference.
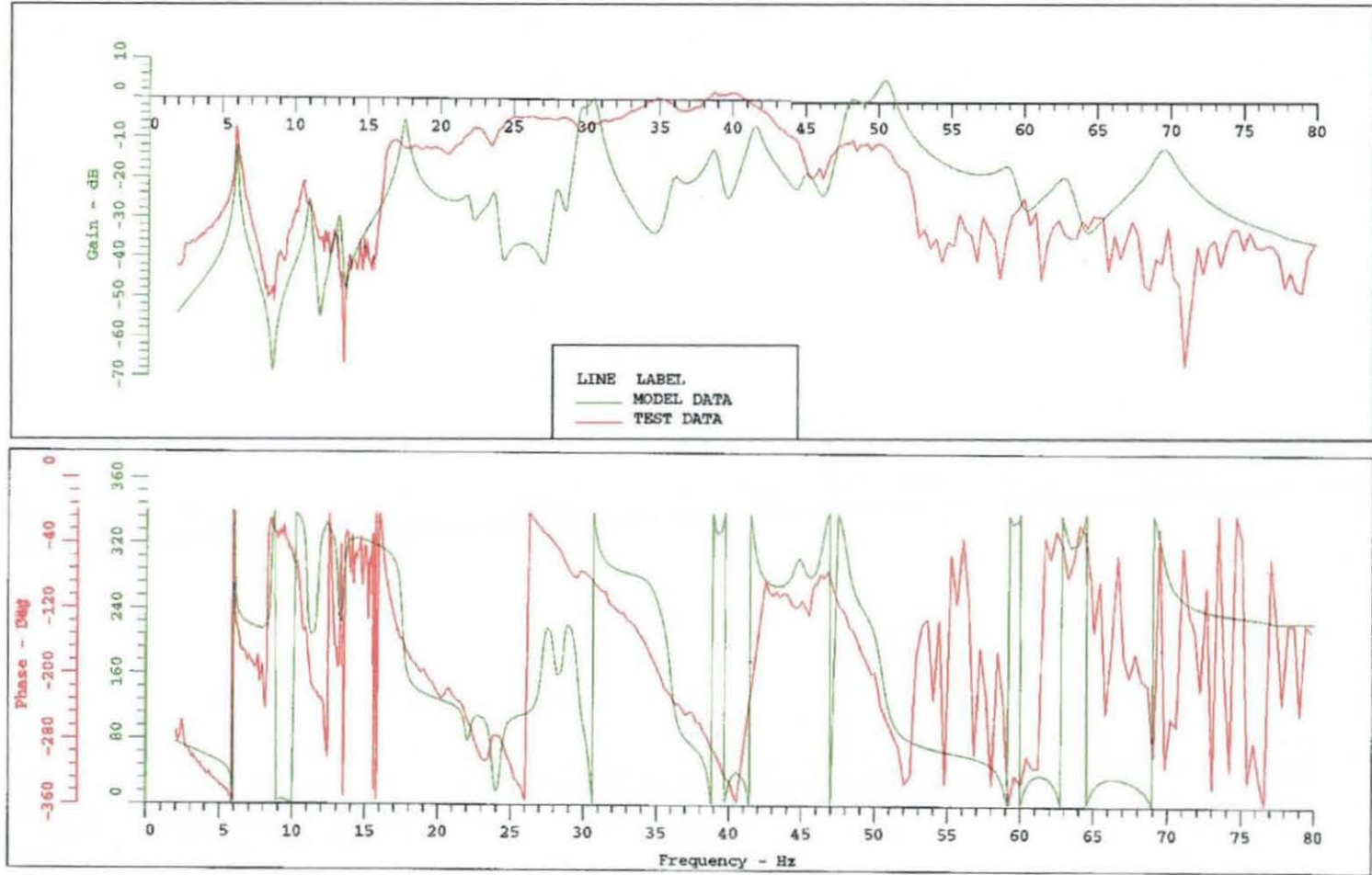
Figure 2-5. Comparison between Model and Test Data

As can be seen from the comparison, whilst at low frequencies the model provides a good comparison with the test data, at higher frequencies there are large differences in the model

In order to reach a solution it may be necessary to use a number of techniques to overcome low frequency phase lag problems If a flexible mode only effects a particular sensor, then placing the notch filter on that sensor path will ensure the phase lag does not affect the other paths Also the location where the notch filter is placed in the path can have an effect, especially in a digital system, where placing the filter before or after an analogue to digital converter (ADC) can impact the amount of phase lag

2.3   Kalman Filter

The Kalman filter is a statistical filtering and estimation technique, which was developed as part of a United States Air Force research project stemming from a need to maintain aerodynamic integrity by deriving the best information out of numerous and continuous data streams that inherently contained imprecise data It is a set of mathematical equations which allows the estimation of both observable and non observable states, and can be used even when a precise model of the plant is available

The majority of the work described in this thesis uses the continuous form (non time-varying) of the Kalman filter, block diagram of which is shown in fig 2
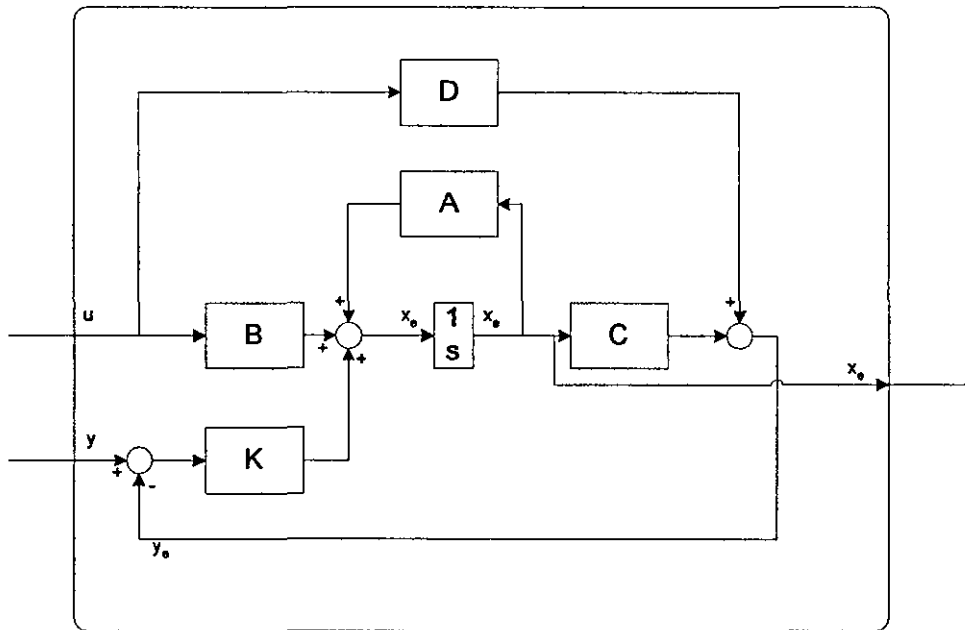
Figure 2-6. Kalman Filter Block Diagram

The inputs to the Kalman filter are typically the inputs to the plant, and the measured outputs of the plant   The inputs are used to calculate an estimate of the plant functions, which are compared to the actual outputs from the plant   The difference between the actual and estimated outputs is multiplied by the Kalman filter Gain, and is used to correct the estimation of the plant states

For a plant which can be represented by the following equations

$$\dot{x} = Ax + Bu + Gw$$
$$y = Cx + Du + v$$

where w represents the process noise of the plant, and v represents the sensor noise The Kalman filter estimate of the plant states is given by

$$\dot{x}_e = Ax_e + Bu + K(y - Cx_e - Du)$$

where K is the Kalman filter gain matrix   The calculations for the Kalman filter gain matrix include additional parameters which allow the co-variances of the process and sensor noise parameters to be included

The sensor noise can normally be measured, allowing the co-variance (R) to be calculated The process noise is however normally very difficult (or impossible) to measure, as a result the co-variance (Q) is normally represented by an estimated number, which the designer feels is appropriate, and choice of the elements of Q constitutes the tuning of the filter

2.4   Stability Margins

There are a number of ways in which the stability of a system can be checked (e g . the existence of closed loop poles in the right hand half of the s-plane or by application of the Nyquist criterion)   These assess whether a system is stable or not, but do not indicate how stable the system will be

Since the model used to assess a system will never be an exact representation, it is possible for a model to indicate that the system is stable, when the uncertainty means that in fact it is not, for this reason, the relative stability of the system is used Frequency domain stability assessment, which forms the basis of the Nyquist criterion, can be extended using two relative stability indicators· the gain and phase margins of the open loop system   These are defined as

> Gain Margin the magnitude of the open loop function of a stable closed loop system at the -180° crossover on the Nyquist diagram   This is usually defined in decibels

> Phase Margin the magnitude of the angle through which the Nyquist diagram must be rotated in order to intersect the (-1,0) point for a stable closed loop system

In order that an acceptable level of stability can be achieved, minimum stability margins are set out. For a combat aircraft, these are given by the relevant military standards (Ref 30)

The standards specify that, to ensure an acceptable level of stability, the designer must ensure phase margins of 35° and 90° to the right and left respectively of the -180° region, with a gain margin of -6dB at this point For structural coupling purposes additional regions are defined· in the -540° region the phase margin is 90° on both sides and the gain margin is -9dB Above -900° the magnitude of the frequency response is not permitted to rise above -9dB, to the right of this point there is a phase margin of +90° These margins can be seen graphically on the Nichols chart as shown in fig 1 and are called the exclusion regions
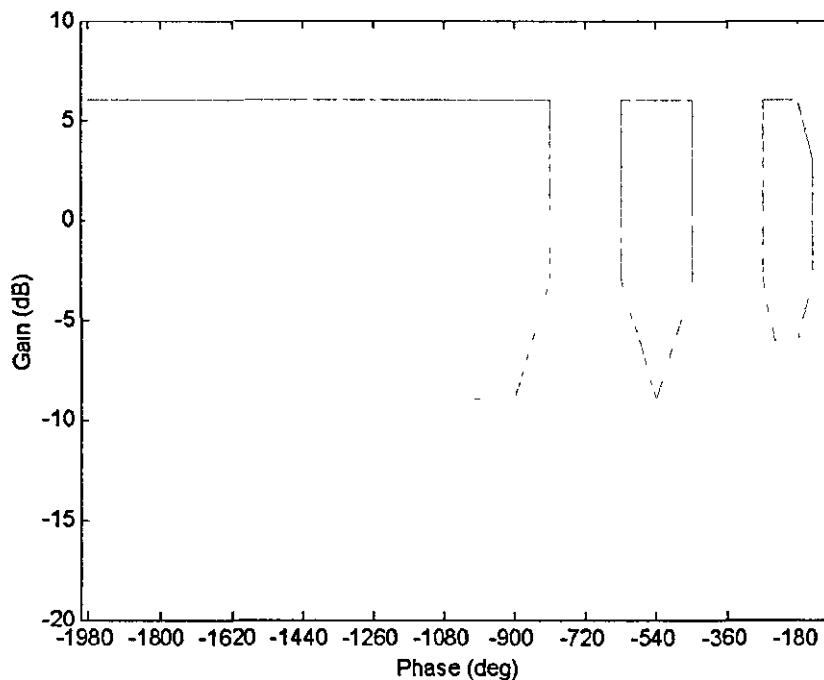
Figure 2-7. Structural Coupling Exclusion Regions

2.5   Motivation

A previous research project (Ref 29), examined the use of model based estimation techniques in aerospace applications The project focused primarily upon aircraft state estimation for FCS, but it also briefly examined the use of model based estimation as a possible alternative solution to the structural coupling problem

The results from this project indicated the potential for a reduction in the low frequency phase lag, if an estimator was used to replace the notch filters which currently provide the solution

2.6 Proposed Solution

The research will look at the potential of a Kalman filter to successfully filter out undesirable flexible mode frequencies by using sensor outputs and control inputs to estimate both the contribution to the sensor output of each of the flexible modes and the rigid mode. It is proposed that the estimated rigid mode sensor data is used as in the feedback of the control loop, as opposed to the notch filtered approach

The aims of this research project are to develop techniques for the use of model based estimators, in particular a Kalman filter, and to examine the performance of the Kalman filter approach in comparison with a notch filter solution

It is intended to use models which provide a close representation of the aircraft system, defining the models to provide flexible modes at similar frequencies to those found on an aircraft

2.7 Outline of Research

This section briefly describes the stages of this research project

2.7 1 Model with a single flexible mode

The first stage of this project looked at a simple model, which provided a single flexible mode with which to examine the problem. Using the model developed, the feasibility of using a Kalman filter in place of the notch filter was assessed

After the initial comparison had been successfully completed, a more in depth analysis of the Kalman filter performance was made, by altering the parameters of the system, and examining the response of the unaltered Kalman filter to the resulting frequency changes

2.7.2 Model with two flexible modes

This stage of the research used a slightly more complex model, which provides a closer representation of the aircraft pitch loop As in the previous stage, a model was developed, and the resulting solution was compared to the traditional solution

After the Kalman filter solution had been developed, the performance of the filter was examined, especially when there were changes in the system which the filter was not aware of The effect of optimising the Kalman filter was also examined to see if this had an effect on the performance

2 7 3 Experimental Validation of model with two flexible modes

From an industrial perspective, it is important that any new techniques developed have been tested on a real system, and not just in simulations This stage of the project developed an experimental rig, based upon the model used in the previous section

The intention of the development of the rig was be to validate the model used, and to compare the experimental performance of the filter with results predicted by the simulation

2 7 4 Model with many flexible modes

The final stage of the project used a model of a flexible aircraft, similar to that used in the aerospace industry Using this model, the Kalman filter approach was examined on a complicated model, where the flexible modes cover a wide range of frequencies

The Kalman filter was compared with the notch filter solution, and then modified to examine the potential for further improvement

3 Single Mode Assessment

This chapter describes the first stage of the project, which has focused upon a simple model consisting of a system that has a single flexible mode

3.1 Introduction

This stage of the work has been used to examine the effectiveness of the Kalman filter as a replacement for notch filters A simple model has been used, since this would allow the examination of the problem and a general proof of the concept, without the complexity of a more complicated model

3.2 Model Description

The model that has been used consists of a large mass and a smaller mass These are connected together via a spring and damper placed in parallel There is a position sensor attached to the smaller mass, and the information supplied by this is used to control the position of the larger mass, A controller and an actuator connected between the large mass and ground are used to provide the control for this loop Figure 3-1 shows this arrangement
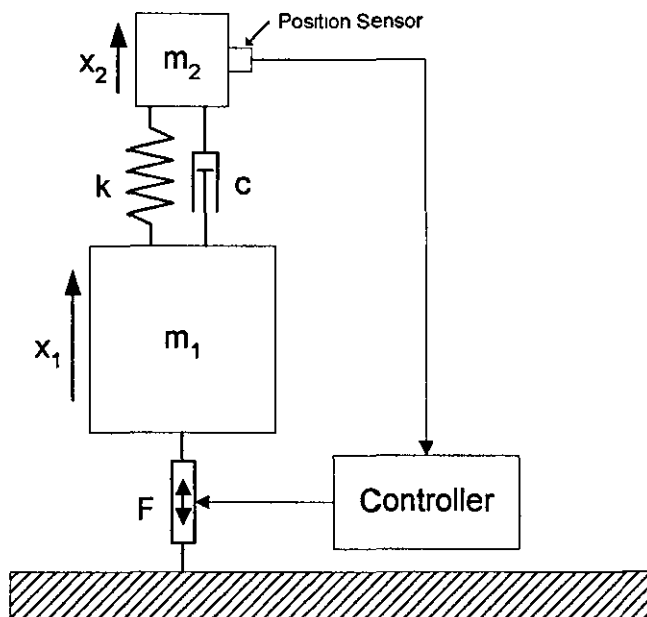
Figure 3-1. Two mass model

Although this model is not representative of the complexity of flexible modes in an aircraft, it is nevertheless a typical problem that is encountered in control engineering, for example a motor driving a load via a resilient shaft and gearbox

The Matlab m-files and Simulink models which have been used to simulate this model are included in Appendix C

3 2.1 Assumptions

For the purposes of this model, two main assumptions have been made.

    a) The system contains negligible process noise

    b) The dynamics of the sensor and actuator cause negligible problems

These assumptions have been made to simplify the problem, but will be examined in detail in the more advanced models later in the theory

3 2 2 Model Parameters

The model has been designed using the following parameters

    Large mass (m_1)   -   50 kg

    Small mass (m_2)   -   25 kg

    Spring constant (k)   - $20000 \ Nm^{-1}$

    Damping constant (c) - $3 \ Nsm^{-1}$

These values have been selected to provide a flexible mode that is comparable to the first flexible mode of an aircraft, and with a low damping factor of 0 2%

3 2 3 System Modelling

In order to examine the model, it must be represented in mathematical form From the model, two state space equations can be developed These equations allow the positions (x) and velocities ($\dot{x}$) of the two masses to be modelled dependent upon the input force (F) The equations are:

$$m_1 \ddot{x}_1 + c(\dot{x}_1 - \dot{x}_2) + k(x_1 - x_2) = F \qquad (3\ 1)$$

$$m_2\ddot{x}_2 - c(\dot{x}_1 - \dot{x}_2) - k(x_1 - x_2) = 0 \qquad (3\ 2)$$

From these equations a state space model can be developed, which will allow analysis of the model   The general state space equations are

$$\dot{X} = AX + BU$$
$$Y = CX + DU \qquad (3\ 3)$$

The block diagram form of these equations is
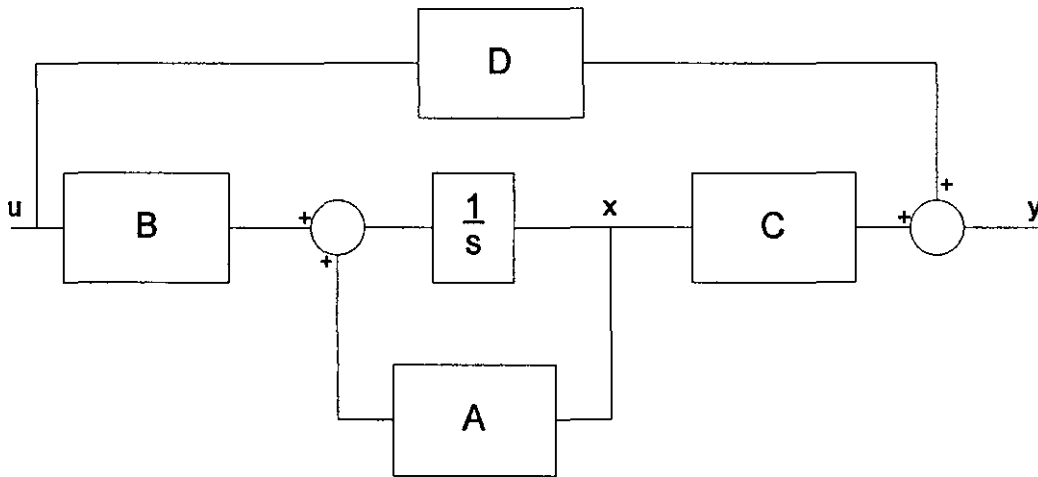
Figure 3-2. State Space Block Diagram

If the state vector X is selected to be

$$X = \begin{bmatrix} x_1 \\ x_2 \\ \dot{x}1 \\ \dot{x}_2 \end{bmatrix} \qquad (3\ 4)$$

Then the model will have the following form (with input U=F)

$$A = \begin{bmatrix} 0 & 0 & 1 & 0 \\ 0 & 0 & 0 & 1 \\ \dfrac{-k}{m_1} & \dfrac{k}{m_1} & \dfrac{-c}{m_1} & \dfrac{c}{m_1} \\ \dfrac{k}{m_2} & \dfrac{-k}{m_2} & \dfrac{c}{m_2} & \dfrac{-c}{m_2} \end{bmatrix} \qquad (3\ 5)$$

$$B = \begin{bmatrix} 0 \\ 0 \\ \dfrac{1}{m_1} \\ 0 \end{bmatrix}$$

(3 6)

$$C = \begin{bmatrix} 1 & 0 & 0 & 0 \\ 0 & 1 & 0 & 0 \end{bmatrix}$$

(3 7)

$$D = 0$$

(3.8)

This provides an output vector containing values x_1 and x_2 (i e the positions of the large and small masses respectively) The large mass position (x_1) is included in the model, but will only be used to provide a comparison between the outputs of the filters, and what they are trying to estimate

The eigenvalues of the uncontrolled system are shown in Table 3-1, and show the frequency and damping of the flexible mode

Eigenvalue	Damping	Frequency (Hz)
0	0	0
-0 09 ± 34 61	0 0026	5 51

Table 3-1. Uncontrolled Eigenvalues

3 2 4   System Controller

In order to allow the system to be used to compare the use of a Kalman filter with a notch filter, a controller must be developed for the system   Figure 3-3 shows the open loop frequency response (force input, position output), and this can be used to assist in the design of the controller   In order to provide a bandwidth of approximately 1Hz, a gain of 1000 has been added to the system
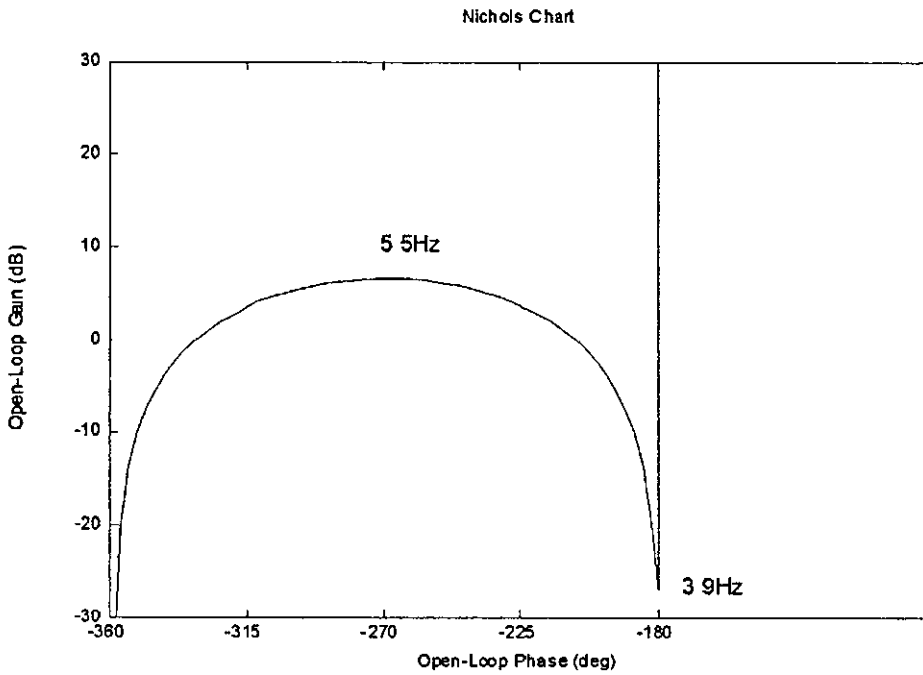
Nichols Chart

Figure 3-3. Open Loop Uncontrolled Frequency Response

Analysis of the Nichols chart shows that the frequency response crosses the 0dB 180° point, indicating that when the control loop is closed, the system will be unstable This response can be improved by adding a phase advance compensator into the system Figure 3-4 shows how this would be inserted into the system
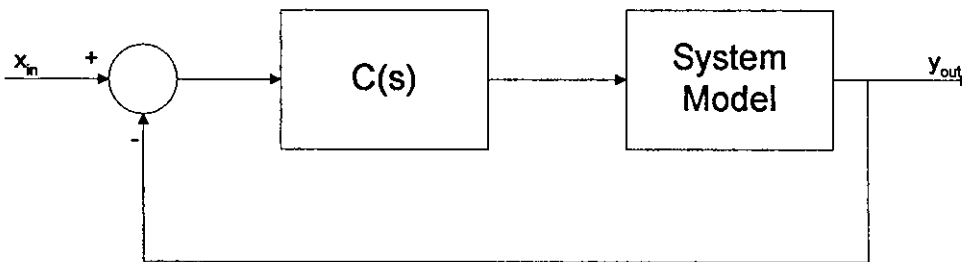
Figure 3-4. Block Diagram of Closed Loop System

In order to provide a basis from which to compare the notch and Kalman filters, it is useful to design the controller so that the controlled system is unstable, and provides a response similar to that found on an aircraft, without the filters Figure 3-5 shows the Nichols chart, when a controller consisting of a gain of 1000 (added in Figure 3-3) combined with a 4 1 phase advance compensator (maximum phase advance at 0 6Hz) is added to the system

Nichols Chart
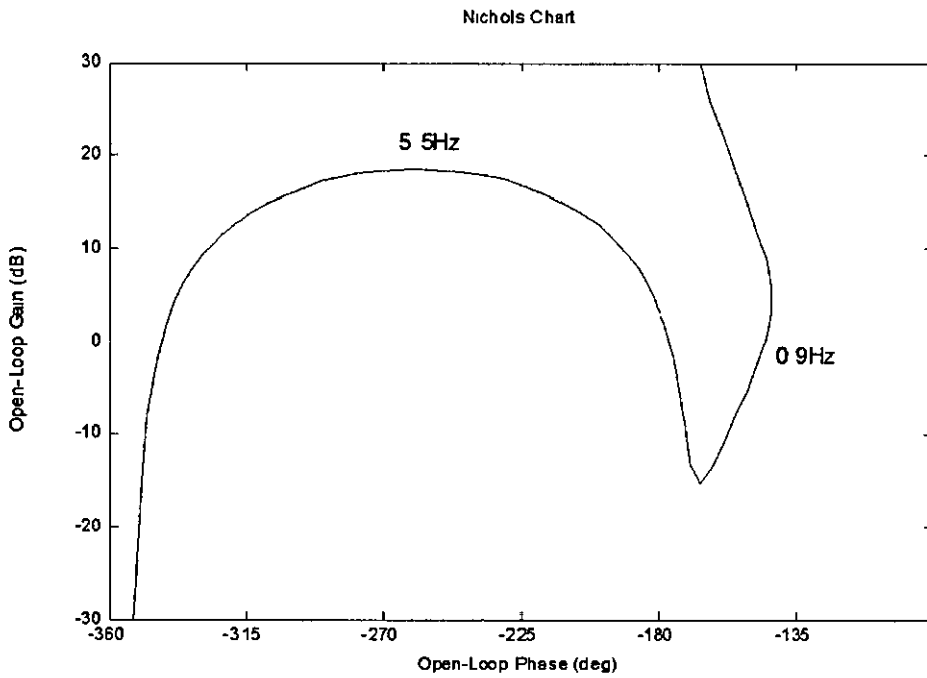
Figure 3-5. Open Loop Frequency Response of Controlled System

The transfer function of this controller is

$$C(s) = \frac{1000(0\ 504s + 1)}{0\ 126s + 1}$$

(3 9)

3.3   Notch Filter Solution

As was seen in Figure 3-5, with this value of gain, the system is unstable   This can be demonstrated through simulation of the model
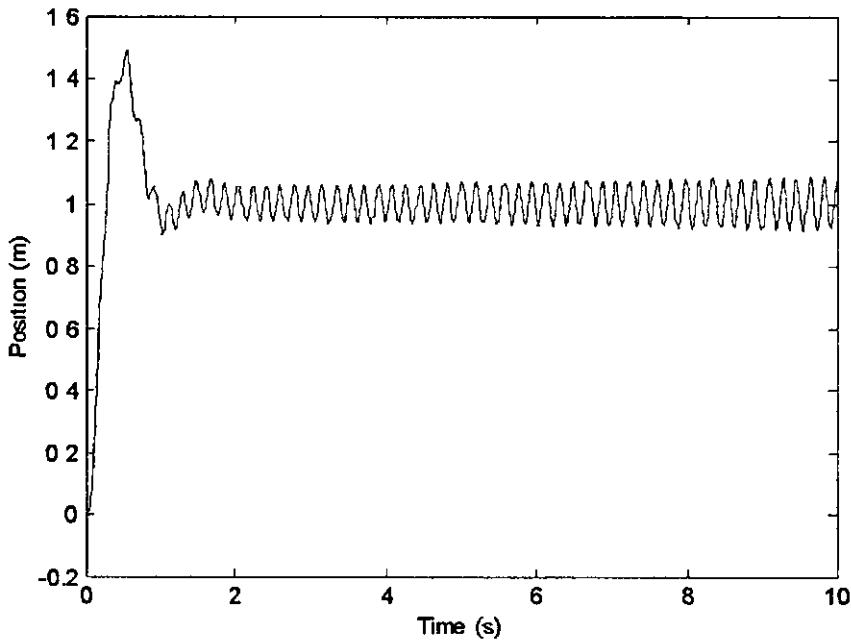
Figure 3-6. Unfiltered System Response

Figure 3-6 shows the time domain response (closed loop) of the model, and it can clearly be seen that the system is unstable when stimulated by a step input of 1m

In order to remove the undesired flexibility effect in the system, a notch filter can be added to the feedback path   The transfer function of the notch filter is

$$F(s) = \frac{s^2 + \varpi^2}{s^2 + s\varpi\zeta + \varpi^2}$$ (3 10)

Where ω is the notch frequency (rad/s) and ζ is the damping of the filter (related to the width of the notch)

The filter used to improve the performance of the system has the following parameters·

Notch frequency	-	34 6 rad/s (5 51Hz)
Damping ratio	-	0 05

The frequency response of this filter is shown in Figure 3-7

Bode Diagram
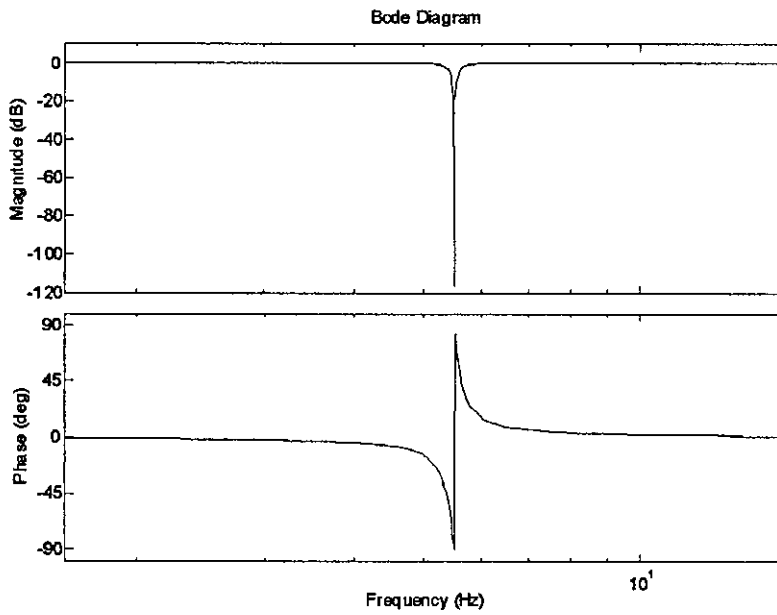
Figure 3-7. Frequency Response of Notch Filter

Since the filter used here has no numerator damping, the filter provides 'perfect' attenuation at the notch frequency When this filter is added to the system, the response of the system is stabilised, as can be seen from Figure 3-8
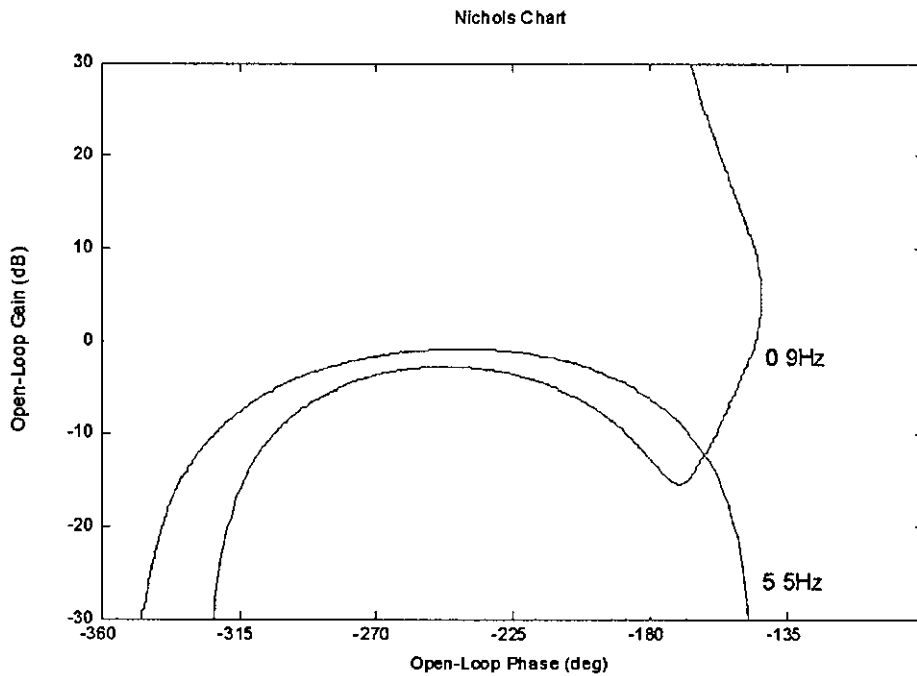
Nichols Chart

Figure 3-8. Frequency response of Notch Filtered System

From the Nichols chart, it can be seen that the filter has reduced the gain of the response around the region where the problem existed. This stability improvement is not without cost. As can be seen from Figure 3-9, the insertion of the notch filter has introduced a small amount of phase lag at lower frequencies, thereby reducing the phase margin.
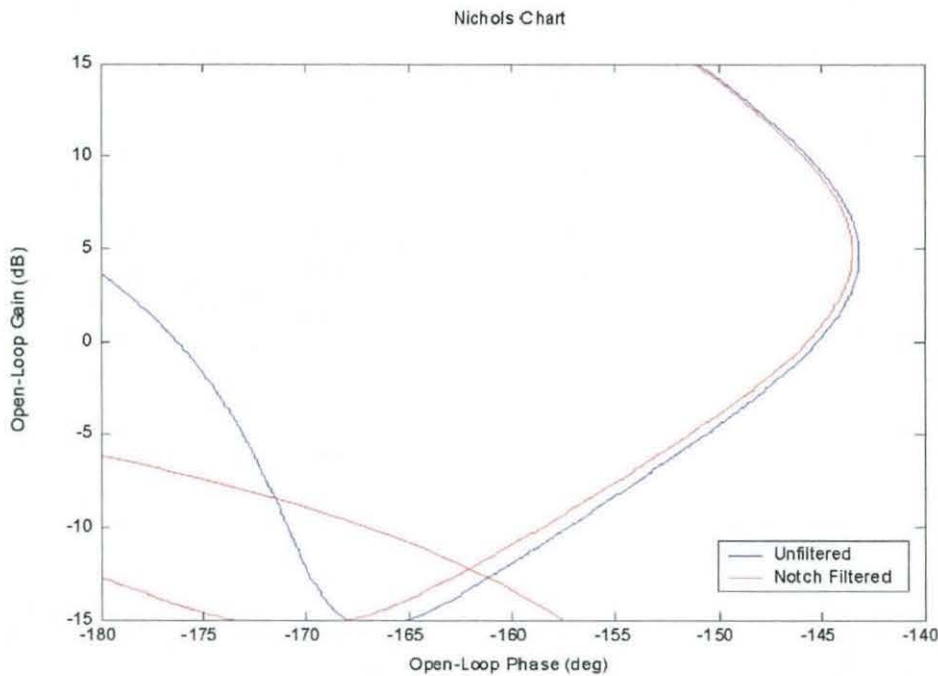
Figure 3-9. Frequency response for the System with and without Notch Filter

Whilst in this model the additional phase lag would not be a problem, in a more complicated model, with more flexible modes and more stringent stability margins, then the additional phase lag becomes a serious concern.

3.4 Kalman Filter

As suggested in Chapter 2, replacing the notch filter with a Kalman filter offers an alternative solution. With knowledge of the system, the Kalman filter can provide an estimate of the position of the large mass, given the input to the system (force) and the sensor readings (position of smaller mass). The positioning of the Kalman filter in the system can be seen in Figure 3-10.
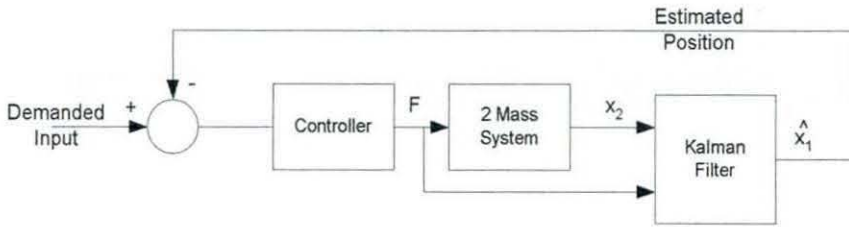
Figure 3-10. Block Diagram of System Including the Kalman Filter

The Kalman filter design uses the same basic state space model derived in Section 3.2.3, with some additional information. These provide information about the sensor noise in the model, the process noise in the model, and how the process noise affects the states.

The process noise can be added to the state equation, as shown in Equation (3.11):

$$\dot{x} = \mathbf{A}x + \mathbf{B}u + \mathbf{G}w \tag{3.11}$$

Where w is the process noise function and $\mathbf{G}$ is the matrix representing the effect of the noise function on the state vector. It is assumed that each state has its own process noise. An identity matrix represents this:

$$G = \begin{bmatrix} 1 & 0 & 0 & 0 \\ 0 & 1 & 0 & 0 \\ 0 & 0 & 1 & 0 \\ 0 & 0 & 0 & 1 \end{bmatrix} \tag{3.12}$$

Since the system process noise has been assumed to be negligible, so the Q matrix, which relates to the system process noise, can be used to bias the Kalman filter to focus primarily on the rigid mode.

$$Q = \begin{bmatrix} 1*10^{-11} & 0 & 0 & 0 \\ 0 & 1*10^{-9} & 0 & 0 \\ 0 & 0 & 5*10^{-7} & 0 \\ 0 & 0 & 0 & 5*10^{-7} \end{bmatrix} \tag{3.13}$$

Each term in equation (3.13) represents one of the states in the system ($x_1, x_2, \dot{x}_1, \dot{x}_2$).

In order to calculate the Kalman filter output covariance parameter (R), the noise is sampled over 10s; this sample is used to calculate the covariance of the noise. With the noise power of the sensor set at:

noise power = $1*10^{-5}$

the sensor noise covariance is:

$$R = 0.001 \tag{3.14}$$

Using these values, the Matlab function 'lqe' calculates the Kalman gain matrix K to be:

$$K = \begin{bmatrix} 0.1826 \\ 0.1826 \\ 0.0167 \\ 0.0167 \end{bmatrix} \tag{3.15}$$

Figure 3-11 shows the open loop frequency response of the unfiltered (controlled) system and the system when the Kalman filter has replaced the notch filter.
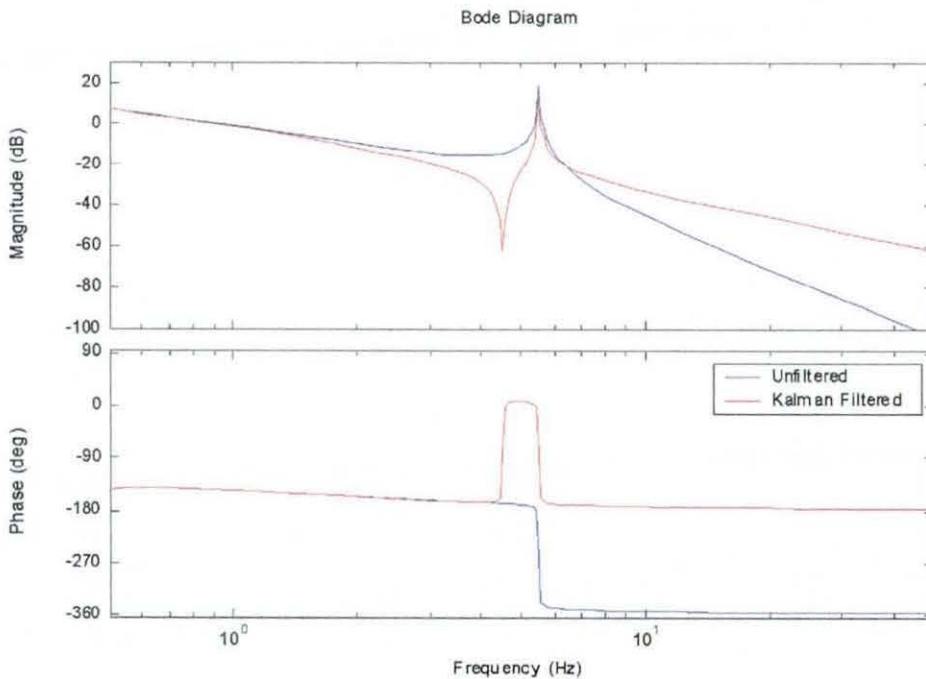
Figure 3-11. System Frequency Response with and without Kalman Filter

As can be seen, the Kalman filter has significantly altered the system response and stabilized the system. Whilst the Kalman filter approach has not significantly reduced the magnitude resulting from the flexible mode, it has fundamentally altered the phase of the system, away from the undesired area.

3.5 Preliminary Results

In order to provide a comparison between the filters, the system has been examined in both the time domain and the frequency domain.

3.5.1 Frequency Domain

The main area of interest to the aerospace industry when considering structural coupling, is the effectiveness of the solution when it is examined in the frequency domain. The main concern is how the solution changes the stability margins; on a typical combat aircraft the phase margin normally occurs at about a frequency of 1 Hz. Figure 3-12 shows the three different options. As can be seen, the Kalman filter provides a better phase response to the notch filtered system.
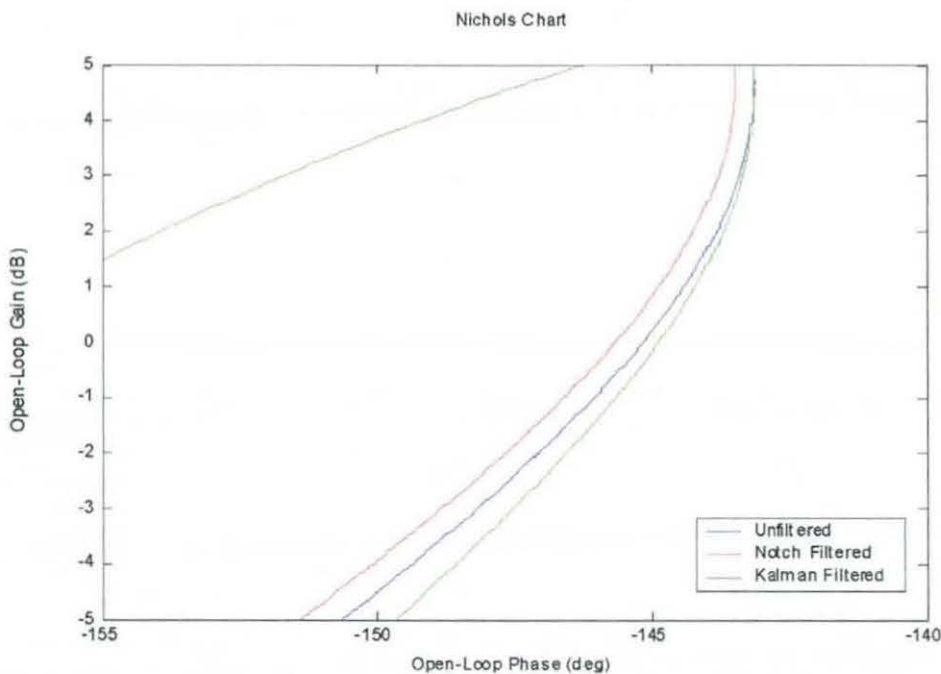
Figure 3-12. Comparison of Phase Lag Between Filters

Examination of the phase of the system as the magnitude of the responses crosses 0dB using Matlab, shows the following results:

	Phase (deg)
Unfiltered	145°
Notch Filter	146°
Kalman Filter	145°

Table 3-2. Filter Type Phase Comparison

The results show that the notch filter introduces 1° of phase to the system, whilst the Kalman filter does not introduce any additional phase. In fact inspection of Figure 3-12 shows that the Kalman filter has slightly lower phase lag than the unfiltered system.

3.5.2   Time Domain Analysis

In order to compare the results in the time domain, the system has been simulated in response to a 1m step input. Sensor noise has been added to the system output.
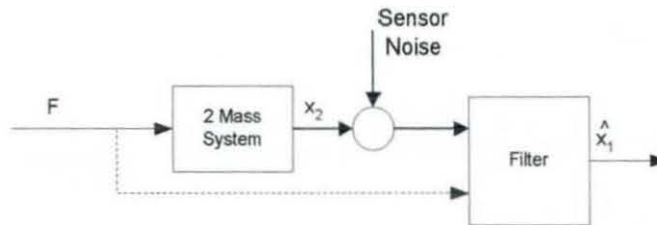
Figure 3-13. Addition of Sensor Noise

The filtered signal, which is passed to the controller (shown as $\hat{x}_1$ in Figure 3-13), is shown in Figure 3-14. This shows that, in addition to removing the effects of the flexible mode, the Kalman filter also reduces the sensor noise.
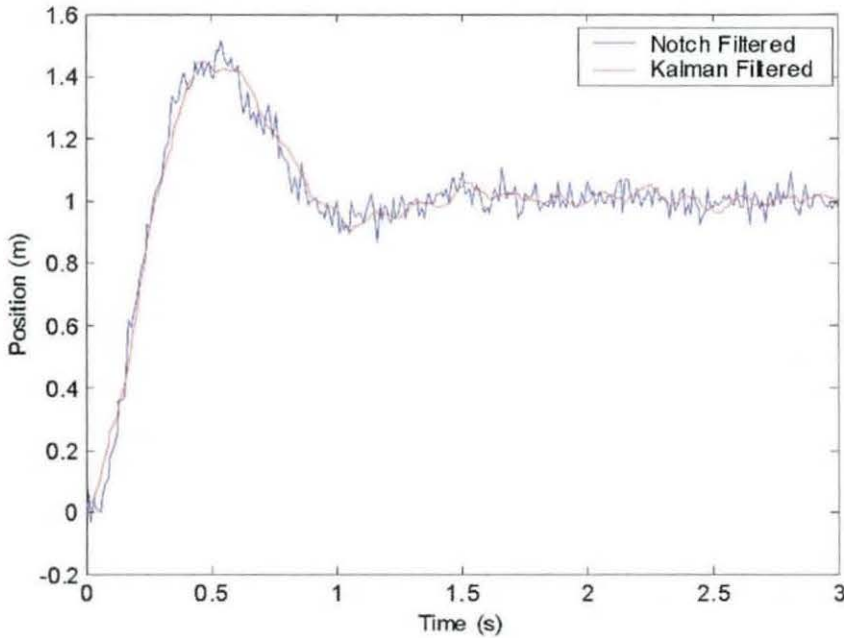
Figure 3-14. Closed Loop Step Response (Feedback)

Comparing the peak and RMS errors in each filter can make a further comparison between the filters. If the feedback signal is compared to the position of m_1, the filter estimation error can be calculated. The notch filter errors are:

Peak: 0.1064

RMS: 3.9×10^{-4}

For the Kalman filter, the errors are:

Peak: 0.0032

RMS: 9.01×10^{-6}

These results demonstrate that the Kalman filter solution provides a better estimate of the position of m_1. This is not unexpected, since while the notch filter operates by attenuating a particular frequency, the Kalman filter operates by providing an explicit estimate of the desired information.

3.5.3   Filter Robustness

As was discussed in Section 2.2.4 all aircraft fly in a number of different configurations. This will affect the frequencies of the flexible modes. As a result of

this it is very important for any solution to the structural coupling problem must be able to accommodate these frequency changes.

In order to assess how the filters manage the changes, errors have been inserted into the model, whilst leaving the filter at the nominal value unchanged. In order to change the frequency in the model, the size of the smaller mass (m_2) has been altered from 50% to 200% of its nominal value, which provides a frequency variation of 4.5Hz to 7.1Hz. The RMS errors across this range for each filter are shown in Figure 3-15.

As can be seen from Figure 3-15, when the difference between the model the Kalman filter expects and the actual model are small, then the Kalman filter operates with lower RMS errors than the notch filter. However when at the extreme differences between the actual and expect models, the RMS errors of the notch filter are better than those of the Kalman filter.
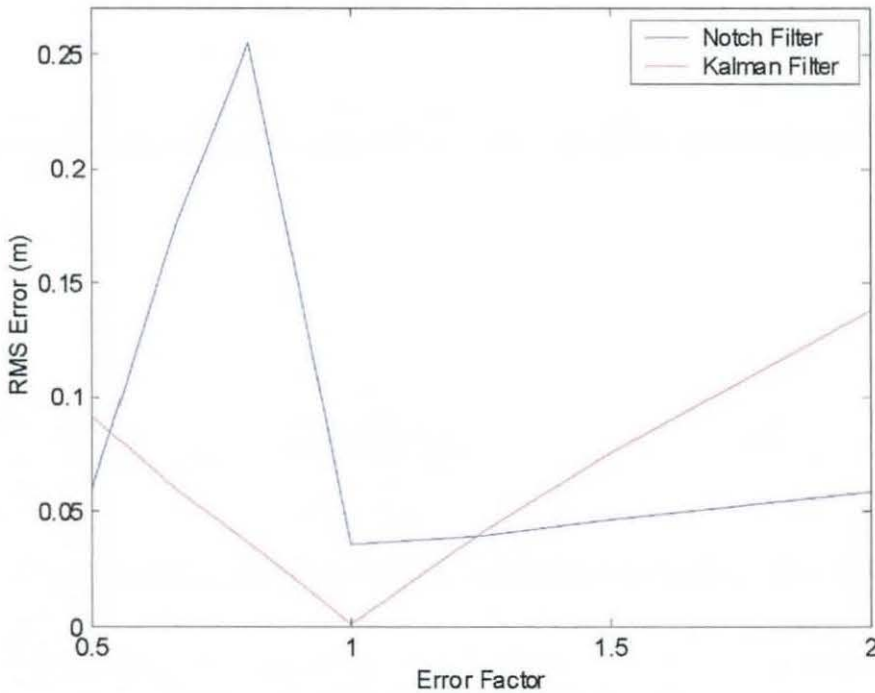
Figure 3-15. RMS Errors of Both Filters

Examination of the time domain responses over the range of model differences help to understand the importance of the results from Figure 3-15.
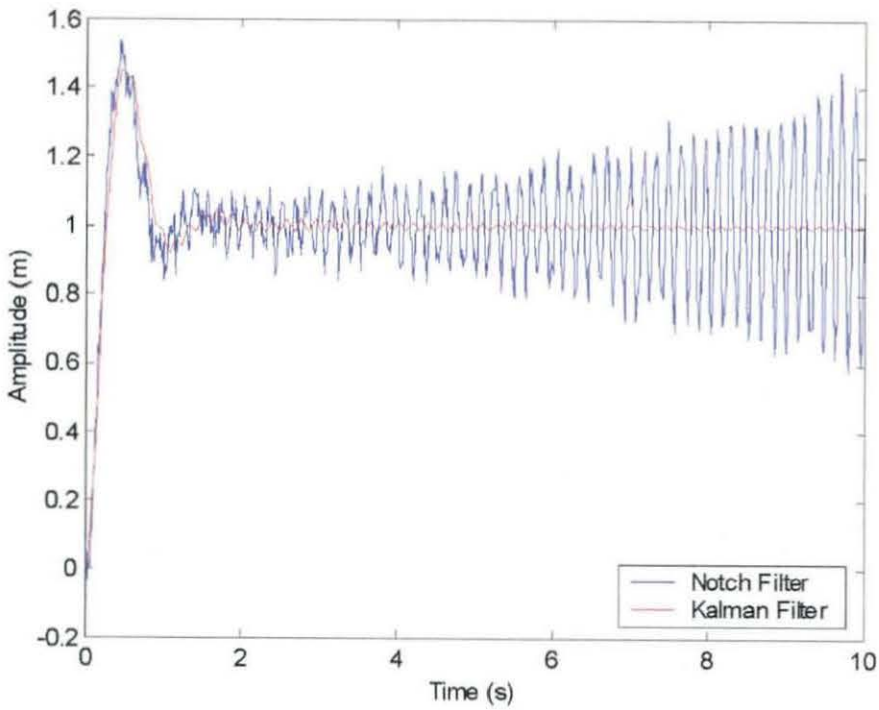
Figure 3-16. Filter Feedback Signal (75% of Expected Mass)

Figure 3-16 shows the closed loop responses (to a step demand of 1m) when the mass is 25% smaller than the filters are expecting. The Kalman filter is stable; however the notch filter in this instance is unstable. This correlates to Figure 3-15, for an error factor of 0.75 the RMS error of the notch filter is significantly higher.
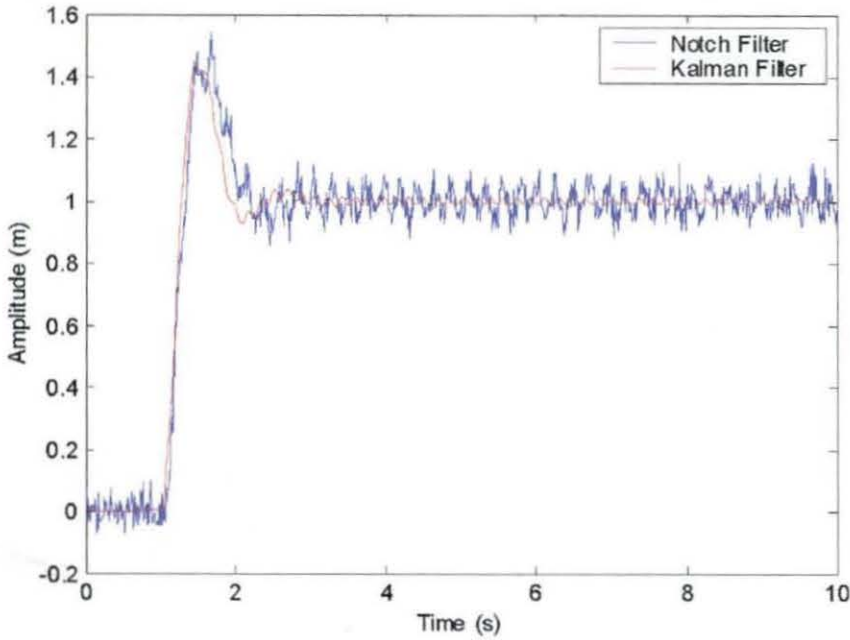
Figure 3-17. Filter Feedback Signal (200% of Expected Mass)

The results shown in Figure 3-17 do not correlate so well with Figure 3-15. The RMS errors suggest that when m_2 is 200% of its nominal value, the notch filter should perform better than the Kalman filter; however the filter outputs do not show this. In order to understand why this is the case, the actual position of m_1 should be looked at.
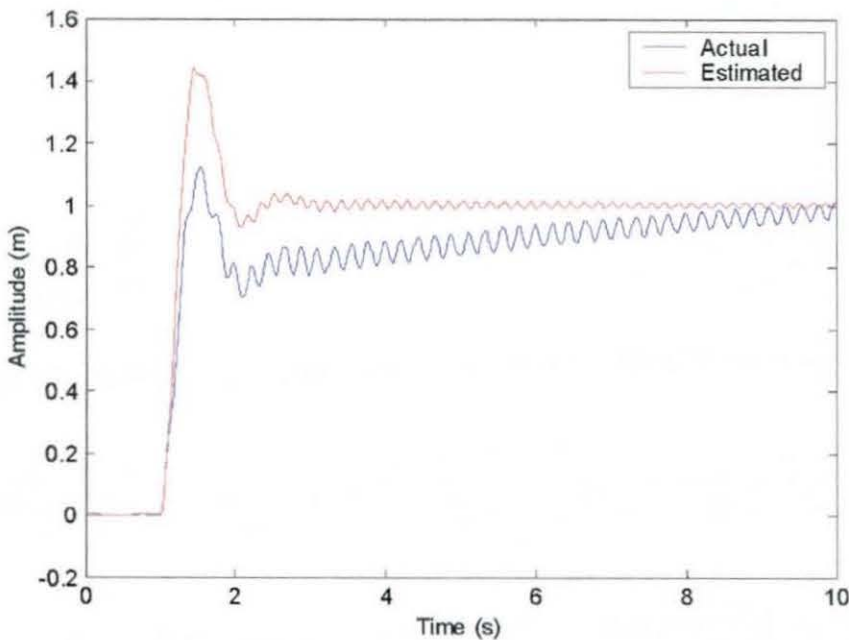
Figure 3-18. Actual and (Kalman Filter) Estimate x_1 Position (200% of Nominal Mass)
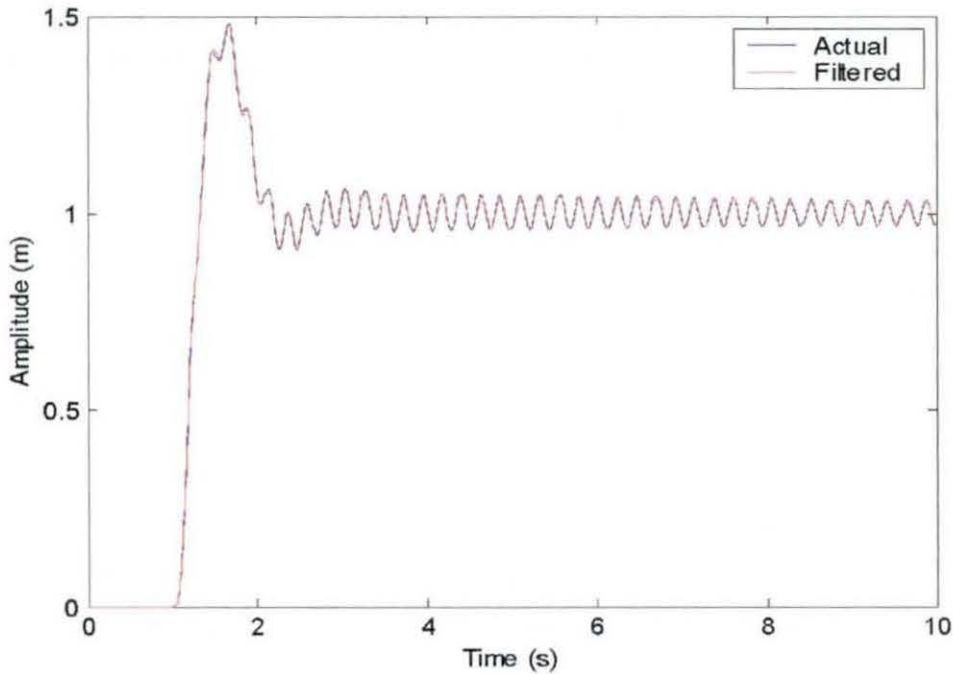
Figure 3-19. Actual and (Notch Filter) Estimate x_1 Position (200% of Nominal Mass)

The comparison between the notch filter (Figure 3-19) and the Kalman filter (Figure 3-18), clearly highlights the reason for the difference in the RMS errors; whilst the Kalman filter estimate removes the contribution of the flexible mode, it does not correctly estimate the position of the mass.

3.5.4 Improvements to the Kalman Filter

The results of the previous section show that the Kalman filter is stable over the range tested. However, when there are significant differences between the expected and actual models, then the Kalman filter does not correctly estimate the position of the large mass.

By adjusting the parameters of the Kalman filter (tuning the Kalman filter) it may be possible to improve filter performance. The Kalman filter has two parameters that can be altered, without affecting the model contained within the filter; these are the Q and R matrices. The R matrix relates to the sensor noise, so should be left unchanged. The Q matrix relates to the process noise within the system itself, and since this is

generally less well known than the sensor noise, there is more freedom to change this parameter.

Through a process of trial and improvement, the Q matrix can be altered to use the following values:

$$Q = \begin{bmatrix} 1*10^{-7} & 0 & 0 & 0 \\ 0 & 1*10^{-5} & 0 & 0 \\ 0 & 0 & 5*10^{-3} & 0 \\ 0 & 0 & 0 & 5*10^{-3} \end{bmatrix} \qquad (3.18)$$

Then the Kalman filter gain matrix changes to:

$$K = \begin{bmatrix} 1.8159 \\ 1.8480 \\ 1.6487 \\ 1.7026 \end{bmatrix} \qquad (3.19)$$

As can be seen the parameters of the gain matrix have all increased, placing more emphasis upon the sensor output than was previously used. In particular the parameters relating to the velocity components of the model have a greater significance. Figure 3-20 shows the RMS errors for the Kalman filter after these changes.
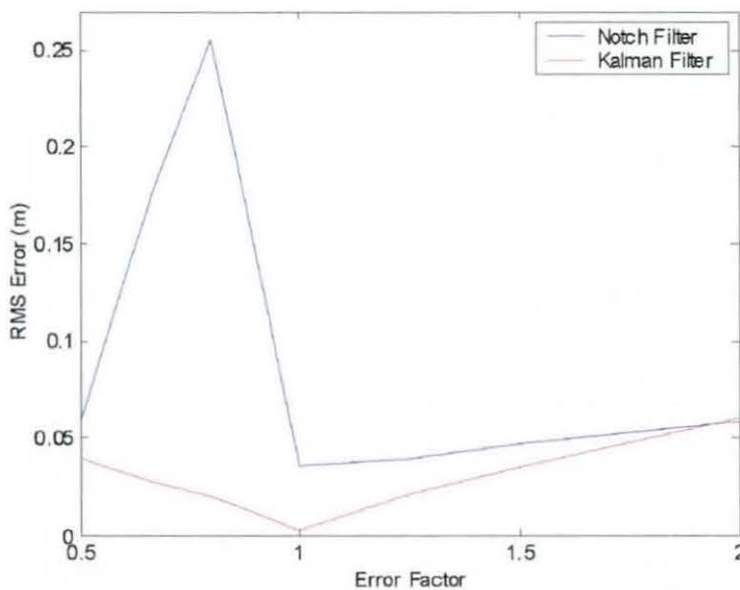
Figure 3-20. RMS Errors with Adjusted Q Matrix

As can be seen from Figure 3-20, the changes to the Q matrix have reduced the RMS errors to below those of the notch filter. Figure 3-21 compares the actual and estimated positions of the large mass.
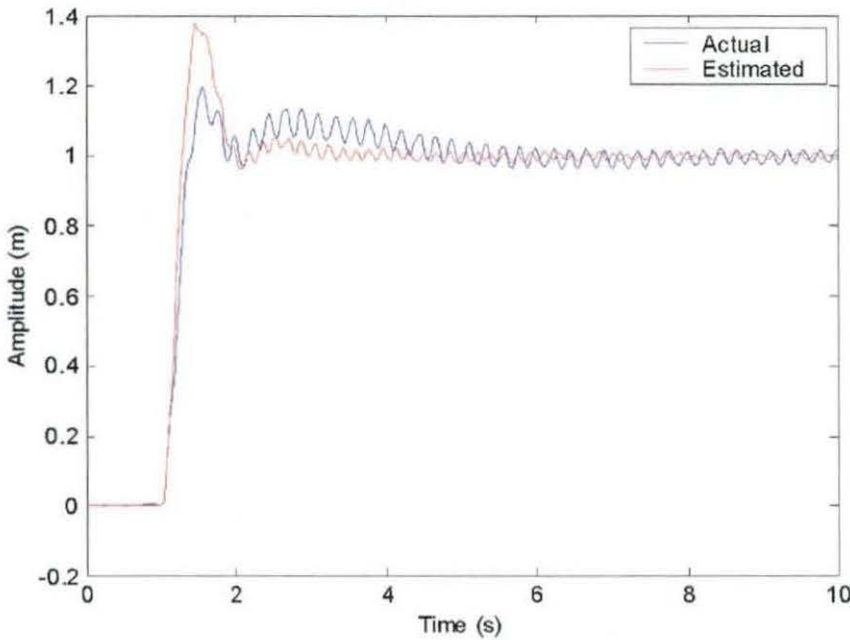
Figure 3-21. Actual and Estimate x_1 Position (200% of Nominal Mass)

This comparison shows that the changes to the Kalman filter have resulted in a more accurate estimate of the large mass position being provided.

Whilst it has not been needed here, the same approach could be used if there was a need to increase the range over which the Kalman filter is stable. The robustness of the Kalman filter, and how to improve it, will be examined in more depth in Chapter 4

3.6   Combined Outputs

Whilst the Kalman filter successfully overcomes the structural coupling problem, it does not remove the flexible mode. Instead it alters the feedback in such a way to reduce its impact upon the system stability margins. Figure 3-22 shows a Bode plot of the unfiltered and Kalman filtered systems.
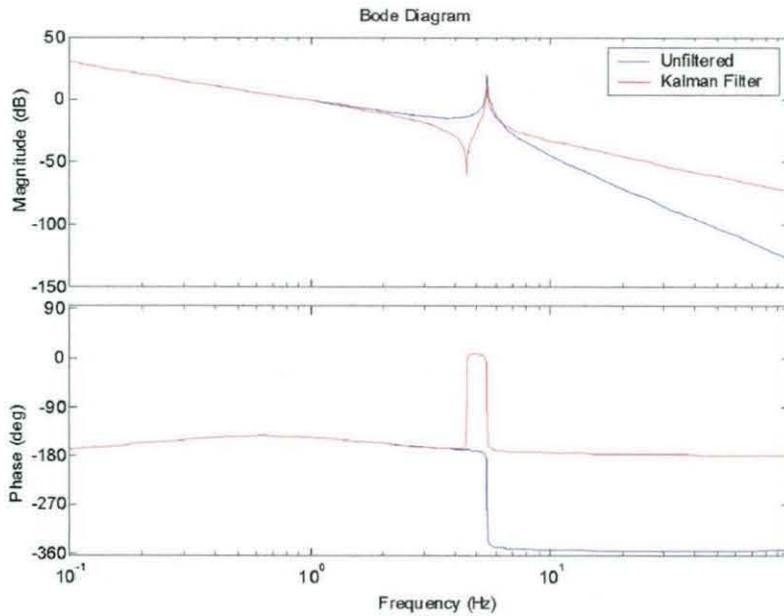
Figure 3-22. Comparison Between Unfiltered and Kalman Filtered Responses

The Kalman filter overcomes the problem here by altering the phase of the system away from the stability point. The gain of the response at the mode frequency has remained unchanged.

Whilst this has not been a problem with this model, it may become more significant in a more complicated model with a larger number of modes. This section will look at the possibilities of using a combination of the positions of the two masses in order to overcome this.

3.6.1   Linear Transformation

In order to provide an output that is a combination of the positions of the two masses, a linear transformation is required. A simple equation has been used to achieve this:

$$feedback = nx_1 + (1-n)x_2 \tag{3.20}$$

where n is varied between 0 and 1 (purely position of x2 and purely position of x1 respectively). This approach provides a composite feedback signal that is still effectively a position signal. A block diagram representation of this is shown in Figure 3-23.
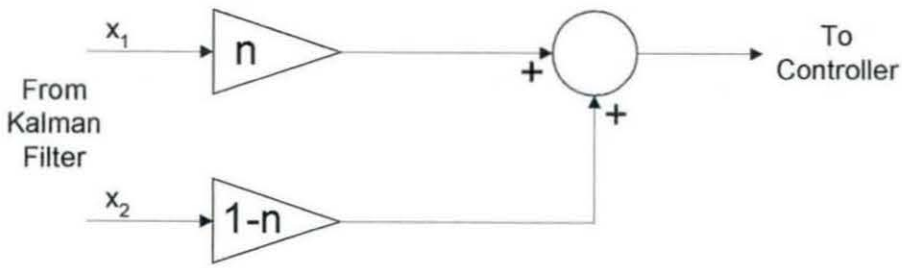
Figure 3-23. Combination of Outputs

Since the states of the model are:

$$X = \begin{bmatrix} x_1 \\ x_2 \\ \dot{x}_1 \\ \dot{x}_2 \end{bmatrix} \tag{3.21}$$

The feedback equation can be converted into a matrix, which can replace the existing Kalman filter output C matrix:

$$C = \begin{bmatrix} n & 1-n & 0 & 0 \end{bmatrix} \tag{3.22}$$

3.6.2   Results

The effects of utilising a feedback signal, which is a combination of a number of states, are shown in the frequency domain. As a comparison, Figure 3-24 shows the two extreme values, where n=1 and n=0. These are identical to the frequency response produced when the feedback is the position of the large mass (n=1) and feedback is provided by the position of the smaller mass (n=0).
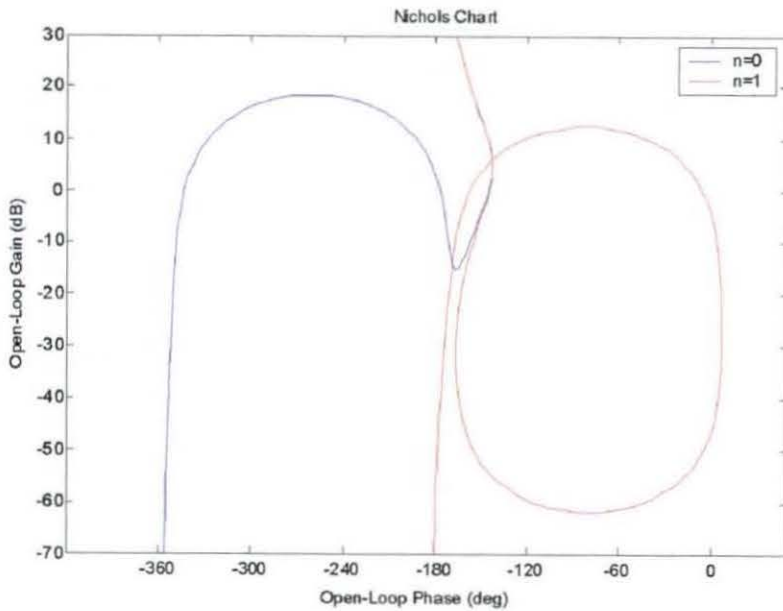
Figure 3-24. Responses for n=0 (x₂) and n=1 (x₁)

As n is increased from 0 to 1, there is a gradual progression between the two extreme responses. Figure 3-25 shows a sample of values of n, which shows this progression.
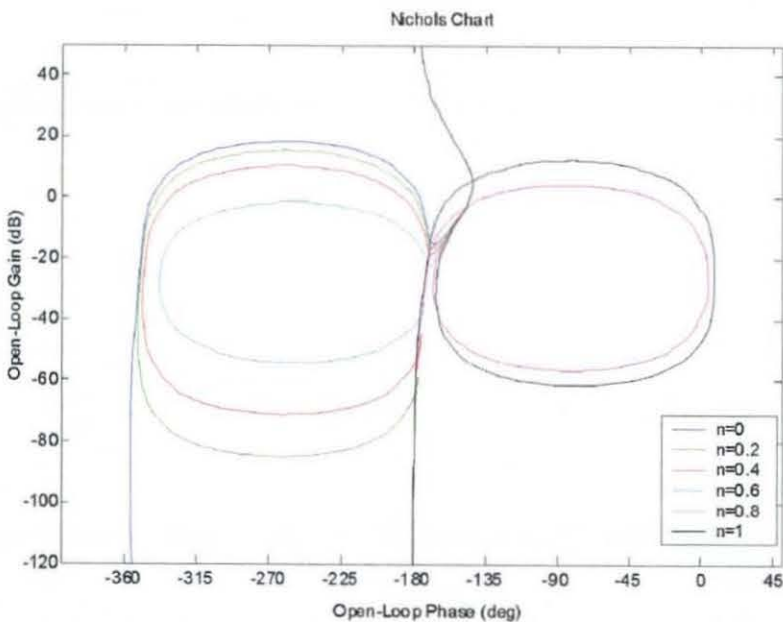
Figure 3-25. Progression from Frequency Response

Examination of Figure 3-25 shows that the phase of the response changes dramatically between n=0.6 and n=0.8. In the ideal response, the phase would be

close to $-180°$, and so the range between $n=0.6$ and $n=0.8$ needs to be examined more closely.

The point at which the flexible mode is removed from the response entirely is when $n=0.667$. This is identical to the ratio of the size of the larger mass (50kg), compared to the total of the two masses combined (75kg). Figure 3-26 compares this response to those for $n=1$ and $n=0$.
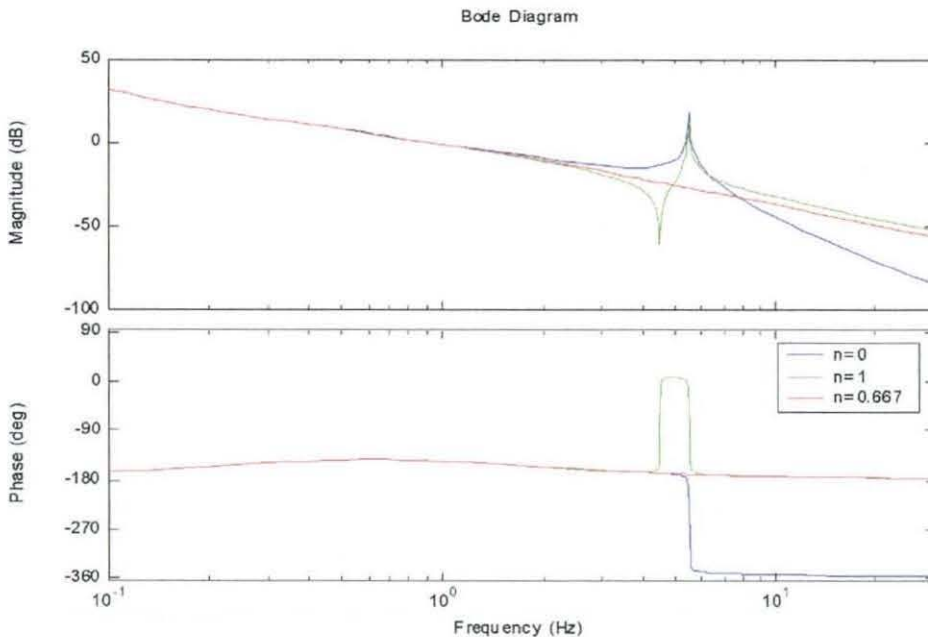
Figure 3-26. Frequency Response for n=0.667

The effects of the mode that can be seen in the other responses (e.g. Figure 3-25) has been removed, leaving the response of the system as if the smaller mass was not present. In nearly all cases (except when $n=1$) the phase margin of the system remains unchanged, the gain margin increases as n increases, until when $n=0.667$ the gain margin becomes infinite.

3.7 Summary

This section has demonstrated the use of the Kalman filter as a replacement for a notch filter in the structural coupling problem, on a basic model. The model used has a single flexible mode, at a frequency comparable to the first mode found on an aircraft.

The use of the two mass model has demonstrated that the Kalman filter can be used to replace a single notch filter, providing a stable solution. In addition it has been shown that the Kalman filter approach provides better tolerance to errors in the model, which affect the frequency of the model mode, than the notch filter solution.

Additional results have shown that the use of a linear combination of the states of the Kalman filter can be used to further improve the frequency response of the Kalman filter approach when there is coupling between the modes of the model.

4   Two Mode Assessment

This chapter discusses the second stage of work of the project, which extends the work of the previous chapter to examine a model with a second flexible mode.

4.1   Introduction

There are two main purposes to this stage of work: to develop and assess the Kalman filter approach on a more complicated model, and also to provide a framework upon which an experimental stage of the project can be based.

The model has been developed to be generally representative of an aircraft model. The material and dimensions of the beam have been chosen to give mode frequencies of similar values to the first modes of the aircraft, additionally the dimensions have been chosen to be consistent with a laboratory rig, so that a comparison between theory and experiment can be made.

4.2   Aircraft Analogy

To ensure that the beam representation that will be used is similar to the pitch loop of a simple aircraft model, a comparison can be made. Figure 4-1 shows the beam overlaid onto an aircraft (also showing the basic aircraft axes).
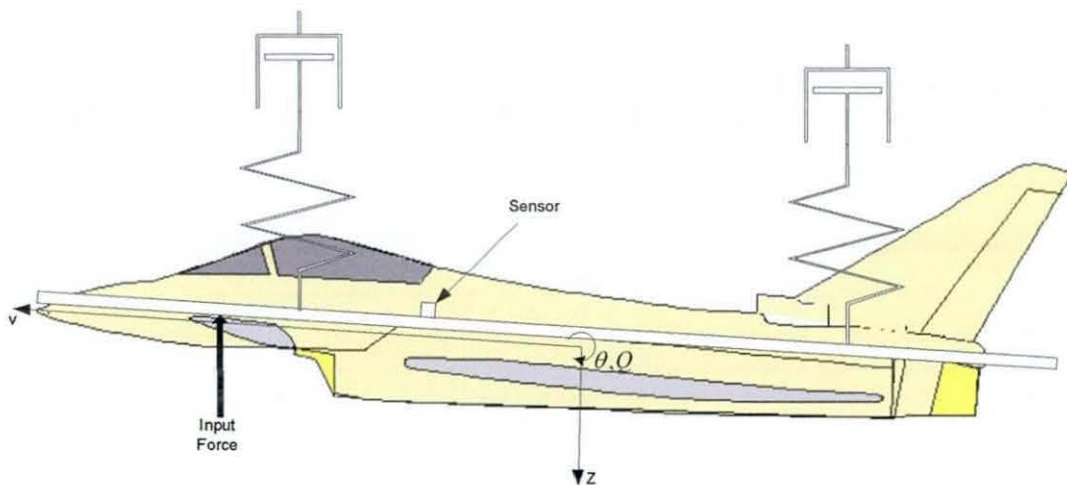
Figure 4-1. Beam – Aircraft Analogy

The aircraft pitching mode can be represented by a torsional mass-spring-damper system [Cook – 1997][28] The torsional spring-damper arrangement can in turn be represented by a pair or series arranged springs and dampers, as described in the next section For all these representations, the pitch rate to input force transfer function can be simplified to.

$$\frac{\theta}{F_\theta} = k\frac{a + bs}{c + ds + es^2}$$

Through careful parameter selection of the mechanical spring and damper, a good representation of the aerodynamic damping and stiffness can be made

4.3   Model Description

The two mode model has been based upon a free – free beam The beam is suspended upon a pair of springs and dampers (in series) These additional components provide the model with a rigid mode An angular rate gyroscope is attached to the beam, an actuator and a controller provide angular rate control of the beam Figure 4-2 shows this arrangement
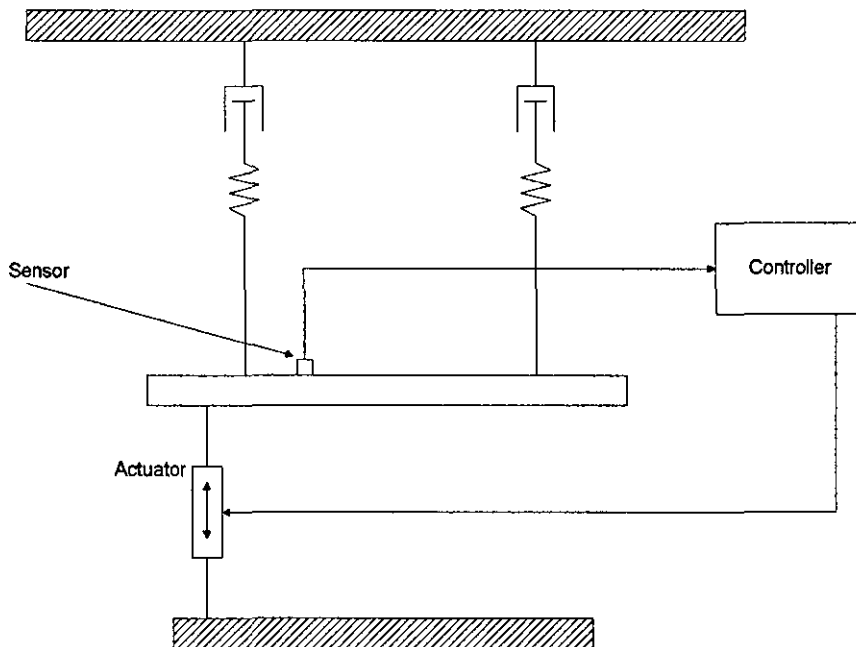
Figure 4-2. Beam Model

The positioning of the actuator and sensor has been selected to provide a comparison with the positions that the equivalent devices would be found on a modern aircraft (sensor placed behind the cockpit, with canards providing primary pitch control)

4 3 1 Assumptions

This stage of the work has made a number of assumptions about the model, these are

    a) The system process noise is negligible

    b) There is no coupling between each mode

4 3 2 Model Parameters

The model has been designed with the following parameters

Length	3 1m
Width	0 1m
Depth	0 01m
Density	2700kgm^{-3} (Aluminium)
Mass	8 37kg
Spring Constant	3000Nm^{-1}
Damping Constant	167Nsm^{-1}
Springs spacing	0 775m (from centre of beam)
Sensor position	0 3875m (from centre of beam)
Actuator position	1 1625m (from centre of beam)

The dimensions of the beam have been selected to produce flexible modes at about 5Hz and 15 0Hz The spring and damper parameters have been selected to provide a highly damped rigid mode at about 3 5Hz

4.4 System Model

The beam model consists of two main components, the rigid mode of the beam, and the flexible modes

4.4 1 Rigid Model

In order to provide pitch information, either a single angular position, or two linear positions must be provided. Two linear positions have been selected, since this allows easy calculation of both linear and angular measurements The states selected are the vertical position and velocity of the beam at the points where the springs are connected
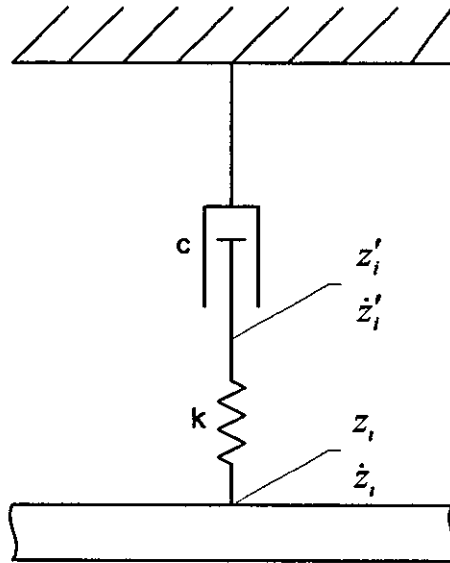
Figure 4-3. Rigid Model States

The force in the spring is

$$F_k = k(z' - z)$$

(4 1)

The force in the damper is.

$$F_c = cz'$$

(4 2)

Since $F_c = -F_k$, substitution and rearrangement gives

$$\dot{z}' = \frac{k}{c}(z - z')$$

(4 3)

The acceleration $\ddot{z}$ can be easily calculated from F_k, the beam mass m, and the force (f) applied to the beam at the spring

$$\ddot{z} = \frac{k}{m}(z' - z) + \frac{f}{m}$$

(4 4)

The state vector is

$$X_i = \begin{bmatrix} z_i \\ \dot{z}_i \\ z_i' \end{bmatrix}$$

(4 5)

Equations (4 3) and (4 4) provide the A and B matrices for the state space model

$$A_i = \begin{bmatrix} 0 & 1 & 0 \\ -\dfrac{k}{m} & 0 & \dfrac{k}{m} \\ -\dfrac{k}{c} & 0 & \dfrac{k}{c} \end{bmatrix} \quad B_i = \begin{bmatrix} 0 \\ \dfrac{a_i}{m} \\ 0 \end{bmatrix}$$

(4 6)

Where a_i is a scaling factor, accounting for the actuator offset from the point of interest This factor can be calculated by taking moments about each of the spring – beam joints (shown as A and B in Figure 4-4) and the centre of gravity (marked COG in Figure 4-4)
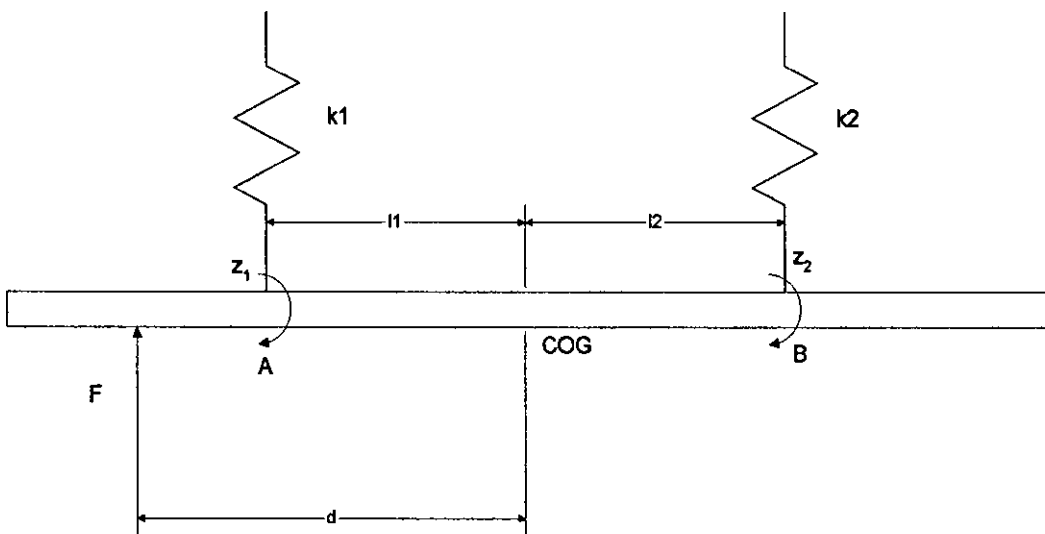
Figure 4-4. Moments on Beam

Assuming steady state conditions, if we take moments about each of A, B, and COG:

Moments about A:

$$F \cdot (d - l1) + z2 \cdot k2 \cdot (l1 + l2) = 0 \qquad (4\ 7)$$

Moments about B

$$F \cdot (d + l2) + z1 \cdot k1 \cdot (l1 + l2) = 0 \qquad (4\ 8)$$

Moments about COG:

$$F \cdot d + z1 \cdot k1 \cdot l1 + z2 \cdot k2 \cdot l2 = 0 \qquad (4\ 9)$$

Rearranging (4 6) in terms of x_1 gives:

$$z1 = \frac{F \cdot (d + l2)}{k2 \cdot (l1 + l2)} \qquad (4\ 10)$$

Rearranging (4 5) in terms of x_2 gives:

$$z2 = \frac{F \cdot (d - l1)}{k1 \cdot (l1 + l2)} \qquad (4.11)$$

If we now substitute the dimensions contained in the specification at the beginning of this section, into equations (4 10) and (4 11) will give us z_1 and z_2 The vertical displacement of the beam at each spring for the force F (when F equals 1N) will be

$$z_1 = 0\ 417mm$$
$$z_2 = -0\ 083mm$$

These values can be checked by substitution into equation (4.9)   In addition multiplying these displacements by the spring constants will provide the resultant force of each spring on the beam   These values are the a_i terms contained in the state space B-matrix

$$k_1 \cdot z_1 = 3000 \cdot 0\ 417 \cdot 10^{-3} = 1\ 25N$$
$$k_2 \cdot z_2 = 3000 \cdot -0\ 083 \cdot 10^{-3} = -0\ 25N$$

Since there are two springs on the beam, and two points are required to provide rotational information, the model requires the matrices developed in equations (4 5) and (4 6) for each spring, i e .

$$A_r = \begin{bmatrix} A_1 & [0] \\ [0] & A_2 \end{bmatrix} \quad B_r = \begin{bmatrix} B_1 \\ B_2 \end{bmatrix} \quad X_r = \begin{bmatrix} X_1 \\ X_2 \end{bmatrix} \tag{4.12}$$

The required output from the model is the angular velocity of the beam   This is produced from the beam velocity, and uses the relationship $\theta = \sin\theta$ for small values of θ

The angular velocity is the difference between the beam velocity components divided by the distance between them

$$\theta = \frac{(\dot{z}_1 - \dot{z}_2)}{0\ 5l} \tag{4 13}$$

This converts to state space form as:

$$C_r = \begin{bmatrix} 0 & \dfrac{2}{l} & 0 & 0 & -\dfrac{2}{l} & 0 \end{bmatrix} \quad D_r = [0]$$

4 4 2   Flexible Modes

This section describes the formulation of the flexible modes   The model has been developed using information contained in [Bishop, Johnson – 1960][12].   A brief description is given below

The differential equation of motion takes the following form

$$\frac{\partial^2 z}{\partial t^2} + \frac{EI}{A\rho} \cdot \frac{\partial^4 z}{\partial x^4} = 0 \tag{4 14}$$

The general solution of this (for a system harmonically excited by frequency ω) is:

$$z = X(x)e^{i\omega t} \tag{4 15}$$

When equation (4 15) is substituted in to equation (4 14), we get an ordinary differential equation

$$\frac{d^4 X}{dx^4} - \lambda^4 X = 0 \qquad (4\ 16)$$

where λ_r is

$$\lambda_r^4 = \frac{\omega_r^2 A \rho}{EI} \qquad (4\ 17)$$

whe solution of this can be written in the following form (for a harmonic force F, with frequency ω)

$$z = \alpha_{xh} F \qquad (4\ 18)$$

where the receptance α_{xh} (where x is the position of the force applied to the beam and h is the position of the sensor on the beam), is

$$\alpha_{xh} = \sum_{r=1}^{\infty} \frac{\Phi_r(x) \cdot \Phi_r(h)}{a_r(\omega_r^2 - \omega^2)} \qquad (4\ 19)$$

$$a_r = A \rho \, l = m \qquad (4\ 20)$$

Here ω_r is the frequency of the rth mode, and $\Phi_r(x)$ is the rth characteristic function of the beam, which in the case of the free-free beam is.

$$\Phi_r(x) = \cosh(\lambda_r x) - \cos(\lambda_r x) - \sigma_r(\sinh(\lambda_r x) - \sin(\lambda_r x))$$
$$\sigma_r = \frac{\cosh(\lambda_r l) - \cos(\lambda_r l)}{\sinh(\lambda_r l) - \sin(\lambda_r l)} \qquad (4\ 21)$$

where λ_r can be calculated from the general solution of (4 16)

$$\cos \lambda_r l \cdot \cosh \lambda_r l = 0 \qquad (4\ 22)$$

the first 4 values of $\lambda_r l$ are.

$$\lambda_1 l = 4\ 730, \quad \lambda_2 l = 7\ 853, \quad \lambda_3 l = 10\ 996, \quad \lambda_4 l = 14\ 137$$

If we add structural damping to (4.19) we obtain

$$\alpha_{xh} = \sum_{r=1}^{\infty} \frac{\Phi_r(x) \cdot \Phi_r(h)}{m(\omega_r^2 + 2\zeta\omega_r(j\omega) + (j\omega)^2)} \tag{4 23}$$

selecting generalised co-ordinates such that

$$z_r = q_r \Phi_r(h) \tag{4 24}$$

$$\theta_r = q_r \Phi_r'(h) \tag{4.25}$$

where z_r is the vertical displacement caused by the rth mode, and θ_r is the angular displacement caused by the rth mode.

substitution of (4 18) into (4 23) and rearrangement gives

$$q = \frac{\alpha_{xh} F}{\Phi_r(h)}$$

$$= \frac{\Phi_r(x)}{m(\omega_r^2 + 2\zeta\omega_r(j\omega) + (j\omega)^2)} \tag{4 26}$$

substituting s for $j\omega$ we get

$$q = \frac{\Phi_r(x)}{m(\omega_r^2 + 2\zeta\omega_r s + s^2)}$$

$$q(\omega_r^2 + 2\zeta\omega_r s + s^2) = \frac{\Phi_r(x)}{m} \tag{4 27}$$

$$\omega_r^2 q + 2\zeta\omega_r \dot{q} + \ddot{q} = \frac{\Phi_r(x)}{m}$$

substitution and rearrangement gives the following

$$\dot{q}_r = \frac{\Phi_r(x)}{m} F - \omega_r^2 q_r - 2\zeta \omega_r \dot{q}_r$$

$$\ddot{z}_r = -\Phi_r(h)\omega_r^2 q_r - 2\Phi_r(h)\zeta \omega_r \dot{q}_r + \frac{\Phi_r(h)\Phi_r(x)}{m} F \tag{4 28}$$

where z_r is the rth mode deflection at the point specified by h. With the states selected as

$$X = \begin{bmatrix} q_n \\ \dot{q}_n \end{bmatrix}$$

These can be written in state space form as

$$A_{fr} = \begin{bmatrix} 0 & 1 \\ -\omega_n^2 & -2\varsigma \, \omega_n \end{bmatrix}, \quad B_{fr} = \begin{bmatrix} 0 \\ \dfrac{\Phi_n(x)}{m} \end{bmatrix}$$

$$C_{fr} = \begin{bmatrix} -\Phi_n(h)\omega_n^2 & -2\varsigma \, \Phi_n(h)\omega_n \end{bmatrix} \quad D_{fr} = \begin{bmatrix} \dfrac{\Phi_n(x) \cdot \Phi_n(h)}{m} \end{bmatrix}$$

(4 29)

Alternatively, if the angular rate is required

$$\dot{\theta}_r = \Phi_r'(h)\dot{q}_r$$

(4 30)

Providing the following state space output equation.

$$C_{fr} = \begin{bmatrix} 0 & \Phi_n' \end{bmatrix} \quad D_{fr} = 0$$

From this basis, any number of modes can be accommodated within the model, simply by replicating the equations above for each required mode, e g for two flexible modes (with angular rate output) the equations would become

$$A_f = \begin{bmatrix} A_{f1} & 0 \\ 0 & A_{f2} \end{bmatrix}, \quad B_f = \begin{bmatrix} B_{f1} \\ B_{f2} \end{bmatrix}$$

$$C_f = \begin{bmatrix} C_{f1} & C_{f2} \end{bmatrix} \quad D_f = \begin{bmatrix} 0 \end{bmatrix}$$

(4 31)

4 4 3   Complete Model

To obtain the complete model, the components for the rigid and the flexible modes (equations (4 12) and (4 31)) are combined   Since it has been assumed that there is no coupling between the modes, the off diagonal terms are zero

$$A = \begin{bmatrix} A_r & [0] \\ [0] & A_f \end{bmatrix}, \quad B = \begin{bmatrix} B_r \\ B_f \end{bmatrix}, \quad C = \begin{bmatrix} C_r & C_f \end{bmatrix}, \quad D = \begin{bmatrix} D_r + D_f \end{bmatrix}$$

(4 32)

From this we have a state vector containing 10 states – 6 rigid states and 4 flexible mode states   The model has been used in Simulink, and the full diagrams for the model are included in Appendix D

The open loop frequency response of the beam is shown in Figure 4-5   From the Bode plot the two flexible modes can clearly be seen by the magnitude peaks and the

180° phase changes   The rigid mode can also be seen, shown by the slight changes in gain and phase around the 3Hz point
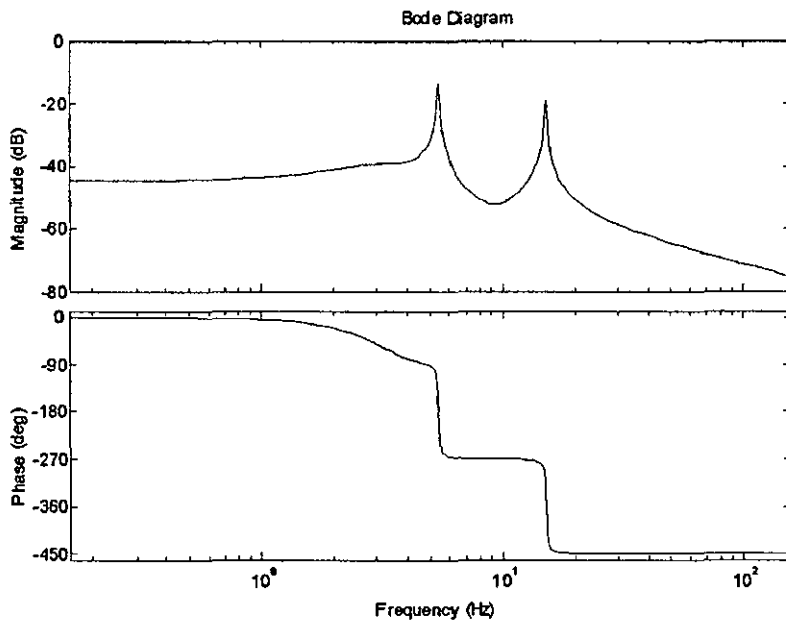
Figure 4-5. Uncontrolled Open Loop Frequency Response of Beam Model

4.5 System Controller

Whilst this system is stable (open loop), the performance of the system is not as good as is desired (i e steady state errors, system bandwidth, etc)   It is therefore necessary to add some form of controller to the system to improve the response

The controller has been designed to control the rigid beam   During the design process, the flexible modes of the beam are removed   This is a similar approach to that used in the design of the control laws for an aircraft

The controller uses a proportional gain, combined with an integral stage and a phase advance stage to produce an improved closed loop response   The gain is set at 7Nm/rad, the integral component has $T_i=0 005$, and the phase advance stage has $T_d=0 01$ and $k=2$ These parameters combine to produce a closed loop system bandwidth of 3Hz

The transfer function for this controller is

$$7 \cdot \frac{0\,005s+1}{0\,005} \cdot \frac{0\,02s+1}{0\,01s+1}$$

Figure 4-6 shows the time domain response of the rigid beam to a 0 01 rad/s demand at t=0s followed by a –0 02 rad/s demand at t=5s As can be seen the response is stable.
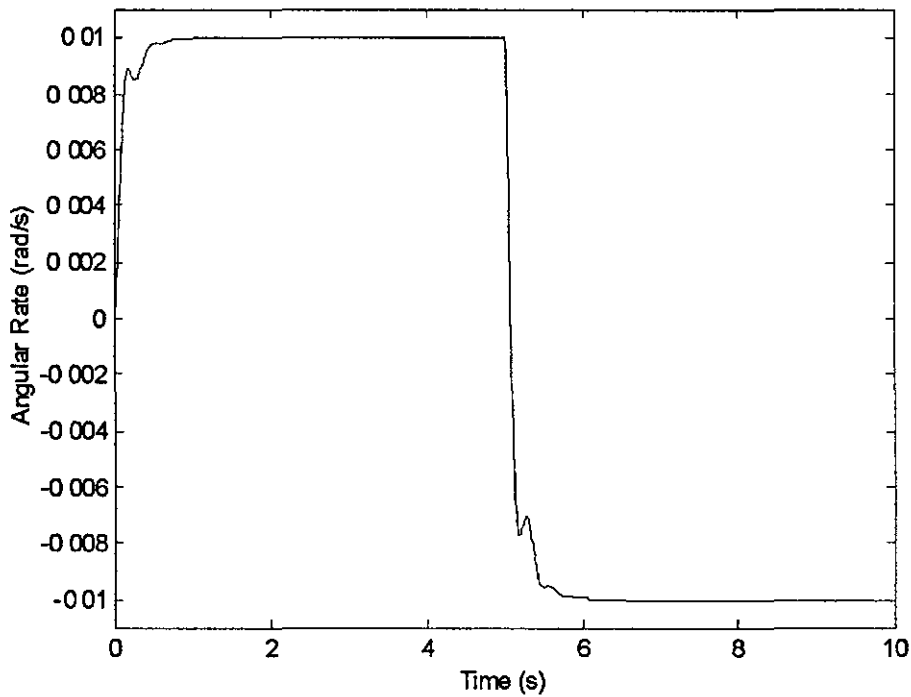
Figure 4-6. Rigid Beam Response (with Controller)

With the controller in the system, the frequency response of the system, with the controller demand as the input and the sensor signal as the output, is:
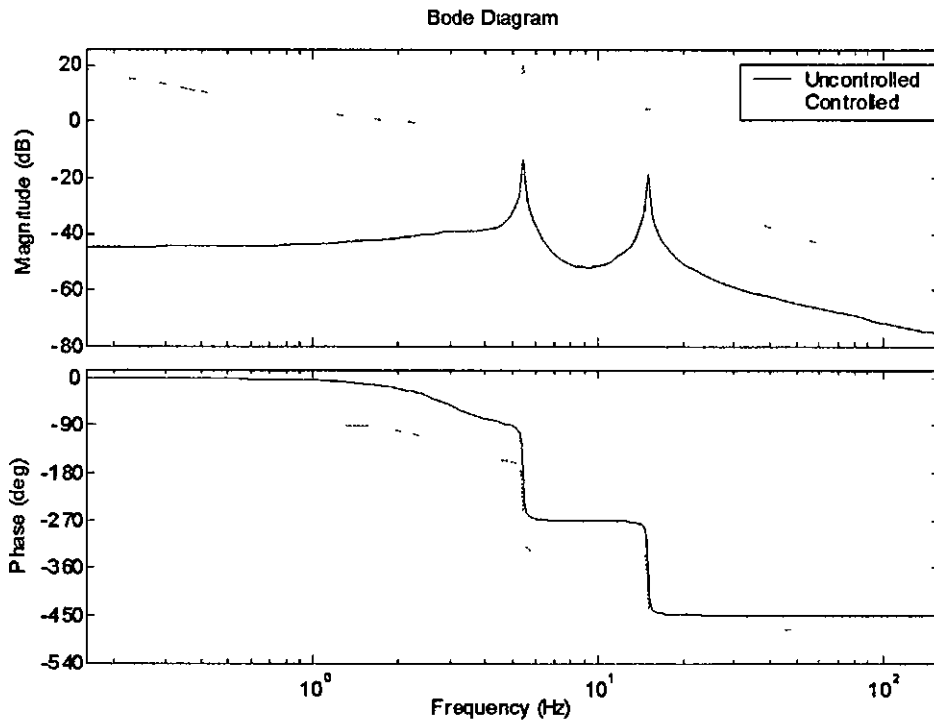
Figure 4-7. Frequency Response of Controlled Beam

As can be seen from Figure 4-7, the controller has added a significant amount of gain across all frequencies, which improves the overall rate of response The integrator has added low frequency (d c) gain, which reduces the steady state errors, however this is at the cost of 90° of additional phase lag The phase advance section of the controller compensates for this around the frequencies of the flexible modes

4 5 1   Actuator Model

In order to provide a more realistic model, a model of an actuator has been used This model has been supplied by BAE Systems, and is comparable to the type of actuator model that they use when modelling aircraft systems The equation of this model is

$$\frac{s^2 - 575s + 243000}{s^2 + 197s + 12073} \cdot \frac{-0\ 0486s^2 + 27\ 5s + 1052}{s^2 + 526\ 6s + 20364}$$

The frequency response of this actuator is shown in Figure 4-8
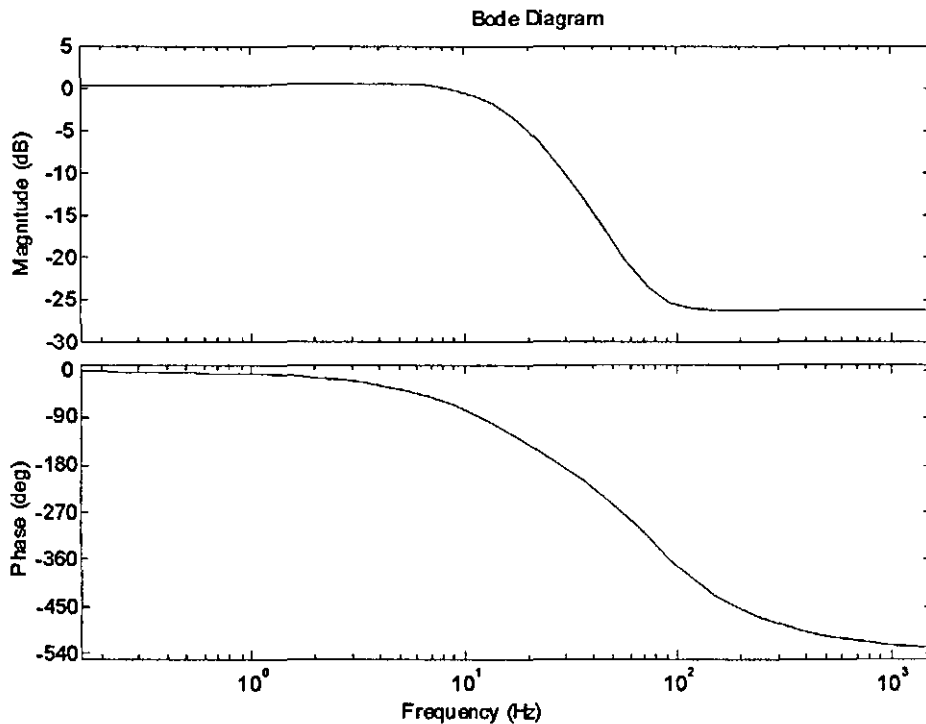
Figure 4-8. Frequency Response of Actuator

4 5 2 Sensor Modelling

The model does provide for sensor noise, in the form of white noise that is added to the sensor output from the model For a sensor output of 0 01rad/s, noise power equal to 1×10^{-9} provides a noise level approximately 1% of the peak sensor reading

4.6 Notch Filters

Whilst the rigid closed loop system (model of beam and controller) is stable, problems arise when the flexible modes are added into the system As is shown in Figure 4-9, whilst the response passes beneath the 0dB −180° point (a key indicator of stability, as discussed in Chapter 2 Section 4), the stability margins are very small As was discussed in Chapter 2, in order to clear an aircraft for flight specified stability margins must be met

It can also be seen from the response that the second flexible mode crosses the 0dB line at a phase of −540°, which is the point at which the second set of stability margins exist This will also need correcting
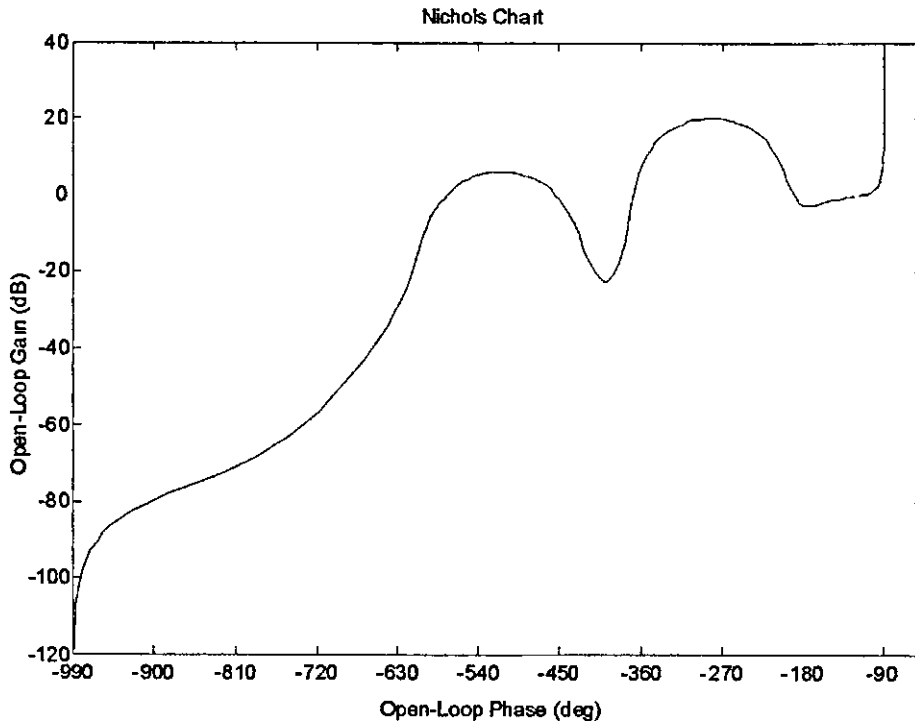
Figure 4-9 - Frequency Response of Unfiltered System

In order to improve the stability margins of the system around the flexible modes, the traditional approach of using notch filters has been used   In this instance the notch filters used have been based upon the following form

$$F(s) = \frac{s^2 + s\omega\zeta_n + \omega^2}{s^2 + s\omega\zeta_d + \omega^2}$$

Where ω is the notch frequency (rads^{-1}), ζ_n is the numerator damping, and ζ_d is the denominator damping

In this model, two notch filters have been used   Although only one filter is required to ensure that the frequency response is below the 0dB −180° point, the second filter attenuates the system to ensure that clearance is achieved at the 0dB −540° point Table 4-1 shows the parameters used in the filters.

	Filter 1	Filter 2
ω	34 2	94 3
ζ_n	0 005	0 004
ζ_d	0 1	0 1

Table 4-1. Notch Filter Parameters

The frequency response for each of these filters is shown in Figure 4-10. The solid line shows filter 1 and the dotted line shows the response for filter 2 As can be expected from the filter parameters, the two filters are of very similar bandwidth and attenuation
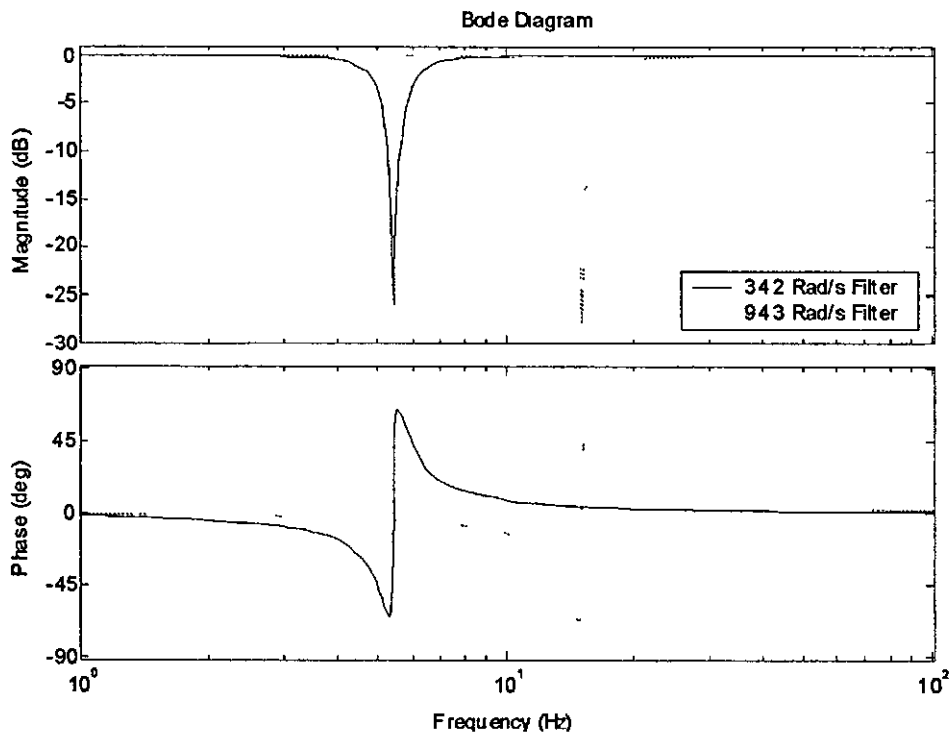
Figure 4-10. Bode Diagram of Beam Model Notch Filters

The effects of these notch filters on the system can be seen from the frequency response shown in Figure 4-11.
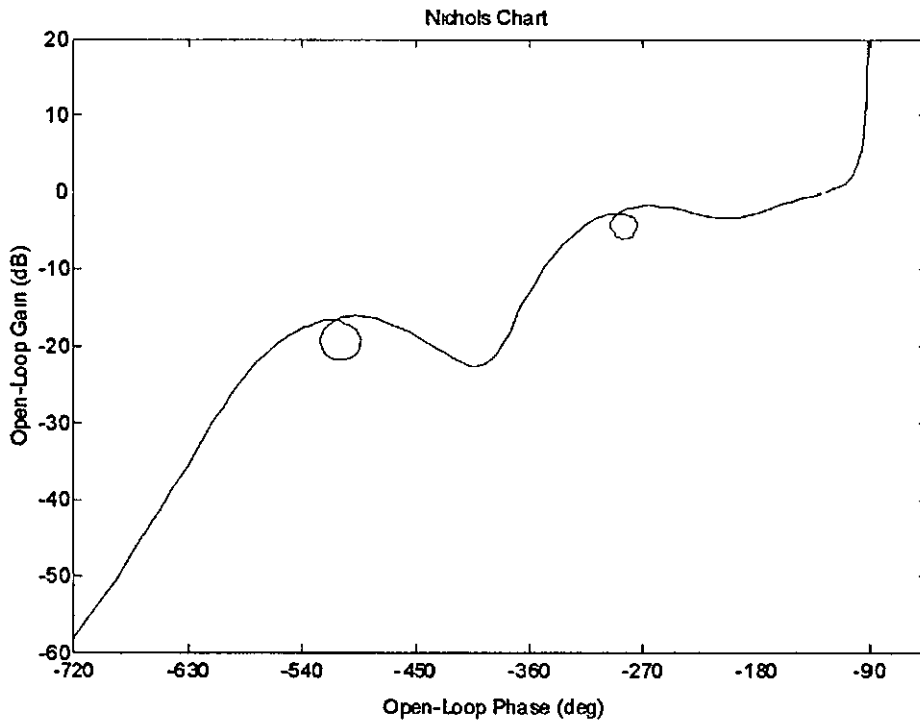
Figure 4-11. Frequency Response of Notch Filtered System

The notch filters have successfully reduced the gain of the flexible modes, and have stabilised the frequency response However, this is not without cost, the notch filters have each added a small amount of phase lag into the system, which reduces the rigid mode stability margins

On a model such as this, where only two notch filters are required, this is not a big problem, but on a more complicated system, where more filters are required, the problem is much more significant.

4.7 Kalman Filter

The Kalman filter has been designed to provide an estimation of the angular rate of the rigid beam. The inputs to the Kalman filter are the controller output and the sensor output

The model used in the Kalman filter is almost identical to that of the beam itself In order to reduce the size, and hence the processing requirements of the Kalman filter, the rigid modes have been minimized using the Matlab command 'minreal' This reduces each rigid mode from 3 to 2 states, and the entire model from 10 to 8 states.

As can be seen from Figure 4-12 there is no noticeable difference between the two models.
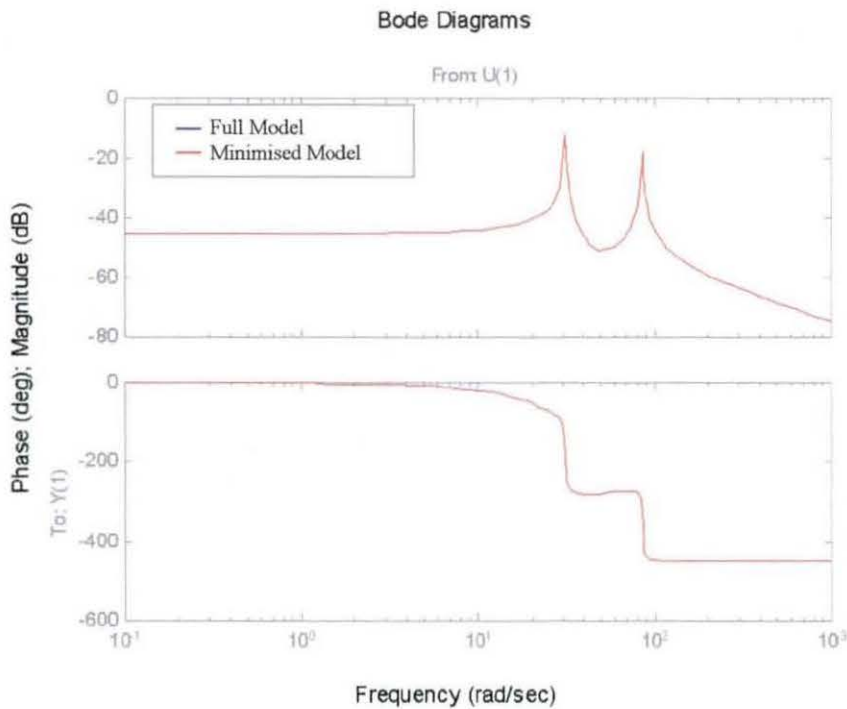
Figure 4-12. Comparison between Full and Minimalised models

Removing the flexible components from the C matrix provides the estimated output. This gives a new output matrix C_{out}, which provides the rigid estimate of the system:

$$C_{out} = \begin{bmatrix} C_r & [0] \end{bmatrix}$$

4.7.1 Filter Parameters

The uncertainty values Q and R used in the generation of the Kalman gain matrix have been selected based upon information in the model. R has been selected to be equal to the variance of the sensor noise (noise power $= 1\times10^{-9}$), and Q has been selected as the variance of the states of the Kalman filter in (open loop) response to a step input. These values are:

$$R = 1.0 \times 10^{-7}$$

The diagonal components of the Q matrix are:

$$
\begin{bmatrix}
5.0440 \times 10^{-4} \\
3.7758 \times 10^{-4} \\
2.7377 \times 10^{-5} \\
1.5922 \times 10^{-5} \\
2.4900 \times 10^{+0} \\
2.9509 \times 10^{-4} \\
9.9605 \times 10^{-2} \\
1.1805 \times 10^{-5}
\end{bmatrix}
$$

4.7.2   Kalman Filter Gain Matrix

Using the parameters given in the previous section, the Kalman filter gain matrix, calculated using the Matlab function 'Kalman', is:

$$
K =
\begin{bmatrix}
5.6634 \times 10^{+1} \\
-1.1151 \times 10^{+3} \\
-1.4705 \times 10^{+1} \\
-1.3359 \times 10^{+2} \\
-3.3078 \times 10^{+3} \\
8.8344 \times 10^{+1} \\
1.3232 \times 10^{+2} \\
-3.5340 \times 10^{+0}
\end{bmatrix}
$$

4.7.3   Frequency Response

With the Kalman filter designed as set out above, and added to the model in place of the notch filters, the model has the frequency response shown in Figure 4-13.

As can be seen from the response, the Kalman filter removes the effects of the flexible modes from the system, leaving only the rigid mode.
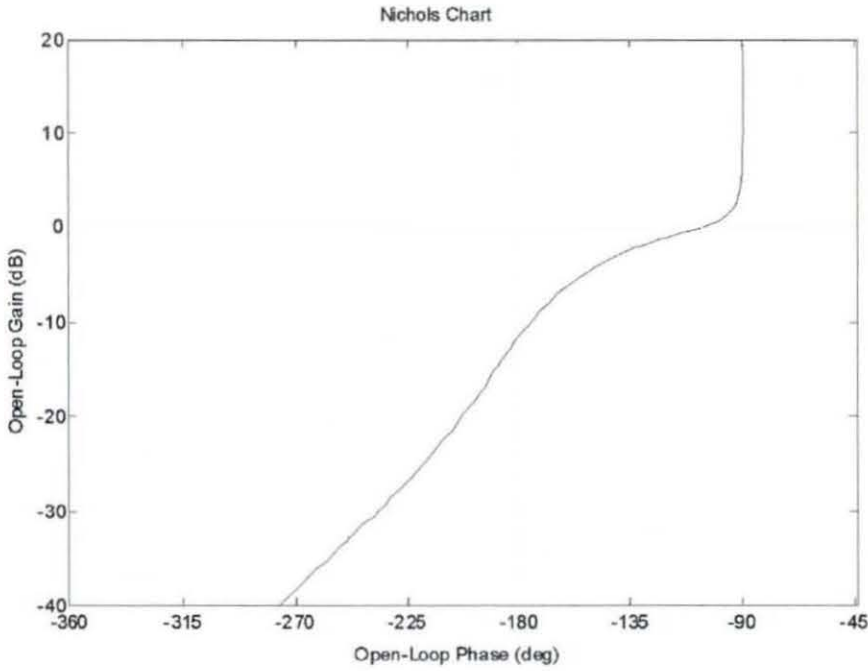
Figure 4-13. Frequency Response of Beam Model with Kalman Filter

4.8 Comparison of Filters

In order to assess the effectiveness of the Kalman filter as a replacement for the notch filters, the frequency responses of the different filters need to be compared on the same chart. Figure 4-14 shows the three different filtering options.
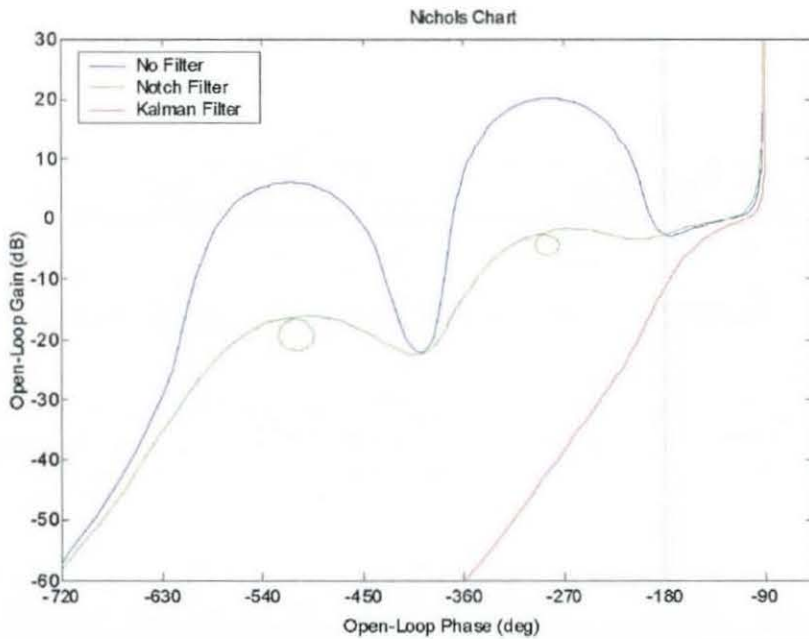
Figure 4-14. Frequency Response of Different Filters

As can be seen, the Notch filters introduce a small amount of phase lag compared to the unfiltered response   The Kalman filter provides a significant improvement, and the phase of the system is lower than the unfiltered response

4 8 1   Kalman Filter Phase Lead

As was highlighted in the previous section, the phase of the Kalman filtered system is lower than the unfiltered system This suggests that the Kalman filter adds phase lead to the system, which could be undesirable.
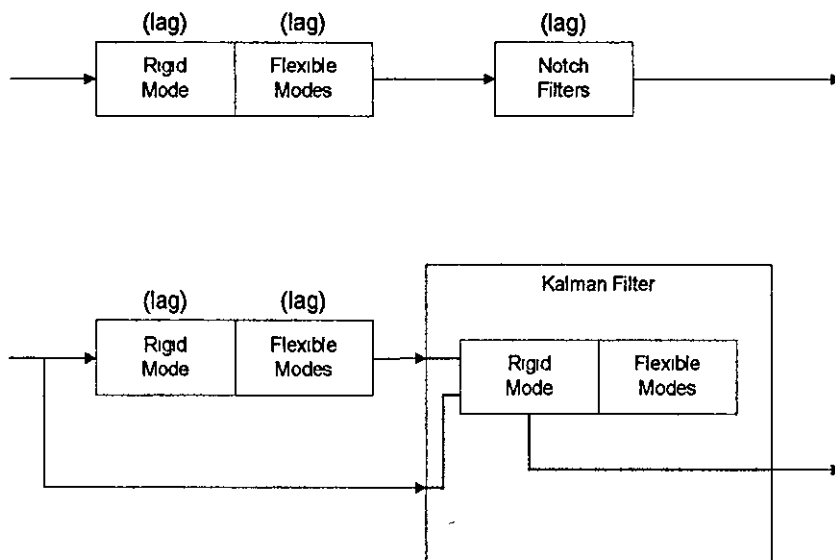
Figure 4-15. Phase Lag Differences between Filters

A comparison of the different techniques shows that the filtered signal, which is fed back to the controller, is developed in significantly different ways   The notch filter method takes the sensor output, and filters out the undesired frequencies   The Kalman filter approach uses the sensor signal and the controller output to produce an estimate of the rigid portion of the sensor signal

As can be seen in Figure 4-15, the notch filter technique produces an output where the phase lag of the system is the sum of the lag introduced by the rigid mode, the flexible

modes, and the notch filters   The Kalman filter output does not use the flexible modes, and hence the phase lag of the system is only that of the rigid mode
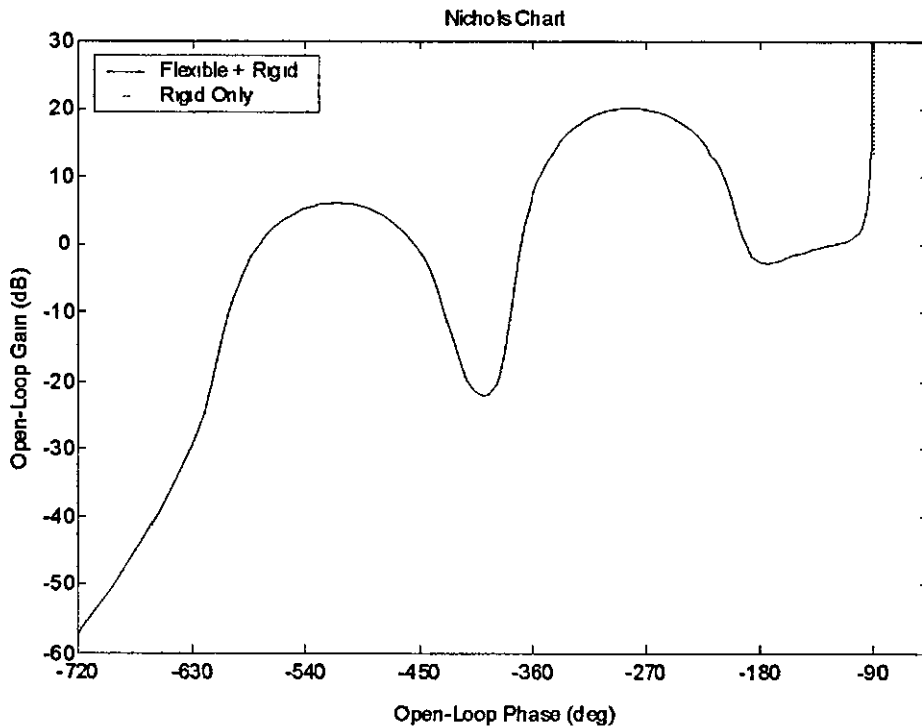
Figure 4-16. Comparison between Rigid and Flexible Models

Figure 4-16 shows the frequency responses for the rigid mode only, and the combination of the flexible and rigid modes   As described above, the rigid mode has less phase lag, and this is reflected in the output of the Kalman filter

4.9   Model improvements

In order to provide a more representative comparison with an aircraft model, some enhancements can be added to the system   These bring the frequency response of the rigid beam much closer to what could be expected from the rigid aircraft; this allows a much fairer comparison between the notch filter and the Kalman filter

4 9 1   Rigid mode compensation

The rigid mode of the beam as used in the previous chapter had quite large stability margins, which would not be seen on an aircraft   This results in much larger phase

margin available for the design of the notch filters, which can lead to an inappropriate design of notch filter

In order to more closely match the beam rigid mode to what would be expected on an aircraft, an additional filter can be added into the system. Figure 4-17 shows the frequency response of the rigid beam, including the exclusion regions used in the aerospace industry, which were discussed in Chapter 2

As can be seen, the response provides 60° of phase margin, which is significantly larger than the 35° that could be expected from an aircraft
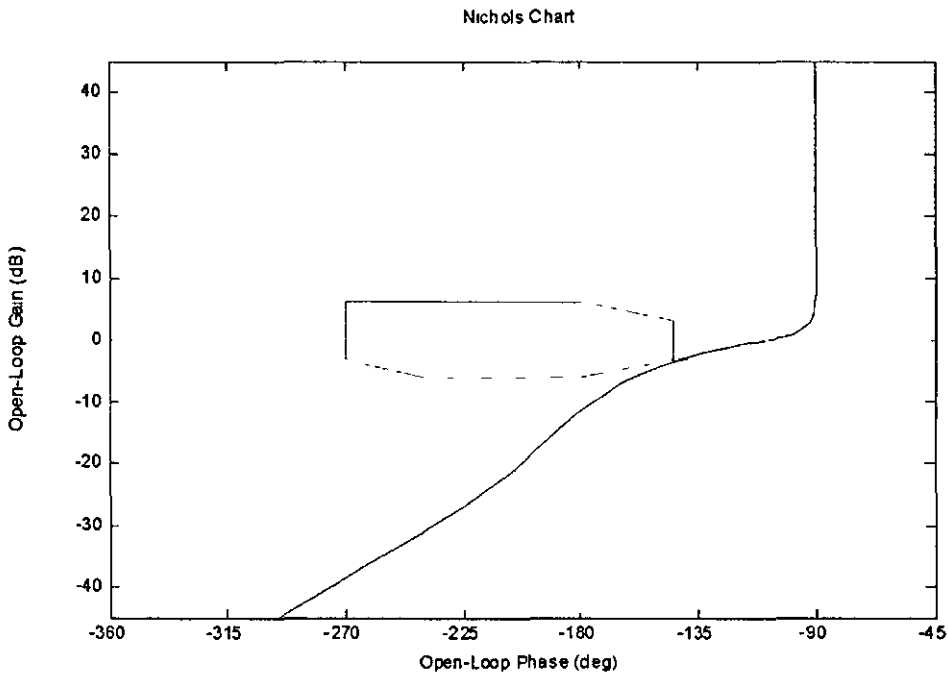
Figure 4-17. Frequency Response of Rigid Beam

More realistic stability margins can be achieved by adding a simple filter that decreases the phase margin at the −180° point, and slightly increases the gain margin at the same point. The following filter has been used to achieve this

$$C(s) = 2.5 \cdot \frac{1 + 0.0675s}{1 + 0.387s}$$

This is inserted into the beam model (between the actuator dynamics and the beam state space model) Figure 4-18 shows the frequency response of the rigid model after the filter has been added

Nichols Chart
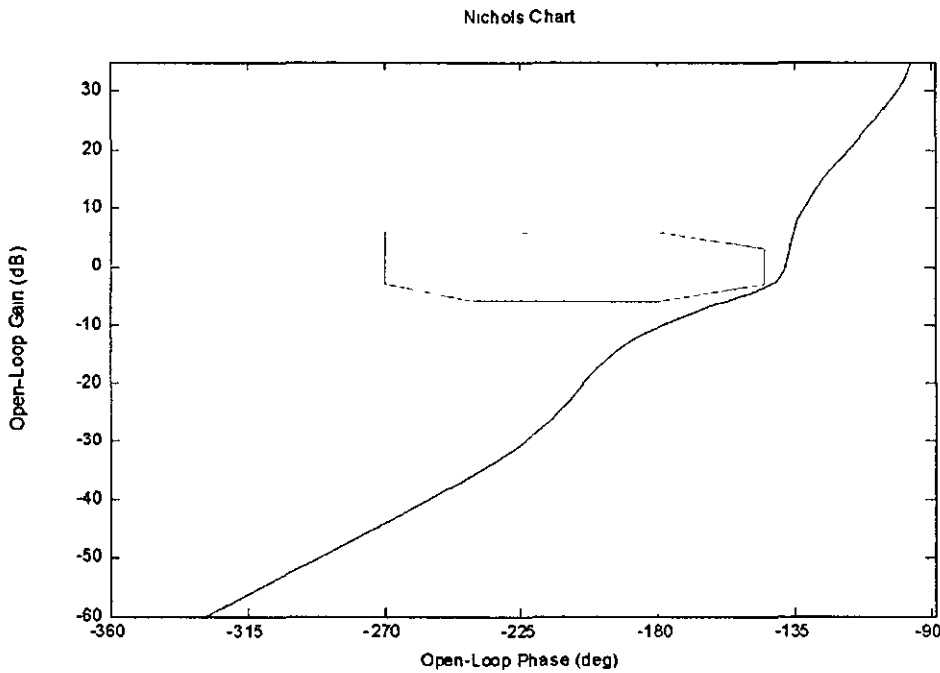
Figure 4-18. Frequency Response of Compensated Rigid Model

The filter has pulled the frequency response much closer to the exclusion region This will ensure that the frequency response of the beam is a better representation of an aircraft, and so a much more representative comparison between the notch and Kalman filter solutions can be undertaken

4 9 2   Modelling frequency changes

The beam model can be readily adapted to examine the effects of changes in the frequencies of the flexible modes   Changing the stiffness (Youngs' Modulus) of the beam by ±15% will alter the flexible modes of the beam by ±7 5%.

4 9 3   Disturbance force

A further expansion of the assessment of the Kalman filter is to see the effect of un-modelled forces acting on the beam, for example to represent a gust of wind acting on

an aircraft   The disturbance can be modelled by adding an additional input component to the beam model, this will not be modelled in the Kalman filter

4 9 4   Improvements to Kalman filter

The parameters of the Kalman filter used in the previous chapter were an initial estimate, which, whilst it does work, may not necessarily be the best solution   When the model and filter are identical, the only difference between the estimated output and the actual sensor reading is the noise on the sensor   When errors are introduced into the model, this will provide a basis from which the Kalman filter can be tuned

4.10 Initial Filter Robustness

When the structural coupling problem is under assessment as part of the FCS design process, the designer needs to take into account variations in the frequencies of the flexible modes   These modes are altered by a number of different factors, including the amount of fuel carried, and the stores carried on the aircraft   The frequency response also changes according to altitude of flight

With the beam model, a simple method to altering the frequencies of the flexible modes is to vary the stiffness (or Youngs Modulus) of the beam   The flexible frequencies of the beam are related to the stiffness of the beam by a factor of a half, a 15% change in stiffness will result in a 7 5% change in flexible mode frequencies

The frequency domain analysis looks at the open loop stability margins of the system with each filter providing the feedback for the controller, and how these margins compare to the aircraft exclusion regions. For the purposes of the frequency analysis, the input to the system is the controller demand, and the output is the estimation provided by the filter

For each filter, the frequency responses for the nominal mode frequency, as well as ±15% mode frequency change, have been shown   These 3 plots will show the range over which the response changes. Figure 4-19 shows the notch filter response, and Figure 4-20 shows the frequency responses of the Kalman filter
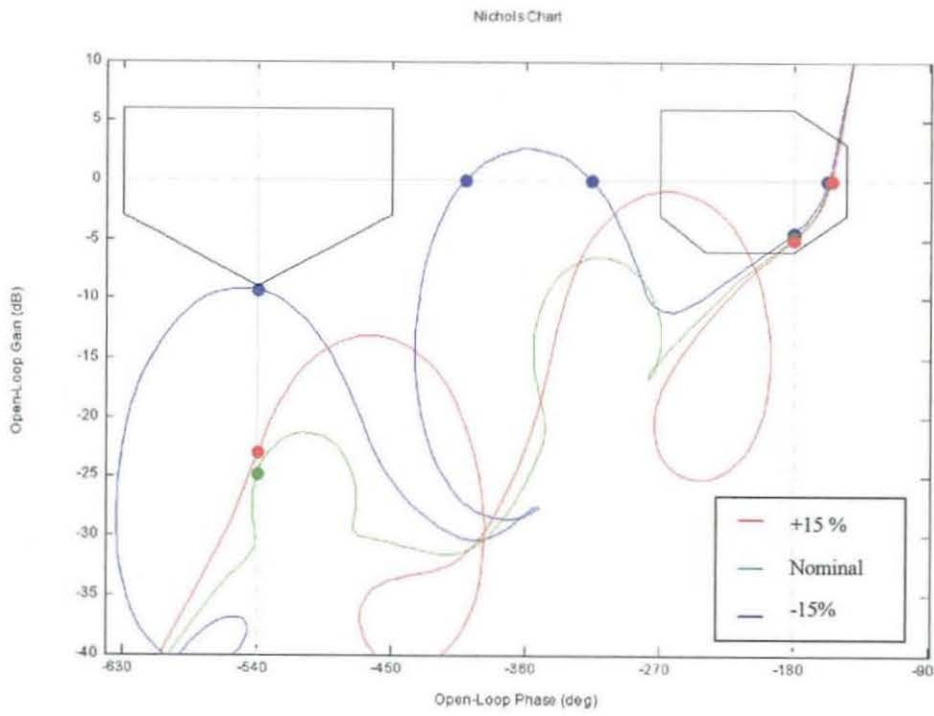
Figure 4-19. Notch Filter Frequency Responses
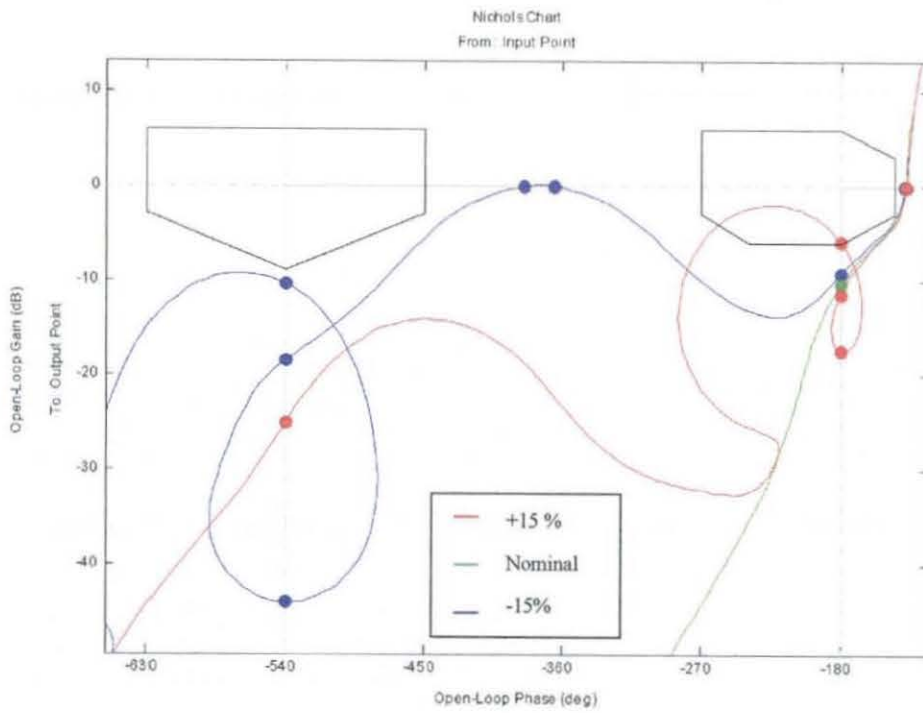
Figure 4-20. Kalman Filter Frequency Responses

When the model frequencies are lower than the notch filter is expecting, the response of the system remains clear of the exclusion region (except for the encroachment caused by the phase lag of the notch filters) However when the model frequencies are larger than the filter expects, there is encroachment into the first exclusion region

When the errors in the model result in lower than expected frequencies, the Kalman filter approach performs slightly better than the notch filter approach, with marginally higher gain and phase margins When the frequencies are higher than expected, like the notch filter approach there is an encroachment into the exclusion region This encroachment is slightly more significant than with notch filter, the encroachment results in a significant reduction in gain margin, and a larger proportion of the exclusion region is enclosed

4.11 Kalman Filter Tuning

The Kalman filter used in the previous section was based upon the variance of the states of the model in response to a step input Whilst the solution provided does work, it does not mean that it provides the ideal solution. Adjustments to each of the individual parameters of the Q matrix and examining the effect on the stability margins will allow an improved Kalman filter to be developed

Each of the diagonal terms of the Q matrix has been scaled (up and down) by a factor of 4 The effects of this scaling have been assessed for each of the extreme error values The effects have been analysed qualitatively, to see the effect each change has on the gain and phase margins around both exclusion regions The following notation has been used to tabulate this analysis

++   significant improvement

+   minor improvement

0   no change

-    minor degradation

--   significant degradation

The results for the model with Young's Modulus changed by ±15% are shown in Table 4-2

		-180°				-540°			
		GM		PM		GM		PM	
		-15%	+15%	-15%	+15%	-15%	+15%	-15%	+15%
Q(1,1)	x 4	+	++	+	-	+	+	++	0
	÷ 4	-	--	-	+	-	-	--	0
Q(2,2)	x 4	0	0	0	0	0	0	0	0
	÷ 4	0	0	0	0	0	0	0	0
Q(3,3)	x 4	0	+	0	0	++	+	+	0
	÷ 4	0	-	0	0	--	-	-	0
Q(4,4)	x 4	0	0	0	0	0	0	0	0
	÷ 4	0	0	0	0	0	0	0	0
Q(5,5)	x 4	-	--	-	+	--	--	--	0
	÷ 4	+	++	+	-	++	++	++	0
Q(6,6)	x 4	0	-	0	+	-	-	-	0
	÷ 4	0	+	0	0	+	+	+	0
Q(7,7)	x 4	0	-	0	0	-	-	-	0
	÷ 4	0	+	0	0	+	+	+	0
Q(8,8)	x 4	0	-	0	0	0	0	-	0
	÷ 4	0	+	0	0	+	0	+	0

Table 4-2. Effects of Changes in Q on Model

As can be seen from Table 4-2, changes to the Q matrix can have a noticeable effect of the stability margins in the system. Most parameters have little or no effect on the response, and the results for both +15% and –15% errors are similar. The parameters which show most interest are Q(1,1) and Q(5,5). Q(1,1) relates to the first flexible mode, and Q(5,5) relates to the rigid mode position at the spring closest to the actuator.

These results indicate the desirability of increasing Q(1,1) and decreasing Q(5,5), which are the co-variances of the first flexible mode and the position of the beam at the spring nearest the actuator respectively. The frequency responses corresponding to each of these changes are shown in Figure 4-21 and Figure 4-22. In these plots

Blue - -15% Young's Modulus error

Green - nominal model

Red - +15% Young's Modulus error
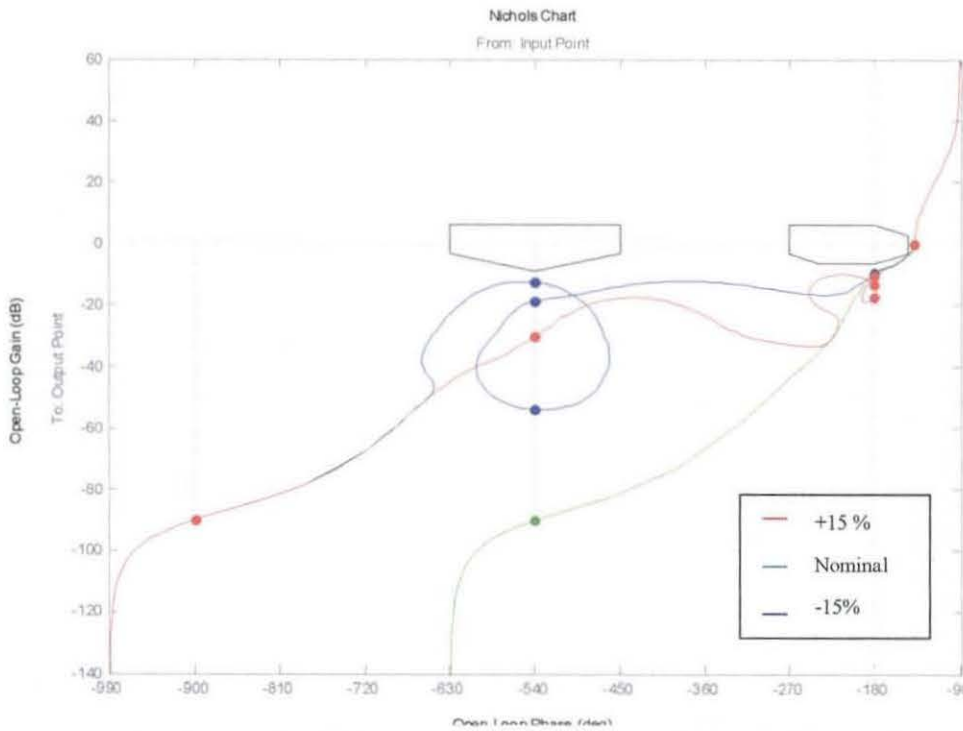
Figure 4-21 - Response of system (Kalman Filter) with Q(1,1) multiplied by 4

The two sets of frequency responses are very similar. In both sets, the exclusion regions have been cleared, but the different changes provide slightly different benefits to this clearance. The responses shown in Figure 4-21 provide slightly better margins around the first (-180°) exclusion region, whilst the responses shown in Figure 4-22 provide better clearance around the second (-540°) exclusion region.
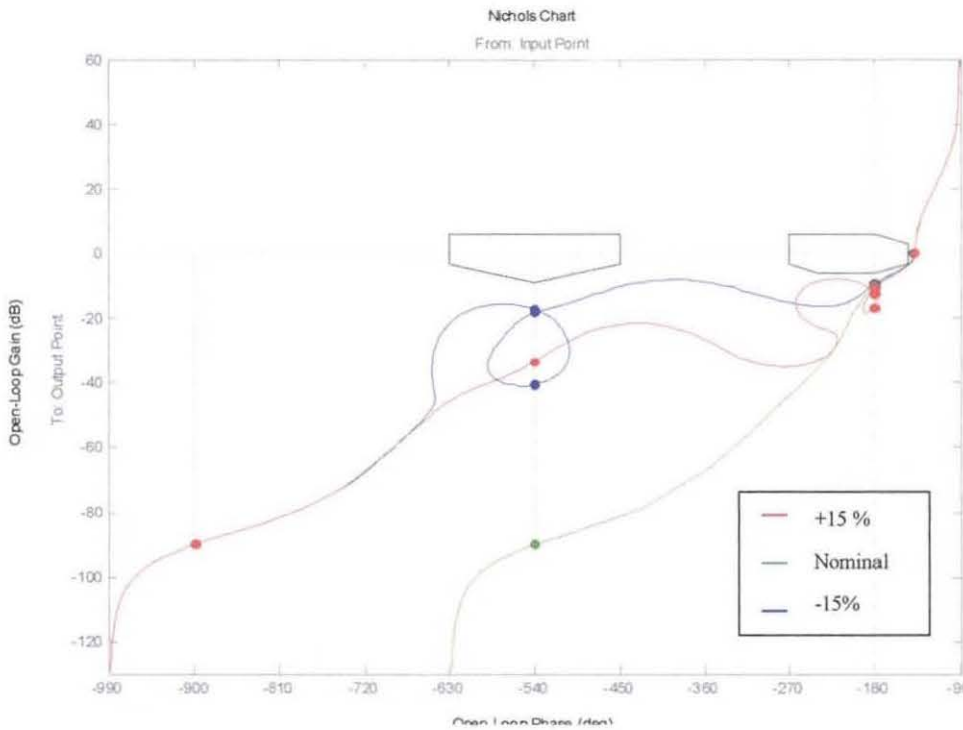
Figure 4-22 - Response of system (Kalman Filter) with Q(5,5) divided by 4

Both of these changes result in clearance of the exclusion regions, so the effects of applying both at the same time have not been shown. It is likely that the combination of both changes would result in a further improvement in the stability margins.

4.12 Un-modelled Disturbances

In flight an aircraft is affected by a number of disturbances (e.g. wind gust, downdraft, etc.) which could not be included in the Kalman filter model. This section will examine the effects of a disturbance to the beam, which the filters do not model.

The disturbance which has been used is an additional force which is applied momentarily to the beam. The model has been simulated to see the effect of this disturbance on the filter's ability to overcome the effects, and provide a stable control loop.

4.12 1 Disturbance model

The placement of the disturbance force has been selected to maximise the distance between the two forces, Figure 4-23 shows the positioning of the disturbance force
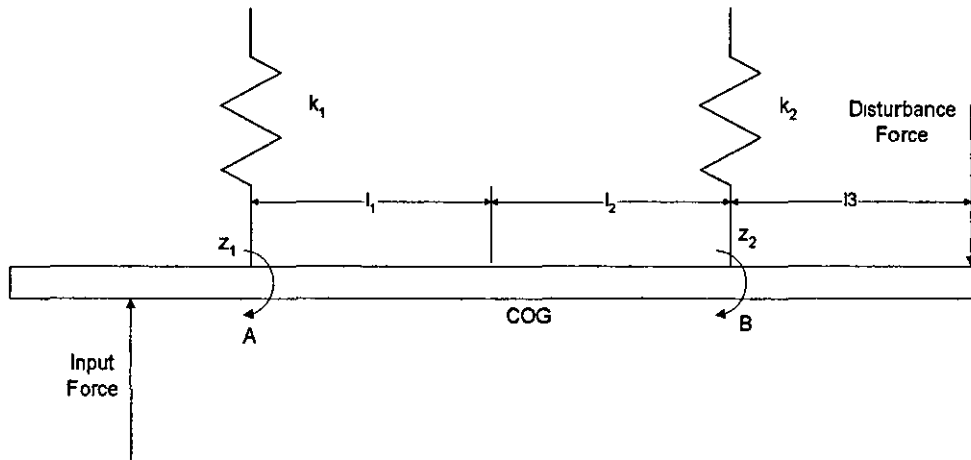
Figure 4-23. Position of Disturbance Force

The disturbance can readily be added to the model as an additional input   The A and C matrices from the state space model developed in Section 4 4 remain unchanged The B and D matrices each gain an additional column

As with the modelling of the input force, the effect of the disturbance force on the flexible modes is calculated using the receptance value for the position on the beam where the force occurs   The effect on the rigid modes is calculated by taking moments about A, B, and the Centre of gravity (COG) as shown in Figure 4-23.

Moments about A·

$$F \cdot (l1 + l2 + l3) + f2 \cdot (l1 + l2) = 0 \tag{4 33}$$

Moments about B

$$F \cdot (l3) + f1 \cdot (-l1 - l2) = 0 \tag{4 34}$$

Moments about COG.

$$F \cdot (l2 + l3) - f1 \cdot l1 + f2 \cdot l2 = 0 \tag{4 35}$$

Rearranging (4 34) in terms of f1 gives

75

$$f1 = \frac{F \cdot (l3)}{(l1 + l2)} \tag{4 36}$$

Rearranging (4 33) in terms of f2 gives

$$f2 = -\frac{F \cdot (l1 + l2 + l3)}{k1 \cdot (l1 + l2)} \tag{4 37}$$

Since the distances between the disturbance force, the springs and the centre of gravity are all equal (i e $l1 = l2 = l3$) equations (4 36) and (4 37) can be reduced to

$$f1 = \frac{1}{2}F \tag{4 38}$$

$$f2 = -\frac{3}{2}F \tag{4 39}$$

These values can be checked by substitution into equation (4 35). These are the values of the effect of the disturbance force on the rigid modes   The B matrix becomes

$$B = \begin{bmatrix} 0 & 0 \\ \dfrac{\Phi_1(x_i)}{m} & \dfrac{\Phi_1(x_d)}{m} \\ 0 & 0 \\ \dfrac{\Phi_2(x_i)}{m} & \dfrac{\Phi_2(x_d)}{m} \\ 0 & 0 \\ \dfrac{1\,25}{m} & \dfrac{-0\,5}{m} \\ 0 & 0 \\ \dfrac{-0\,25}{m} & \dfrac{1\,5}{m} \end{bmatrix}$$

The D matrix is unchanged

4 12 2 Results

The effect of applying an un-modelled disturbance can be examined by applying an impulse function to the disturbance input   The controller input to the beam remains the same as in the previous chapter (i e the beam is responding to a demanded 0 01rad/s step at t=0, followed by a -0 02 rad/s step at t=5)   The impulse represents a

very short duration disturbance, such as a wind gust or downdraft, and is applied after the system has settled down following the initial transient.

The impulse function is represented by a 3N force applied for 0.1s. This is applied after the simulation has been running for 1s. Figure 4-24 shows the effect of this disturbance to a 10 second simulation. The system runs closed loop, with the feedback supplied by the Kalman filter.
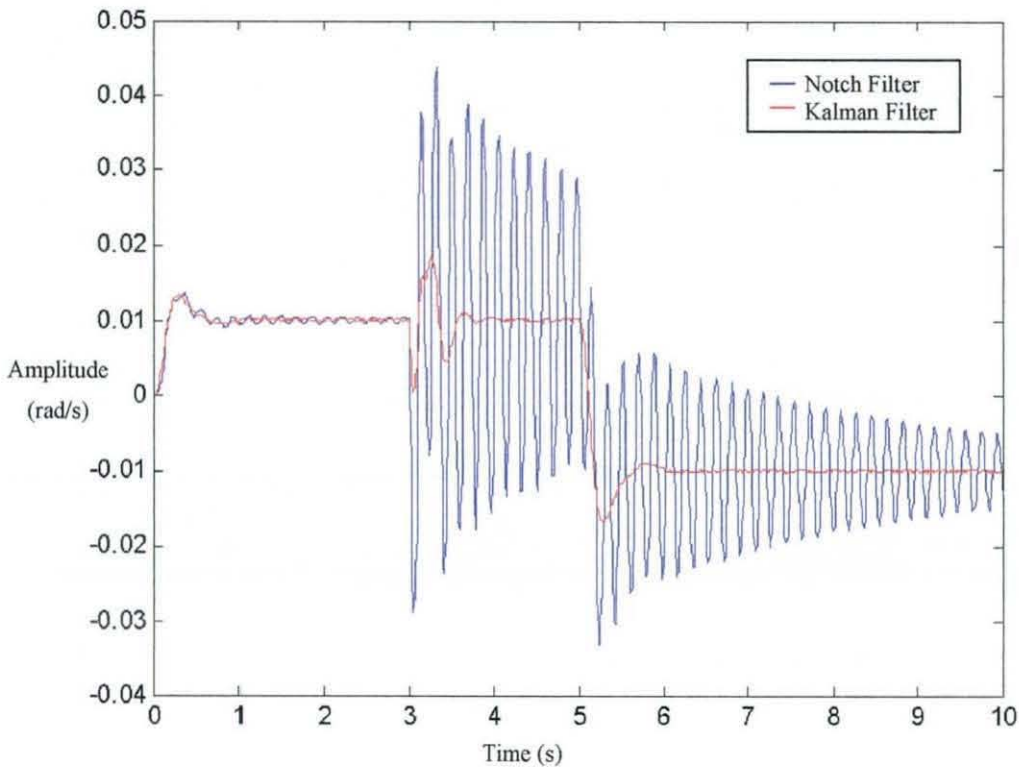
Figure 4-24. Effect of Disturbance on Beam Model

The disturbance has quite a large effect on the beam, and this is reflected in the sensor output (blue). However, the Kalman filter (red) filters out most of this, feeding back to the controller only enough of the disturbance signal to prevent the system from becoming unstable.

The effect of the disturbance could be more significant if it occurred at the same time as a change in the demanded signal. Figure 4-25 shows the system response to a disturbance force of the same magnitude occurring at t=5s.
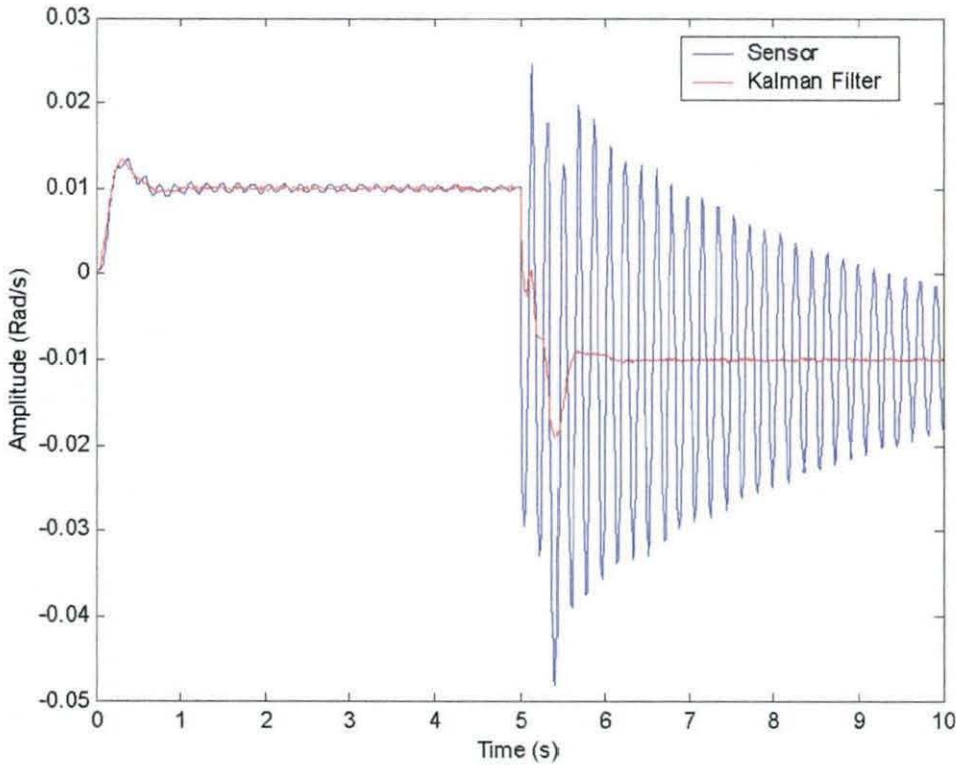
Figure 4-25. Effect of Disturbance at t=5s

Even with the disturbance occurring at the same time as a change in the demand signal, with the Kalman filter in the system, the beam remains stable.

4.13 Summary

This chapter has discussed the use of the Kalman filter as replacement for a pair of notch filters. The parameters of the model used in this chapter have been developed so as to allow the construction of an experimental rig. The experimental rig will be discussed in detail in Chapter 5.

The Kalman filter approach provides an improvement over the use of notch filters to overcome the problems associated with the flexible modes. It also provides additional phase benefits over the unfiltered response.

It has been shown that the model can be modified to more closely represent the aircraft system, with a more stringent set of stability margins. It has been shown that

the Kalman filter approach will operate under adverse conditions, either when the model is not an accurate representation of the system, or when the system is affected by un-modelled forces

5 Experimental Rig

This chapter describes the design of the experimental rig, which has been used to validate the two-mode beam model work

5.1 Introduction

An important part of the development of a new approach is to validate any modelling carried out on a physical system.

The two-mode model, as discussed in Chapter 4 was modelled on such a scale that it could be developed into an experimental system in order to provide validation of the model
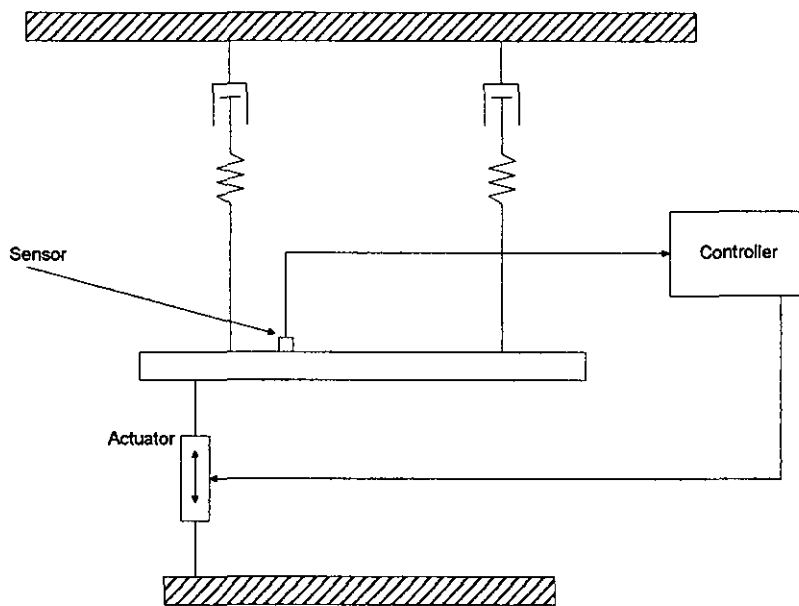
Figure 5-1. Beam Model

Figure 5-1 shows the original layout of the beam model This diagram implies that the motion of the actuator is in the vertical direction One of the key assumptions made before the modelling started, was that the effects of gravity could be ignored This meant that only the actuator would provide stimulation to the beam

If the experimental rig were to be mounted in the vertical plane, then the model used in earlier chapters would not be entirely valid for comparison with this stage of work. In order to overcome this, the rig has been designed to operate in the horizontal plane, an arrangement which also facilitates supporting the beam in a largely unconstrained manner. Figure 5-2 shows a photo of the experimental rig.
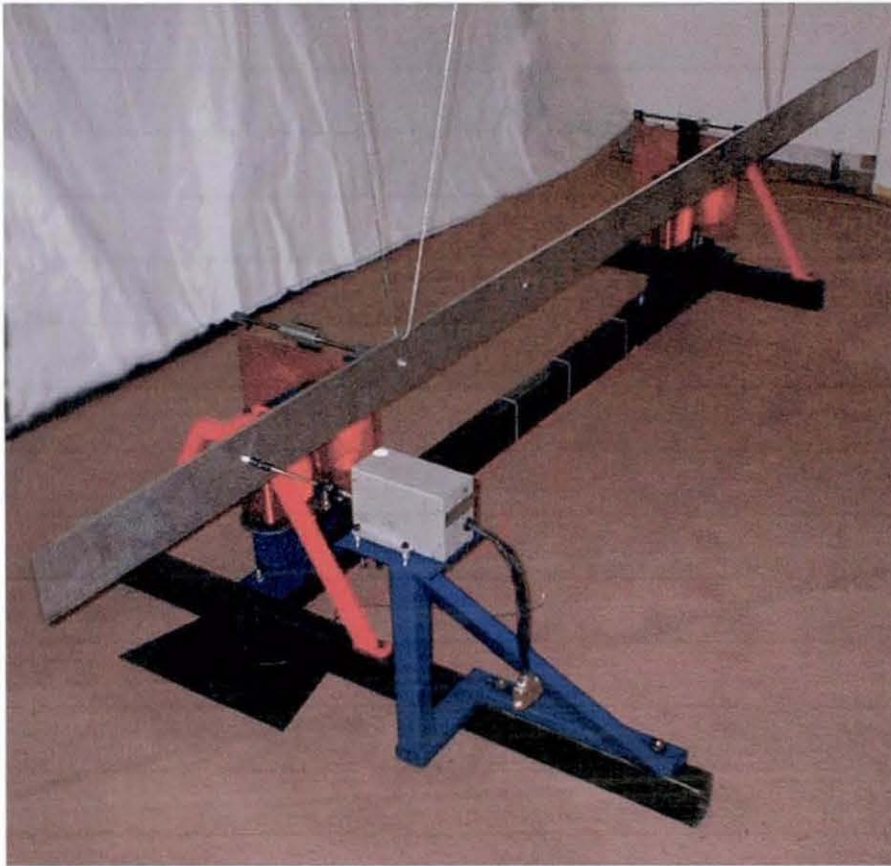
Figure 5-2. Experimental Rig

5.2 Components of the Rig

The rig consists of a number of different components, which are described in this section.

5.2.1 Beam

The beam has been designed to give a first bending frequency of around 5Hz and manufactured from Aluminium (density of aluminium is 2700kgm^{-3}). The dimensions of the beam are:

Length	-	3 1m
Width	-	10cm
Depth	-	0 9cm
Mass	-	7 533kg

The beam is suspended from long wires attached to the ceiling, in order to ensure that the lateral forces on the springs and actuator caused by the suspension are as small as possible

5 2 2 Springs

The springs used are compression springs They have the following dimensions

Wire Diameter (d)	-	0 91mm
Outside Diameter (OD)	-	12 7mm
Free Length (FL)	-	38 1mm
Free Coils (n)	-	6
Modulus of shear (G)	-	76GPa

These dimensions provide a spring constant of 0 6 Nmm^{-1}.

5 2.3 Dampers

In order to reduce the amount of friction in the system, electromagnetic dampers have been used

The damping is produced by passing a copper sheet through a magnetic field The copper sheet is supported on a bar that can move freely through a pair of linear bearings Two circular runners at the bottom of the copper sheet prevent lateral movement. A full description of the design of the dampers is given in Appendix G

5 2 4 Actuator

A moving coil actuator has been used on the rig. This type of actuator has low levels of friction The basic specification of the actuator is show below·

Stroke	50mm
Maximum Force	60N
Coil Resistance	12Ω
Maximum Current	2.5A
Sensitivity	22N/A

The actuator also provides high accuracy position feedback information. The data sheet for the actuator is included in Appendix E. A photo of the actuator is shown in Figure 5-3.
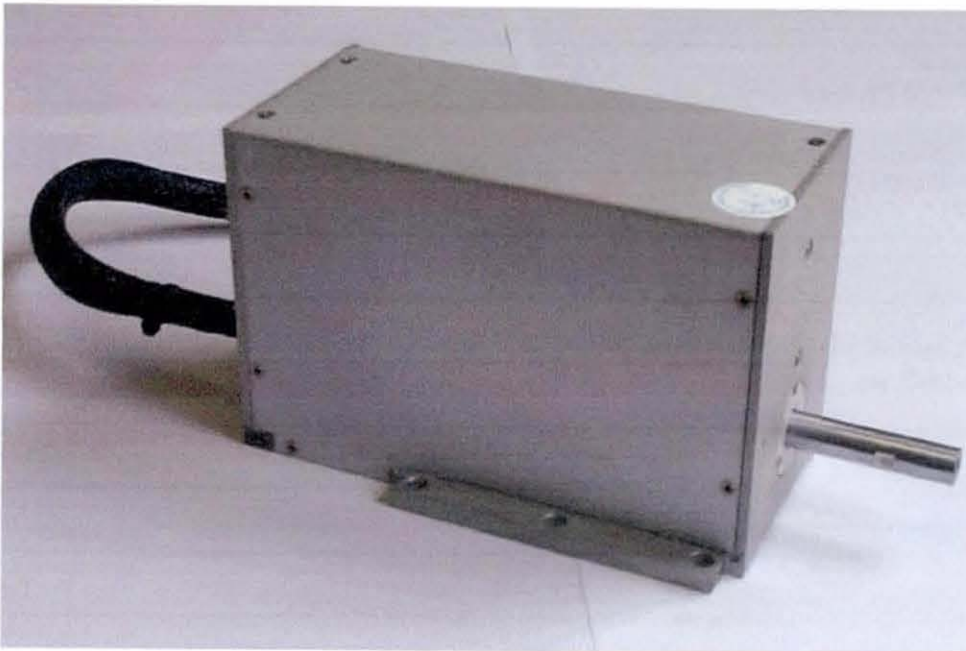
Figure 5-3. Actuator

5.2.5   Sensor

A small solid state gyroscope has been supplied by BAE Systems for use as part of the control system, discussed in Chapter 4. The basic specification of the sensor is shown below:

Maximum rate	±110°/s
Noise	0.25°/s
Sensitivity	18.2mV/°/s

The datasheet for the gyroscope is included in Appendix F. A photo of the sensor is shown in Figure 5-4.

Figure 5-4. Sensor

5.2.6 Controller

A Digital Signal Processing (DSP) card has been used to develop the controller and filtering for the rig. This approach allows development of the software required to operate the system under a number of different conditions. Full details of the design of the controller can be found in Section 5.4.

5.2.7 Data Logging

Variables from inside the controller have been recorded using the interface between the DSP and a PC. The sensor output is saved into the memory on the DSP, and then can be downloaded to the PC at the end of the test cycle.

5.3 Electromagnetic Damper Design

The electromagnetic damping occurs due to the interaction between eddy currents induced in a thin conducting sheet (e.g. copper) and a magnetic field. Figure 5-5 shows a generalisation of this arrangement.
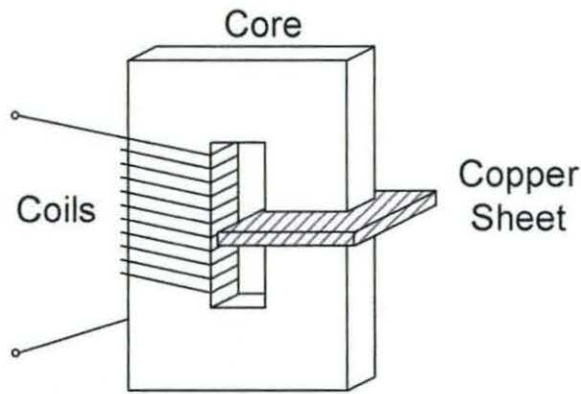
Figure 5-5. Concept of Electro-magnetic Damper

This approach to damper design produces a solution with potentially very low friction, but, in order to generate the required field, the solution is likely to be bulky.

The design of this damper is included in Appendix G. Figure 5-6 shows a drawing of the damper and its support structure.
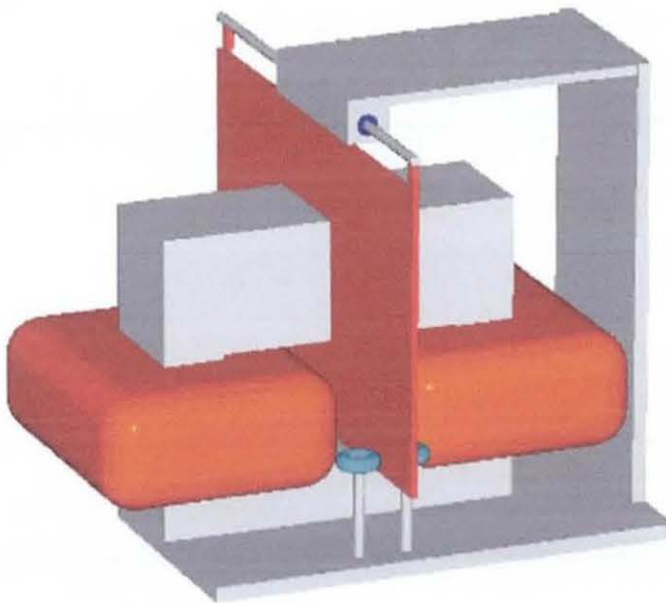
Figure 5-6. 3-Dimensional Drawing of Electromagnetic Damper

The drawing shows two small rollers at the base of the copper sheet; these keep the sheet orientated correctly in relationship to the damper core, and prevent the sheet from fouling on either pole.

5.4 Controller Design

The controller routines have been designed to run on a Texas Instruments (TI) digital signal processor (DSP) card, based upon the TI TMS320C31 processor. Figure 5-7 shows a picture of the processor card.

This processor card provides a simple development environment from which to design the routines required to control the rig. The card provides a parallel port for communication with a host PC. External DAC and ADC devices have been used; these are mapped to memory locations of the DSP.
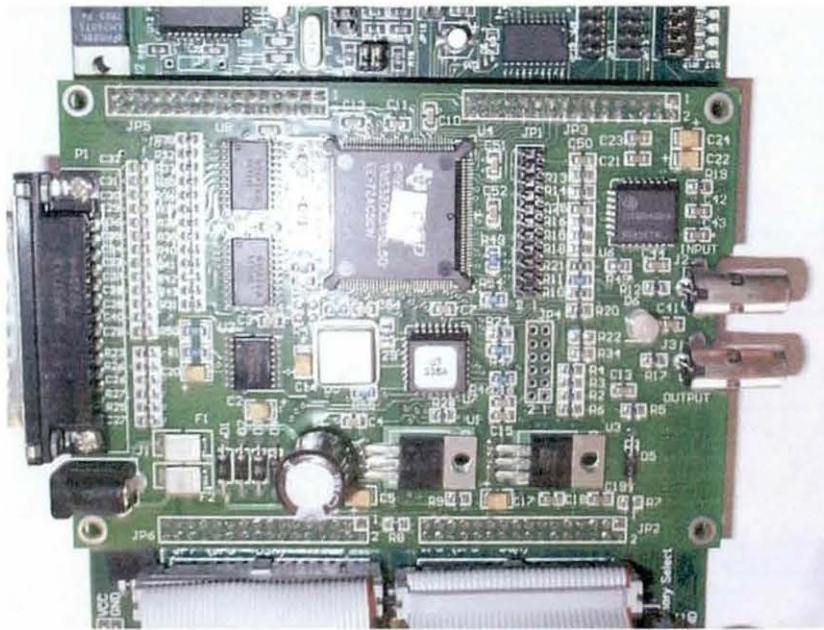
Figure 5-7. TMS320C31 Based DSP Card

The controller consists of two main components; these are:

    Control routines

    Kalman filter routines

5.4.1 Control Routines

The controller designed in Chapter 4 is formed for a continuous model. This would not work on the DSP, since the DSP operates in discrete steps. In order to develop a

controller which does work on the DSP, the continuous model needs to be converted to discrete form

The transfer function of the controller was

$$7 \cdot \frac{0\,005s + 1}{0\,005s} \cdot \frac{0\,02s + 1}{0\,01s + 1} \tag{5 10}$$

This can be converted into state space form using the Matlab function tf2ss The state space matrices produced by this function are

$$A = \begin{bmatrix} -100 & 0 \\ 1 & 0 \end{bmatrix}, B = \begin{bmatrix} 1 \\ 0 \end{bmatrix}, C = \begin{bmatrix} 2100 & 1\,4 \cdot 10^5 \end{bmatrix} D = \begin{bmatrix} 14 \end{bmatrix} \tag{5 11}$$

These parameters define the controller using the state space equations

$$\dot{x} = Ax + Bu$$
$$x = Cx + Du \tag{5.12}$$

The same equations can be described in discrete state space form

$$x_{n+1} = A_d x_n + B_d u_n$$
$$x_n = C_d x_n + D_d u_n \tag{5.13}$$

The matrices for the discrete model can be calculated from the continuous matrices (5 11) using the Matlab function c2d With a sampling period of 0 001s, these are

$$A = \begin{bmatrix} 3\,68 \cdot 10^{-1} & 0 \\ 6\,32 \cdot 10^{-3} & 1 \end{bmatrix}, B = \begin{bmatrix} 6\,32 \cdot 10^{-3} \\ 3\,68 \cdot 10^5 \end{bmatrix}, C = \begin{bmatrix} 2100 & 1\,4 \cdot 10^5 \end{bmatrix} D = \begin{bmatrix} 14 \end{bmatrix} \tag{5 14}$$

5 4 2   Kalman Filter Routines

As with the controller, the Kalman filter used in the modelling stage of work was designed for use in the continuous domain, and therefore need to be converted to discrete form

Unlike the previous section, where the continuous controller could be readily converted to a discrete form, the Kalman filter needs to be redesigned for the discrete form   The Kalman filter gain matrix is developed from the system state space

equations, and before the discrete form of the Kalman filter can be created, the system must be converted to discrete form (as before using the Matlab command c2d)

Using the parameters for the rig outlined in Section 5 2, the continuous domain state space matrices used in the Kalman filter are

$$A = \begin{bmatrix} 0 & 1 & 0 & 0 & 0 & 0 & 0 & 0 \\ -9\,5x10^2 & -4\,9x10^{-1} & 0 & 0 & 0 & 0 & 0 & 0 \\ 0 & 0 & 0 & 1 & 0 & 0 & 0 & 0 \\ 0 & 0 & -7\,2x10^3 & -1\,4x10^0 & 0 & 0 & 0 & 0 \\ 0 & 0 & 0 & 0 & -4\,4x10^1 & -1\,0x10^3 & 0 & 0 \\ 0 & 0 & 0 & 0 & 1\,3x10^0 & 1\,3x10^1 & 0 & 0 \\ 0 & 0 & 0 & 0 & 0 & 0 & -4\,4x10^1 & -1\,0x10^3 \\ 0 & 0 & 0 & 0 & 0 & 0 & 1\,3x10^0 & 1\,3x10^1 \end{bmatrix}$$

$$B = \begin{bmatrix} 0 \\ 1\,4x10^{-1} \\ 0 \\ 2\,5x10^{-1} \\ -1\,7x10^{-1} \\ 7\,1x10^{-3} \\ 3\,3x10^{-2} \\ -1\,4x10^{-3} \end{bmatrix}$$

$$C = \begin{bmatrix} 0 & -9\,0x10^{-1} & 0 & 7\,3x10^{-1} & -6\,4x10^{-1} & 2\,8x10^{-2} & 6\,4x10^{-1} & -2\,8x10^{-2} \end{bmatrix}$$

$$D = \begin{bmatrix} 0 \end{bmatrix}$$

Using a sampling period of 0 001s, the Matlab command c2d produces the following discrete state space matrices

$$A = \begin{bmatrix} 9\,53x10^{-1} & 9\,82x10^{-3} & 0 & 0 & 0 & 0 & 0 & 0 \\ -9\,31 & 9\,48x10^{-1} & 0 & 0 & 0 & 0 & 0 & 0 \\ 0 & 0 & 6\,62x10^{-1} & 8\,78x10^{-3} & 0 & 0 & 0 & 0 \\ 0 & 0 & -6\,33x10^1 & 6\,50x10^{-1} & 0 & 0 & 0 & 0 \\ 0 & 0 & 0 & 0 & 5\,93x10^{-1} & -8\,7008 & 0 & 0 \\ 0 & 0 & 0 & 0 & 1\,07x10^{-2} & 1\,0768 & 0 & 0 \\ 0 & 0 & 0 & 0 & 0 & 0 & 5\,93x10^{-1} & -8\,7008 \\ 0 & 0 & 0 & 0 & 0 & 0 & 1\,07x10^{-2} & 1\,0768 \end{bmatrix}$$

$$B = \begin{bmatrix} 6\,87x10^{-6} \\ 1\,36x10^{-3} \\ 1\,15x10^{-5} \\ 2\,16x10^{-3} \\ -1\,64x10^{-3} \\ 6\,53x10^{-5} \\ 3\,28x10^{-4} \\ -1\,31x10^{-5} \end{bmatrix}$$

$$C = \begin{bmatrix} 0 & -8\,98\text{x}10^{-1} & 0 & 7\,26\text{x}10^{-1} & -6\,45\text{x}10^{-1} & 2\,78\text{x}10^{-2} & 6\,45\text{x}10^{-1} & -2\,78\text{x}10^{-2} \end{bmatrix}$$

$$D = \begin{bmatrix} 0 \end{bmatrix}$$

In addition, the covariance matrices for the process noise (Q) and measurement noise (R) as discussed and developed in Chapter 4 are required   These are

$$R = 1\,0 \times 10^{-7}$$

$$Q(diagonal\ terms) \begin{bmatrix} 5\,0440 \times 10^{-4} \\ 3\,7758 \times 10^{-4} \\ 2\,7377 \times 10^{-5} \\ 1.5922 \times 10^{-5} \\ 2\,4900 \times 10^{+0} \\ 2\,9509 \times 10^{-4} \\ 9\,9605 \times 10^{-2} \\ 1\,1805 \times 10^{-5} \end{bmatrix}$$

The Matlab command 'kalman' produces two matrices which define the discrete Kalman filter. These are the Kalman gain matrix (K) and the innovations gain matrix (M)   The values of these matrices are

$$K = \begin{bmatrix} 3\,89x10^{-3} \\ -4\,77x10^{-1} \\ -8\,72x10^{-4} \\ 2\,92x10^{-1} \\ -6\,04x10^{-1} \\ 9\,41x10^{-3} \\ 2\,42x10^{-2} \\ -3\,77x10^{-4} \end{bmatrix}$$

$$M = \begin{bmatrix} 8\,41x10^{-3} \\ -4\,20x10^{-1} \\ -3\,17x10^{-3} \\ 1\,40x10^{-1} \\ -7\,77x10^{-1} \\ 1\,65x10^{-2} \\ 3\,11x10^{-2} \\ -6\,59x10^{-4} \end{bmatrix}$$

These matrices along with the state space matrices are used to calculate the state and output estimates. The equations used are.

$$x(n \mid n) = x(n \mid n-1) + M(y(n) - Cx(n \mid n-1) - Du(n))$$ (5 15)

$$y(n \mid n) = C_o x(n \mid n) + Du(n)$$ (5 16)

$$x(n+1 \mid n) = Ax(n \mid n-1) + Bu(n) + K(y(n) - Cx(n \mid n-1) - Du(n))$$ (5 17)

Equation (5 16) uses a slightly different C matrix to that discussed above (and used in equations 5 15 and 5 17). In order that the estimated output of the beam angular velocity provides only the rigid portion, and not the flexible components, the components of the C matrix relating to the flexible modes are set to zero (this is the same method used in Chapter 4).

$$C_o = \begin{bmatrix} 0 & 0 & 0 & 0 & -645\text{x}10^{-1} & 278\text{x}10^{-2} & 645\text{x}10^{-1} & -278\text{x}10^{-2} \end{bmatrix}$$

5.5 DSP Operation

The DSP system has been designed to continuously loop through the program until the host (PC software) sends the command to stop. In each loop, the software requests a new sample from the ADC, updates the Kalman filter output and produces the rigid mode estimate. This is passed to the controller which produces an output which is sent to the DAC. Figure 5-8 shows the program flowchart
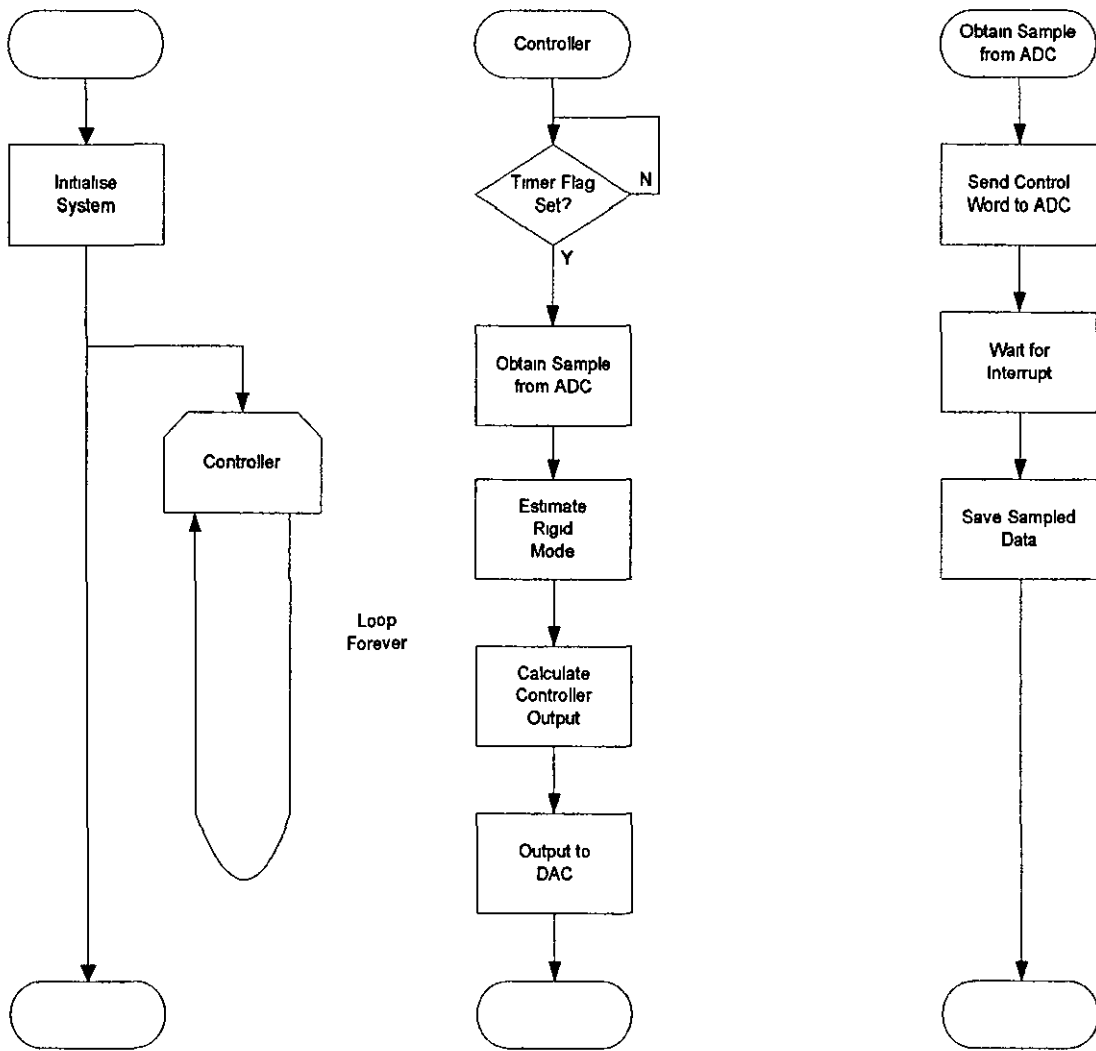
Figure 5-8. DSP Software Flowchart

Before the controller loop is entered, the system is initialised, this sets up the DSP to produce a 1 kHz timer function, which is used to control the sampling rate of the program The controller, the Kalman filter, and the model parameters are initialised at the same time

Obtaining a new sample from the ADC is a two stage process   First a control word must be sent to the address of the ADC, this sets the ADC to look at the correct channel (the ADC supports 6 channels), and to sample at the correct voltage level When the ADC returns an interrupt the sampled value can be read from the ADC

5.6 Results

5 6 1 Model Validation

The first stage when commissioning a rig is to ensure the validity of the model of the system In this case it is of particular importance, since the Kalman filter needs a good model of the system in order to operate properly

Using a Voltech Instruments TF2000 frequency response analyser, the frequency response of the uncontrolled beam was measured The results of this, and the model response for comparison, are shown in Figure 5-9
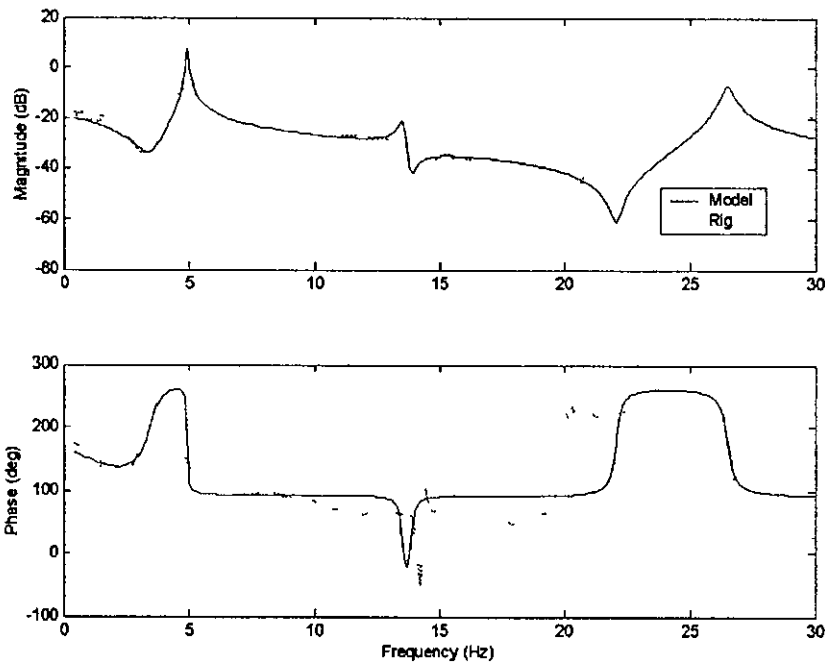
Figure 5-9. Model and Rig Frequency Response

The response shows a good comparison between the model and rig, especially below 5Hz This should allow the Kalman filter to estimate the rigid portion of the sensor output with a good degree of accuracy.

The model isn't quite so good at the higher frequencies, suggesting a second flexible mode lower than the actual frequency of the rig The same is true of the third mode However, this is of less importance, since this will allow the Kalman filter to be initially tested with small known errors in some of the flexible modes

5 6 2   Future Results

At present, the results from the beam have been limited to the validation of the model shown in the previous section   Results will be obtained which will validate the operation of the Kalman filter. The rig can be extended to allow the tolerance of the Kalman filter approach to changes in the flexible mode frequencies by adding small masses to the beam

5.7   Summary

An experimental rig has been designed and implemented which can be used to verify the simulation work carried out in Chapter 4   Whilst only the validation of the model of the beam has been produced to date, the rig will be used to validate the Kalman filter approach.

6   Aircraft Model

This chapter discusses the development of an pitch axis aircraft model, which has been used to examine the concepts introduced in earlier chapters in the same environment that is used to produce the notch filter solution

6.1   Introduction

The design of a solution to the structural coupling problem includes the use of an aircraft model. As was discussed in Chapter 2, whilst a model of the aircraft cannot be relied upon as the sole source of information, it does form a significant part of the design process, especially in the early stages of the process

The model has been developed in close conjunction with BAE Systems, and has been corrected to improve the comparison between the model data and the data recorded from ground testing

6.2   Model Components

The model of the aircraft system consists of two main sections; the model of the aircraft, and the model of the FCS

6.2 1   Aircraft model

The aircraft modelled is a generic Agile Combat Aircraft (ACA)   It is built up from a matrix differential equation

$$\mathbf{A}_a \ddot{q} + \left(\mathbf{D}_a + \sigma V \mathbf{B}_a\right)\dot{q} + \left(\mathbf{E}_a + \sigma V^2 \mathbf{C}_a\right)q = 0 \tag{6 1}$$

Where V is the true airspeed, σ is the relative air density, and q is the vector of generalised coordinates   The matrices A_a, B_a, C_a, D_a and E_a are respectively the inertia, the aerodynamic damping and stiffness, and the structural damping and stiffness   Each of these matrices is a square matrix with 80 rows, with each row (and column) representing a different mode. There are 74 flexible modes, 3 control modes,

and 3 rigid modes   The control modes represent the rotation of the aircraft control surfaces

> Inboard flap rotation
>
> Outboard flap rotation
>
> Foreplane rotation

The output matrix (Z) provides 3 sensor outputs at 19 locations on the centre line of the fuselage   The sensors are

> Angular displacement (θ)
>
> Forward velocity (x)
>
> Vertical velocity (z)

This formulation of the model can readily be converted into state space form, allowing the model to be used in the Matlab environment   The traditional state space form is

$$\dot{x} = Ax + Bu$$
$$y = Cx + Du$$

(6 2)

Keeping the generalised coordinates from the differential form of the aircraft model, the state vector x becomes

$$x = \begin{bmatrix} q \\ \dot{q} \end{bmatrix}$$

(6 3)

Rearranging equation (6 1) in terms of $\ddot{q}$ gives·

$$\ddot{q} = -\left(\frac{\mathbf{D}_a + \sigma V \mathbf{B}_a}{\mathbf{A}_a}\right)\dot{q} - \left(\frac{\mathbf{E}_a + \sigma V^2 \mathbf{C}_a}{\mathbf{A}_a}\right)q$$

(6 4)

From this, the state space a matrix can be obtained

$$A = \begin{bmatrix} [\mathbf{0}] & [\mathbf{I}] \\ \left[-\left(\frac{\mathbf{E}_a + \sigma V^2 \mathbf{C}_a}{\mathbf{A}_a}\right)\right] & \left[-\left(\frac{\mathbf{D}_a + \sigma V \mathbf{B}_a}{\mathbf{A}_a}\right)\right] \end{bmatrix}$$

(6 5)

The inputs to the model are moments applied to the control surfaces. The input matrix **ip** (3 columns) is

$$\mathbf{ip} = \begin{bmatrix} [0] \\ [\mathbf{E}_a(ctrl)] \\ [0] \end{bmatrix}$$ (6 6)

where *ctrl* is the location (in the $\mathbf{E}_a$ matrix) of the control modes. The state space input matrix **b** is:

$$\mathbf{B} = \begin{bmatrix} \begin{bmatrix} [0] \\ \begin{bmatrix} \dfrac{\mathbf{ip}}{\mathbf{A}_a} \end{bmatrix} \end{bmatrix} \end{bmatrix}$$ (6 7)

The output from the state space model is identical to the differential form, since the outputs are based on the same set of generalised coordinates, if for example, a pitch rate measurement was required from the point closest to the nose of the aircraft, then this would be obtained by the following:

$$\dot{\theta} = \begin{bmatrix} [0] & [\mathbf{Z}(row1)] \end{bmatrix} \begin{bmatrix} q \\ q \end{bmatrix}$$ (6 8)

The FCS uses the output from 4 sensors (pitch rate and vertical velocity from one location, and pitch angle and vertical velocity from a second location), the **c** matrix which provides these is

$$C = \begin{bmatrix} [0] & [\mathbf{Z}(row27)] \\ [0] & [\mathbf{Z}(row26)] \\ [\mathbf{Z}(row51)] & [0] \\ [0] & [\mathbf{Z}(row50)] \end{bmatrix}$$ (6 9)

The **D** matrix is a zero matrix, with 4 rows and 3 columns

The aircraft model has been initially developed with 80 modes, but this leads to a state space model with 160 states. A model of this size would require a significant amount of processing power to simulate. To overcome this, the model can be reduced in size by removing the rows and columns (in the differential equation form of the model)

relating to the higher flexible modes. To obtain a 20 mode (40 state) model, modes 15 to 74 would need to be removed.

Figure 6-1 shows a frequency response comparison between the 80 mode, 40 mode, and 20 mode models. The system includes the FCS (detailed in section 6.2.2), and is an open loop system with single input (foreplane hinge moment) and a single output (sensor 1 pitch rate).
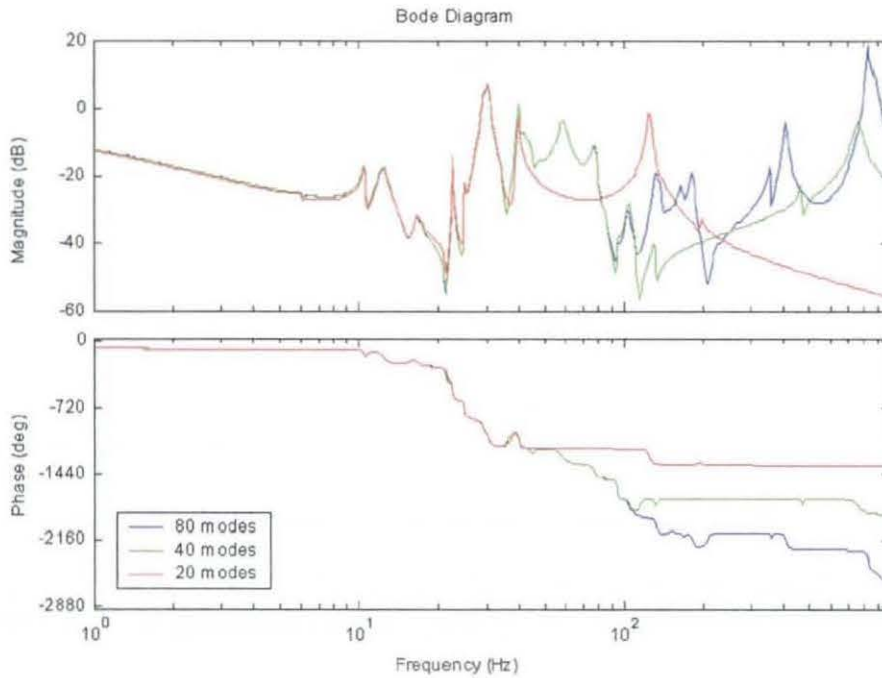
Figure 6-1. Comparison of Different Size Models

At frequencies lower than about 40Hz there is very little difference between the models and up to 100Hz there is almost no difference between the 80 mode and 40 mode models. Since, as was discussed in Chapter 2, the model is only accurate to about 20Hz, the model with 20 modes will provide enough data.

6.2.2 FCS model

The FCS model consists of a number of transfer functions which represent the flight control laws. It also contains the notch filters, and distribution paths linking the sensors, the control laws, and the actuator demand paths.

The 4 aircraft model sensors are used to provide 3 inputs (pitch rate, vertical acceleration, and angle of attack) Inputs are also provided in the FCS model to allow the control surfaces to be stimulated (as in ground vibration testing) The output from the FCS is the demanded rotational displacement for the 3 control surfaces These outputs are passed through models of the actuators

Since the model uses hinge moments as inputs, the output from the FCS needs to be compared with the actual control surface position, before conversion into a moment The actual surface positions are obtained by augmenting the state space **c** matrix with a further 3 rows

$$\mathbf{c}(rows5 - 7) = [[0] \quad [\mathbf{I}] \quad [0]]$$
(6 10)

Where the identity matrix **I** starts in the column relating to the first control mode (column 75 in the 80 mode model) Figure 6-2 shows the connections between the Aircraft model and the FCS
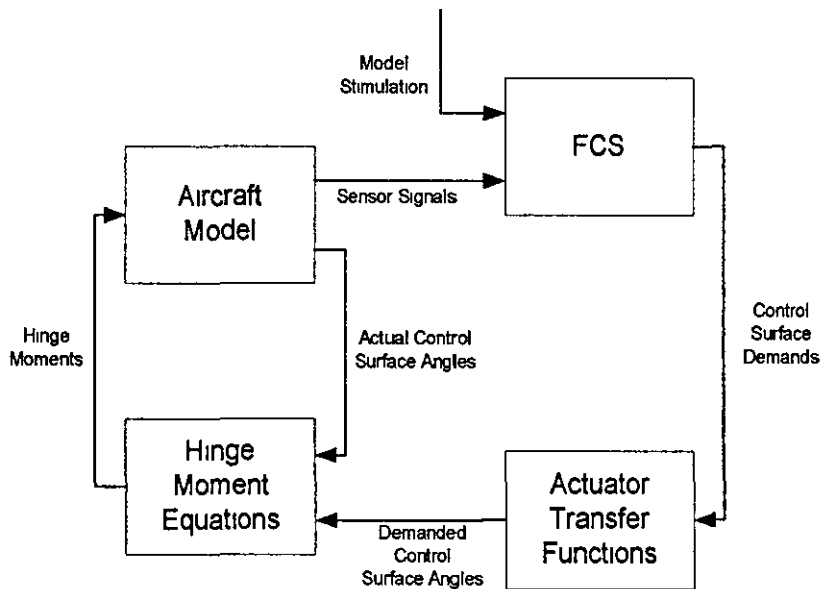
Figure 6-2. Aircraft Model and FCS

The Matlab files for the model are included in Appendix H

6.3 Kalman Filter

The Kalman filter which will be used in conjunction with the aircraft model has been designed to estimate the rigid mode output using 3 control surface moment inputs and the 4 aircraft model sensors   The system model used in the Kalman filter is initially identical to that used in the aircraft model

6 3 1   Uncertainty Parameters

The R matrix provides the Kalman filter with information on the noise on each of the sensors   It has been set up, with 1 row for each sensor, using the same value for each sensor as was used on the beam model.   Since there are 4 sensors and it has been assumed that the noise on each sensor is identical, using the same noise levels as used on the beam model (noise power $= 1 \times 10^{-9}$) the R matrix used is

$$\mathbf{R} = \begin{bmatrix} 1\,0 \times 10^{-7} & 0 & 0 & 0 \\ 0 & 1\,0 \times 10^{-7} & 0 & 0 \\ 0 & 0 & 1\,0 \times 10^{-7} & 0 \\ 0 & 0 & 0 & 1\,0 \times 10^{-7} \end{bmatrix} \qquad (6\ 11)$$

The Q matrix, which provides the Kalman filter with information about the accuracy of each of the states in the model, has as many rows as there are states in the Kalman filter   It has been developed from the covariance of the states in the Kalman filter, calculated from the closed loop response of the states in the Kalman filter to a unity sine wave input applied to the FCS input (shown as STK in the model diagrams) to the system   For the 20 mode model (40 states) the diagonal terms of the Q matrix are

$$
rows\ 1\text{-}20
\begin{bmatrix}
1\ 0129e+0 \\
8\ 9829e-4 \\
2\ 7100e-5 \\
5\ 1050e-4 \\
6\ 5733e-3 \\
1\ 5550e-5 \\
1\ 8791e-5 \\
5\ 6536e-5 \\
9\ 2266e-5 \\
6.3356e-3 \\
2\ 8510e-4 \\
7\ 2006e-5 \\
4\ 3713e-7 \\
2\ 0538e-6 \\
8\ 8506e-1 \\
8\ 9112e-1 \\
4\ 5939e-1 \\
2\ 7968e-1 \\
1\ 9504e-1 \\
2\ 3046e-4
\end{bmatrix}
\qquad
rows\ 21\text{-}40
\begin{bmatrix}
1\ 0520e+3 \\
9\ 3263e-1 \\
2.8317e-2 \\
5\ 2792e-1 \\
6\ 8034e+0 \\
1\ 7081e-2 \\
1\ 9837e-2 \\
6\ 1279e-2 \\
9\ 5969e-2 \\
6\ 6261e+0 \\
3\ 0332e-1 \\
7.5385e-2 \\
4\ 5622e-4 \\
2\ 1244e-3 \\
9\ 1668e+2 \\
9\ 2356e+2 \\
4.7762e+2 \\
1\ 5549e+0 \\
1\ 7984e+0 \\
2\ 1310e-1
\end{bmatrix}
\qquad (6.12)
$$

These parameters have been used to develop the Kalman gain matrix using the Matlab function Kalman   The Kalman gain matrix is included in Appendix H

6.4   Comparison of Filters

The Kalman filter developed in the previous section needs to be added to the system before a comparison can be made between the notch filter and Kalman filter approaches   Figure 6-3 shows a block diagram of the system with the Kalman filter added
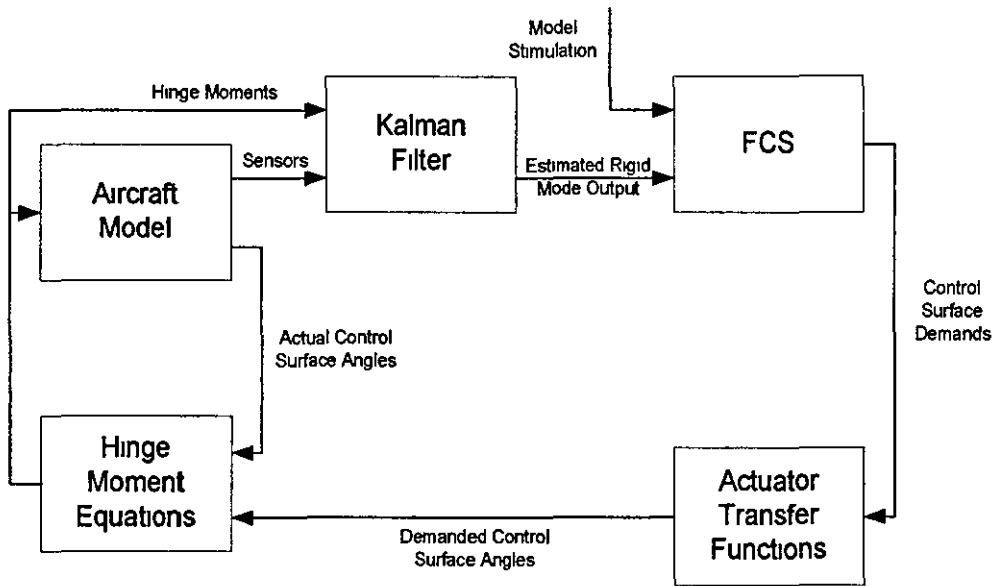
Figure 6-3. Aircraft System including Kalman Filter

The notch filters, which are included in the FCS, have been set up in the Simulink model in such a way that they can easily be excluded from the model, allowing quick comparisons between the models

The model of the aircraft system has been developed for frequency response analysis Since it includes a low frequency instability, which would be corrected by the pilot, it is not suited to time domain analysis   For this reason, the approaches have only been compared in the frequency domain   To allow the mode frequencies and the effects on stability to be compared, both Bode diagrams (Figure 6-4) and Nichols charts (Figure 6-5) are shown   The unfiltered system is included (blue plot) to allow provide a full comparison, and to allow evaluation of the improvement that each filter provides
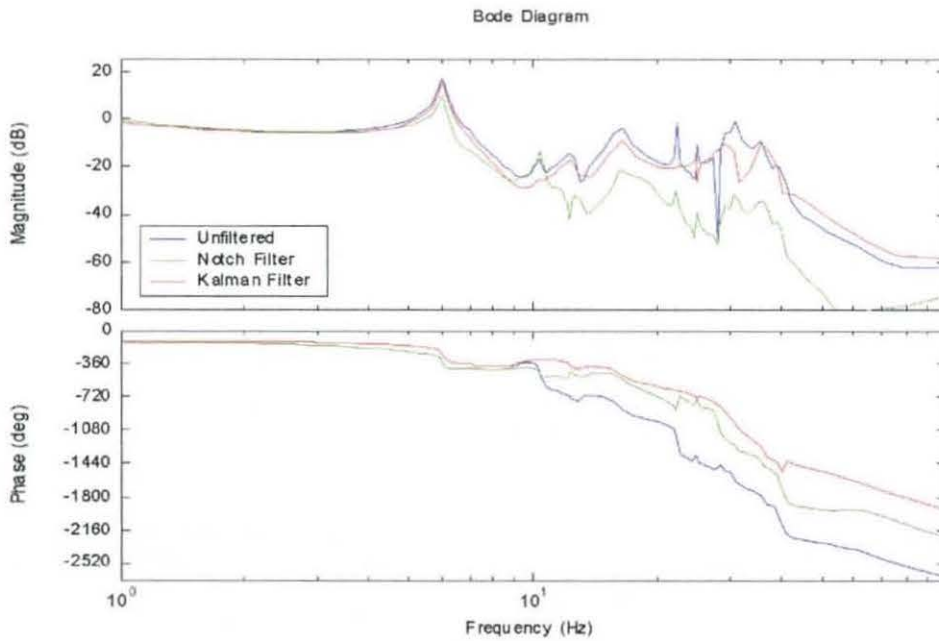
Bode Diagram

Figure 6-4. Bode Diagram Comparison of Filters with Aircraft Model

The Bode diagram shows that the notch filters (green plot) have attenuated the response across all of the flexible modes (from about 6Hz upwards). The notch filters have also added phase lag across all of these frequencies. The Kalman filter has attenuated some of the flexible modes, although very little on the first (6Hz) mode. The diagram also shows that the Kalman filter has not added any additional phase lag at low frequencies, and removes a significant amount at higher frequencies.
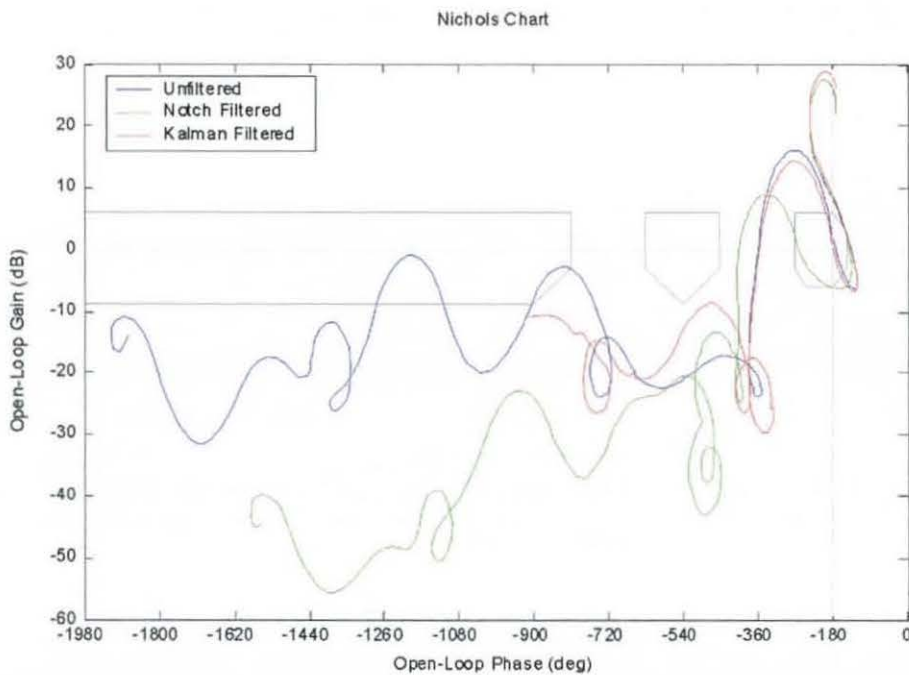
Nichols Chart

Figure 6-5. Nichols Chart Comparison of Filters with Aircraft Model

The Nichols chart shows that whilst the notch filter has attenuated the response, it has not quite achieved the goal of providing clearance of the exclusion regions. It can also be seen that the Kalman filter provides almost no benefit at low frequencies, although at most other frequencies the Kalman filter provides a small amount of attenuation (not as much as the notch filters), and so provides clearance of the second and third exclusion regions.

In order to see the effect of the filter on the stability margins, much closer inspection is required. Figure 6-6 shows the same responses, but zoomed in around the rigid and first flexible modes.
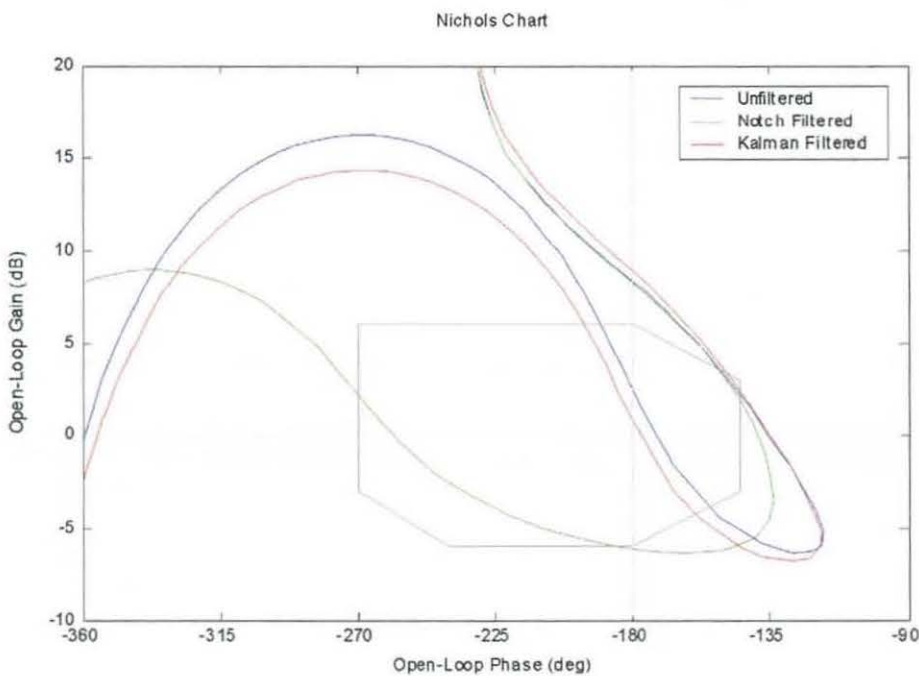
Figure 6-6. Comparison of Filters with Aircraft Model (Nichols Chart)

The Nichols chart shown in Figure 6-6 concentrates on the area around the first stability region (which is crucial in this model). Examination of the chart using Matlab shows the Phase Margins for the 3 plots to be:

	Phase Margin (deg)
Unfiltered	45°
Notch Filtered	41°
Kalman Filtered	46°

Table 6-1. Phase Margins of Different Filter Approaches

These results show that the Kalman filter has improved the phase margin, not only compared to the notch filter, but also the unfiltered system. The reasons for this were discussed in Chapter 4.

In order to improve the response of the Kalman filter either some modifications are required, or a notch filter would need adding to the system to alter that mode.

6.5 Filter Improvements

Figure 6-5 and Figure 6-6 showed that the Kalman filter in its initial form does not satisfactorily reduce the structural coupling problems in the aircraft model. Examination of Kalman filter frequency response in the Bode diagram (Figure 6-4) indicates that it is not filtering out the flexible modes as well as it did for the beam model.

The beam model was developed with no coupling between the rigid and flexible modes, and when the system and filter models were identical, the Kalman filter removed the flexible mode data entirely. The aircraft model includes some coupling between all of the modes (rigid and flexible). This results in a more accurate model, but means that even with the output from the Kalman filter flexible mode states set to zero, there will still be some influence from the flexible modes. This section looks at reducing this effect.

From equations (6 1) to (6 6), the Inertia matrix (**A**) influences both the **a** and **b** matrices in state space form. This matrix would then be a sensible choice for where to start looking at reducing the effects of the coupling between rigid and flexible modes.

The **A** matrix is broken down into 3 main regions (flexible modes, control modes, and rigid modes), with coupling between each region.

$$A = \begin{bmatrix} [\mathit{flexible}] & [c-f] & [r-f] \\ [f-c] & [control] & [r-c] \\ [f-r] & [c-r] & [\mathit{rigid}] \end{bmatrix} \qquad (6\ 13)$$

Equation (6 13) shows these regions The coupling between the control modes and the other modes (marked [f-c] and [c-r] above) are very important to the operation of the model, so will not be touched The coupling between the rigid and flexible modes is less important, and removing this is less likely to have an effect

$$A = \begin{bmatrix} [\textit{flexible}] & [c-f] & [0] \\ [f-c] & [\textit{control}] & [r-c] \\ [0] & [c-r] & [\textit{rigid}] \end{bmatrix} \tag{6 14}$$

In equation (6 14), the regions marked [f-r] have been set to zero This new matrix can then be used to make a new state space model for the Kalman filter (the system model remains unchanged), and update the Kalman filter matrices

6 5.1   Kalman Filter

Using the model altered in the previous section, the Q matrix and the Kalman filter gain matrix (K) need to be updated (This is included in Appendix H) The diagonal terms of the Q matrix become.

$$
rows\,1\text{-}23\begin{bmatrix} 2\,1516e\text{-}2 \\ 2\,6282e\text{-}5 \\ 7\,2384e\text{-}6 \\ 1.7928e\text{-}4 \\ 2\,0517e\text{-}3 \\ 7\,5877e\text{-}6 \\ 4\,8722e\text{-}6 \\ 6\,2936e\text{-}6 \\ 2\,5238e\text{-}6 \\ 7.1161e\text{-}4 \\ 3\,8875e\text{-}5 \\ 2\,3150e\text{-}5 \\ 1\,3385e\text{-}7 \\ 4\,2648e\text{-}7 \\ 1\,8820e\text{-}1 \\ 1\,7713e\text{-}1 \\ 8\,0749e\text{-}2 \\ 3.1891e\text{+}1 \\ 2\,2012e\text{+}1 \\ 2\,8729e\text{-}3 \\ 3\,1891e\text{+}1 \\ 2.2012e\text{+}1 \\ 2\,8729e\text{-}3 \end{bmatrix} \qquad rows\,24\text{-}46\begin{bmatrix} 8\,8731e\text{-}1 \\ 1.1229e\text{-}3 \\ 2.9216e\text{-}4 \\ 7\,1650e\text{-}3 \\ 8\,2009e\text{-}2 \\ 2\,9272e\text{-}4 \\ 1\,9592e\text{-}4 \\ 2\,6359e\text{-}4 \\ 1\,1737e\text{-}4 \\ 2\,9164e\text{-}2 \\ 1\,5996e\text{-}3 \\ 9\,3367e\text{-}4 \\ 5\,8142e\text{-}6 \\ 2\,5315e\text{-}5 \\ 7\,5430e\text{+}0 \\ 7\,1011e\text{+}0 \\ 3\,2354e\text{+}0 \\ 1.9448e\text{+}1 \\ 2\,2910e\text{+}0 \\ 1\,0621e\text{-}1 \\ 1\,9462e\text{+}1 \\ 2\,2478e\text{+}0 \\ 1\,0276e\text{-}1 \end{bmatrix} \qquad (6\,15)
$$

6 5 2   Frequency response

Utilising the frequency responses the modified Kalman filter can be compared to the unfiltered system, and the original Kalman filter. Figure 6-7 the frequency response of the modified filter, whilst Figure 6-8 shows the same chart, focused around the first exclusion region
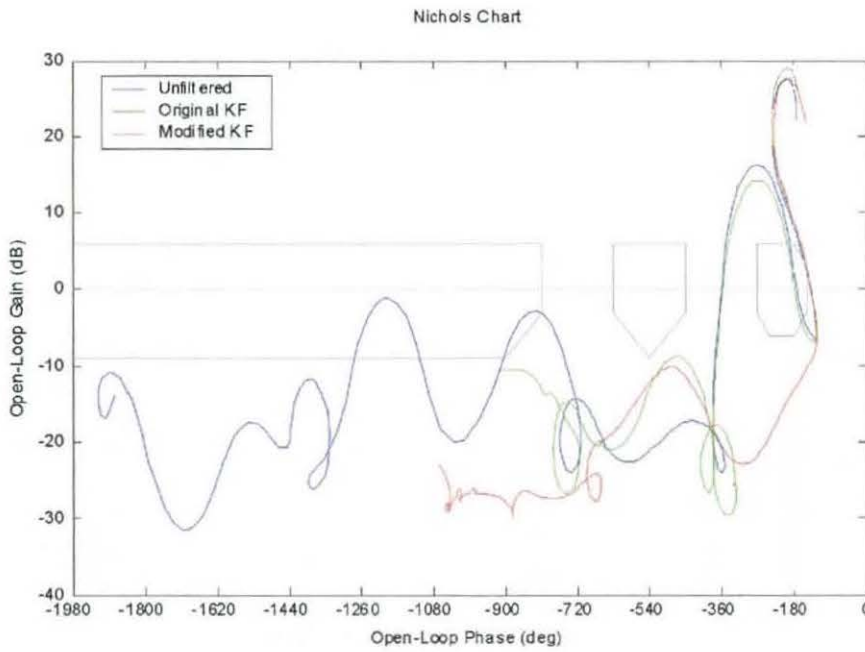
Nichols Chart

Figure 6-7. Frequency Response of Modified Kalman Filter
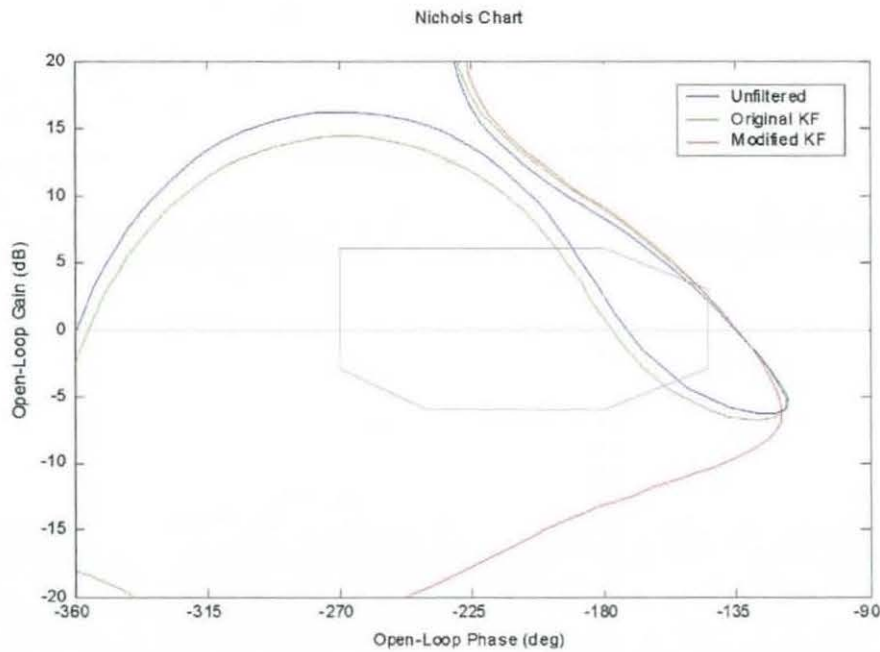
Nichols Chart

Figure 6-8. Frequency Response of Modified Kalman Filter (Nichols Chart)

Figure 6-7 shows that the modified Kalman filter (red plot) has attenuated many of the magnitude spikes associated with the flexible modes, and below 40Hz, the magnitude is lower than both the original Kalman filter (green) and the unfiltered system (blue).

From Figure 6-8, the phase margin or the modified system (using Matlab) can be calculated to be 45°, the modifications have not reduced the phase margin of the system below the unfiltered level. It can also be seen that the first mode has been attenuated to such an extent that the response does not encroach into the exclusion region

6.6   Summary

This chapter has applied the ideas developed on basic models to a highly complicated model of an aircraft system. The aircraft model used is similar to that used as part of the design process for the development of the notch filter solution used at present

When applied to the system using an identical model, the Kalman filter shows some promise, and reduces the effect of a number of the structural modes, although it does not provide a complete solution on its own, leaving the first flexible mode untouched

A modified Kalman filter, which has had some of the coupling between flexible and rigid modes removed, provides a much improved solution, which clears the exclusion regions

7   Conclusions

This thesis has proposed using a Kalman filter to estimate an aircraft's rigid body mode as an alternative to an array of notch filters to overcome the effects of structural coupling   It has been suggested that this approach would reduce the undesirable phase lag added by the notch filters.

The approach has been applied to three models of increasing complexity, and comparisons have been made between the proposed Kalman filter solution, and the traditional notch filter solution

The first model used a combination of two different masses, connected by a spring and damper in parallel, to produce a model with a single flexible mode   This model has been used to demonstrate the principle of the proposed solution   Initial results showed that, whilst the Kalman filter did not significantly alter the magnitude of the flexible mode, it did significantly alter the phase of the mode, and as a result overcame the structural coupling concern   When the performance of the filter was assessed with errors in the system (which the filter was unaware of), the Kalman filter approach showed better tolerance to the changes than the notch filter approach Modifications to the Kalman filter improved this further.

The second model provided two flexible modes by using a model of an aluminium beam   To provide a rigid control mode, which was representative of an aircraft pitch control loop, two sets of spring and damper connected in series were mounted between the beam and a fixed point   Initial results showed that the Kalman filter could remove the effects of the flexible modes and estimate the rigid mode of the beam

With the addition of a simple filter, the model of the beam provided a good representation of the rigid frequency response of an aircraft   This was used to provide a better comparison between the approaches   The effects of altering the flexible mode frequencies by $\pm 7\,5\%$ was examined, and this showed that both approaches to the problem obtained similar performance, although the Kalman filter approach produced

a greater phase margin Neither filter performed especially well when the flexible modes were 7 5% greater than expected

Modifications to the Kalman filter were discussed, and the performance was compared This produced a filter which was more tolerant to both positive and negative changes in the mode frequencies The effects of unmodelled disturbances were also examined, to ensure that the filter did not alter the control characteristics of the system

The beam model has been developed into an experimental rig, which will be used to validate the techniques developed over the course of this research, although to date, only validation of the model has been achieved

The final stage discussed has used a model of an aircraft (developed in conjunction with BAE Systems) to compare the Kalman filter approach to a highly representative system and notch filter solution

In order to achieve a satisfactory response from the Kalman filter, the method used in the previous stages needed to be adapted to take into account the effects of coupling between the rigid and flexible modes The initial Kalman filter did not affect the first flexible mode, this was corrected by the modifications After modifications, the Kalman filter approach provided a response which kept clear of the exclusion regions

The results discussed have demonstrated the potential for the Kalman filter to be used as a replacement for notch filters A particularly valuable feature is that it potentially provides a rigorous model-based approach for structural coupling, whereas the current notch filter approach requires an extremely high level of experience and insight from the designer

7.1   Future Work

Before this technique could be implemented on an aircraft further study is required Some of the questions which need to be answered include·

    a) Does the experimental rig validate the beam model results?

    b) What is the effect of mode frequency changes on aircraft model?

c) How many flexible modes need to be modelled in order to provide a satisfactory response?

d) What process should be used to design the Kalman filter and how can it be proved for flight clearance?

e) How should the Kalman filter be implemented in an aircraft environment?

A three year research project in conjunction with BAE Systems has begun which will look at these questions, and further develop the Kalman filter approach towards an aircraft implementation

References

1 **Aeroservoelastic Encounters**, Felt LR, Huttsell LJ, Noll TE, Cooley DE, *Journal of Aircraft*, Vol 16 No 7, pp477-483

2 **The Effects of Sampled Signals on the Flight Control System of an Agile Combat Aircraft with a Flexible Structure**; Taylor R, Pratt RW, Caldwell BD, *Trans Measurement and Control*, Vol 18 No 3; pp160-164

3 **Effect of Actuator Nonlinearities on Aeroservoelasticity**, Taylor R, Pratt RW, Caldwell BD; *Journal of Guidance, Control and Dynamics*, Vol 19 No 2, pp309-315

4 **Aeroservoelasticity: Key Issues Affecting the Design of Flight Control Systems**, Pratt RW , Taylor R , Caldwell BD ; *Control '94*

5 **Auto-Aeroelastic Mode Coupling, A Comparison of Predicted and Actual Characteristics**, Evans GJ, Beele BJ, *AGARD FMP S&C*, September 1968

6 **Alternative Approach to Aeroservoelastic Design and Clearance**, Taylor R ,Pratt RW ,Caldwell BD , *IEE Proceedings on Control Theory and Applications*, January 1996, Vol 143 No 1; pp1-8

7 **Aeroservoelasticity in the Time Domain**, Cutchins MA , Purvis JW , Bunton RW., *Journal of Aircraft*, Vol 20 No 9 September 1983, pp753-761

8 **ADAM, AN Aeroservoelastic Analysis Method for Analog or Digital Systems**, Noll T , Blair M , Cerra J ; *Journal of Aircraft*, Vol 23 No 11 November 1986, pp853-858

9 **FCS Design for Structural Coupling Stability**, Caldwell BD, *The Aeronautical Journal*, December 1996, pp507-519

10 **Enhanced Vibration Controllability by Minor Structural Modifications,** Haftka RT., Martinovic ZN , Hallauer WL , *AIAA Journal,* Vol 23 No 8 August 1985, pp1260-1266

11 **An Analytical and Experimental Study of a Control Systems Sensitivity to Structural Modifications,** Haftka RT , Martinovic ZN , Hallauer WL , Schamel G , *AIAA Journal,* Vol 25 No 2 Feburary 1987, pp310-315

12 **The Mechanics of Vibration;** Bishop RED, Johnson DC , Cambridge University Press 1960

13 **The Receptance Functions of Uniform Beams,** Milne HK , *Journal of Sound and Vibration;* Vol 131 No. 3 1989, pp353-365

14 **On the Receptance Functions of a Uniform Beam,** Milne HK , *Journal of Sound and Vibration,* Vol 146 No 1 1991, pp176-180

15 **Equivalent Dynamic Beam-Rod Models of Wing Structures,** Lee U , *Aeronautical Journal,* December 1995, pp450-457

16 **A Dynamic Tool for Design and Troubleshooting,** Dovel G, *Mechanical Engineering;* March 1989, pp82-86

17 **A New Approach to Linear Filtering and Prediction Problems,** Kalman RE , *Trans ASME Journal of Basic Engineering,* Vol 82D March 1960, pp35-45

18 **New Results in Linear Filtering and Prediction Theory,** Kalman RE , Bucy RS , *Trans ASME Journal of Basic Engineering,* Vol 83D March 1961; pp95-108

19 **The Kalman Filter Applied to Aerospace and Electronic Systems,** Hutchinson CE , *IEEE Trans Aerospace and Electronic Systems,* Vol 20 No 4 July 1984, pp500-504

20 **Kalman Filtering with Real Time Applications**, Chui CK , Chen G , Springer-Verlag Berlin, ISBN 3-540-18395-7, 1987

21 **Kalman-Bucy Filters**, K Brammer, Siffling G , Artech House Inc , ISBN 0-89006-294-3, 1989

22 **An Introduction to Applied Electromagnetism**, Christopoulos C ; John Wiley & Sons Ltd , June 1995

23 **Forces on Moving Magnets due to Eddy Currents**, Reitz JR., *Journal of Applied Physics*, Vol 41 No 5 April 1970; pp2067-2071

24 **Drag Force of an Eddy Current Damper**, Weinberger MR., *IEEE Trans. Aerospace and Electronic Systems*; Vol 13 No 2 March 1977, pp197-200

25 **Eddy Current Damping Due to a Linear Periodic Array**, Perry MP , *IEEE Trans. Magnetics*, Vol 20 No 1 January 1984, pp149-155

26 **Unipolar Induction Braking of Thin Metal Sheets**, Schieber D , *Proceedings of the IEE*, Vol 119 No 10 October 1972, pp1499-1503

27 **Optimal Dimensions of Rectangular Electromagnet for Braking Purposes**, Schieber D , *IEEE Trans. Magnetics*, Vol 11 No 3 May 1975, pp948-952

28 **Flight Dynamics Principles**, Cook MV , Arnold, 1997

29 **Initial Studies / Concepts for Data Consolidation**, Pearson J T

30 **FCS – Design Installation and Test of Piloted Aircraft, General Specification for, MIL-F-9490D**

KALMAN FILTERS FOR REDUCING THE EFFECTS OF STRUCTURAL COUPLING

J T Pearson[*], R M Goodall[*], S A Halsey[*], B D Caldwell[+]
[*]*Systems and Control Research Group, Loughborough University UK*
[+]*Military Aircraft and Aerostructures British Aerospace*

ABSTRACT

For modern combat aircraft the disturbance to the inertial measurement signals by components caused by the flexibility of the airframe is problematic Current solutions use a series of notch filters to remove these troublesome components, but this introduces phase delay into the safety critical flight control loop This paper presents some preliminary results from a research project investigating the use of Kalman Filters to reduce the effects of structural coupling

1. STRUCTURAL COUPLING PROBLEM

One of the major concerns of the designers of flight control systems (FCS) is the interaction between the aircraft dynamics (both rigid and flexible) and the FCS itself [1]-[4]
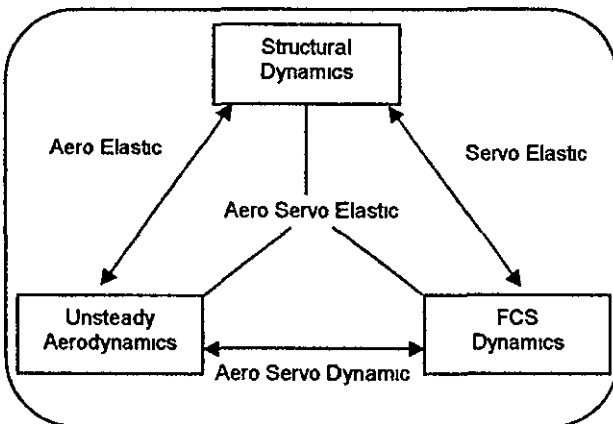

Figure 1 Aircraft Interactions

These interactions are termed Structural Coupling (more commonly known as Aero-Servo-Elasticity ASE in the USA) These interactions need to be examined, and where necessary filtered to limit the feedback of signals (from flexible modes) which can cause instability and which could have safety implications for the aircraft Figure 1 shows these (and other) interactions

The current solution to this problem is to include a number of notch filters in the control loop (Figure 2) These remove the flexible mode frequencies, but at the cost of introducing undesirable phase lag into the system As aircraft systems become increasingly complex, so the structural coupling interactions also become more complicated This in turn requires a solution that is likely to comprise a larger number of

filters to solve the problem The task is made more difficult by the stability margins for the safety of the aircraft, forcing a trade off between desired attenuation and required maximum permissible phase lag
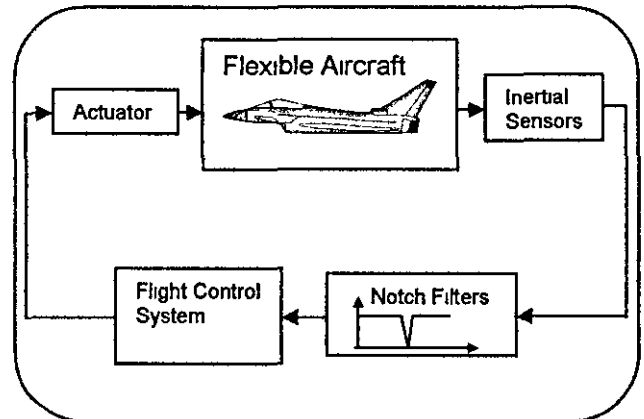
Figure 2 Flight Control Loop

2. THE NOTCH FILTER SOLUTION

The notch filters provide attenuation at the flexible body frequencies, thereby removing the interaction between the FCS and the aircraft's flexible modes However, the filter adds phase lag at low frequencies which has a destabilising effect for the main control loop The design of the notch filter solution is a complicated and time-consuming task

The designer requires knowledge of the frequency response of the aircraft for the various configurations in which it can be flown These responses need to cover all the possible modal frequencies, they can then be combined together to provide an overall response from which the notch filter solution can be developed

The design of the solution is an iterative process, designing a filter for each modal frequency in turn in order to reduce the response gain to the required level

This process involves a trade off between the level of attenuation achieved by the filters, and the rigid aircraft stability margins This can result in the redesign of the solution a number of times to achieve the optimal solution

The notch filters used in this study have been implemented using the following form

$$F(s) = \frac{s^2 + \omega^2}{s^2 + s\omega\zeta + \omega^2}$$

Where ω is the notch frequency (in rad/s), and ζ is the damping ratio

3. THE KALMAN FILTER

The Kalman Filter is a model based estimation algorithm, with different formulations enabling the estimation of past, present and even future states It is implemented using a set of recursive mathematical equations, but these are not repeated here since Kalman filtering is well documented in the literature [5]

The filter estimates the state vector of a system using a form of feedback control At each iteration the filter estimates the system states and then obtains corrective feedback in the form of measurements, which are corrupted by measurement noise
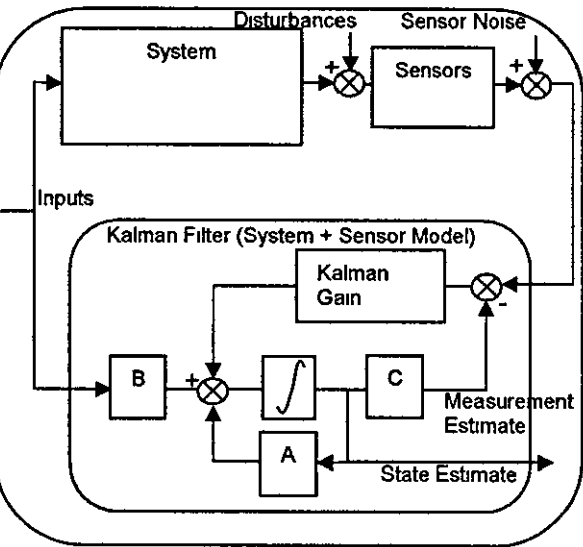

Figure 3 Kalman Filter Block Diagram

The aim of this work is to replace the notch filters shown in Figure 2, with a Kalman filter based solution – refer to Figure 4   The measurements available to the filter will typically be from inertial sensors such as accelerometers and rate gyros   These measurements contain both rigid body information giving the gross movement of the airframe (which is what the FCS is controlling) and the effects of the flexible body   The filter uses these measurements combined with a mathematical model of the aircraft to provide estimates of the rigid body aircraft motion as well as estimates of the flexible body motions

The rigid body information is required by the Flight Control System (FCS)   The flexible body information may prove useful to other systems, for example a Health Usage Monitoring System (HUMS)
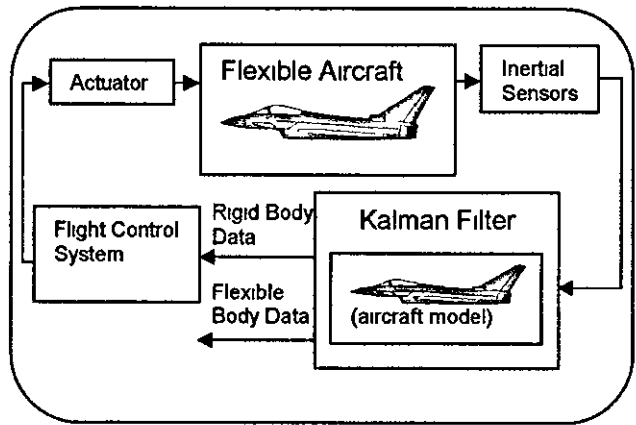
Figure 4 Kalman Filter Implementation

4. TWO MASS MODEL ANALYSIS

The purpose of this stage of work was to develop a solution to the problem on a simple model, and then carry out a comparison between the existing notch filter approach and the model based estimator solution

The model used consists of a large mass (representing the rigid body) and a small mass (to provide a flexible mode) connected together by a spring and damper   There is a position sensor on the smaller mass, and an actuator, which is connected between the large mass and ground, can be used to provide feedback control of the position of the larger mass – see Figure 5

Note that, although this is not directly representative of the FCS problem, it is nevertheless typical of a real problem   Resilience in an actuator can cause a similar flexibility effect, in particular this is encountered with hydraulic actuators
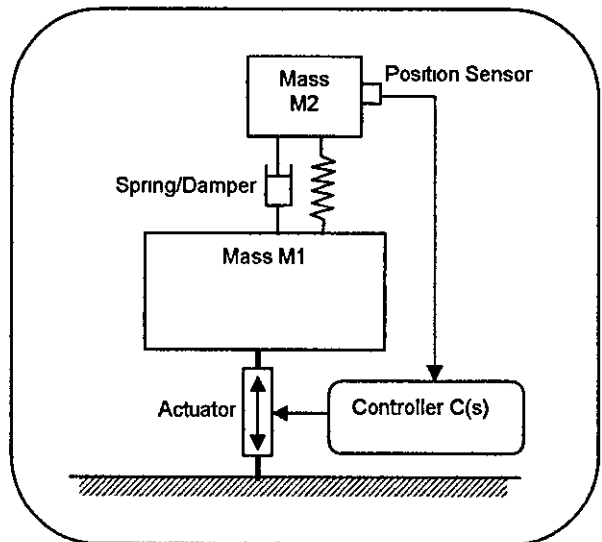
Figure 5- Two Mass Model

The model parameters have been chosen to provide a frequency representation of the first flexible mode of an aircraft   The controller used in this model has deliberately been designed badly, to destabilise the system, so requiring the implementation of filtering This will allow a comparison of how the different techniques are affected by errors in the model parameters that are expected
In this model the notch frequency has been set at 5 51Hz (34 6 rad/s − the frequency of the small mass/spring combination representing the flexible mode frequency) and the damping ratio has been set to the smallest value whereby the system could be stabilised

For this model, a Kalman-Bucy filter implementation has been used The Kalman filter algorithm is not described in this paper as it is widely documented in the public domain
Two inputs are supplied to the filter
          Controller output signal
          Sensor output signal
The filter has a single output
          Estimated position of the large mass
The measurement noise covariance matrix (R) has been set to match the covariance of the measurement noise The process noise uncertainty matrix (Q) has been tuned to provide the desired performance In this model, a steady state Kalman gain matrix has been used

Simulation Results
Figure 6 shows a comparison of open-loop Nichols plots for both the Kalman Filter based system and for the notch filter based system The input is the demand to the actuator and the output is the signal from the position sensor The Kalman filter response clearly shows the effect of using a feedback signal from the position of the principal mass (via estimation) The notch filter response shows the large phase lag introduced at higher frequencies, which is a consequence of filtering measurements from the secondary mass These are preliminary results and it is anticipated that by taking a
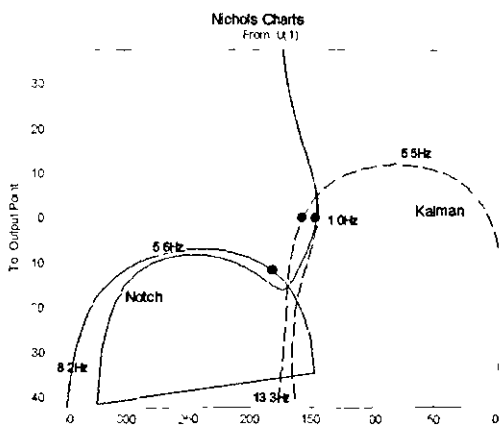
Figure 6- Nichols plot for Kalman Filter and Notch Filter based system

linear combination of state estimates that it should be possible to introduce some phase lead at around 1 0Hz

for the Kalman filter solution, thereby improving the phase margin

As Figure 7 shows the Kalman filter output has a much more accurate estimation of the position of the large
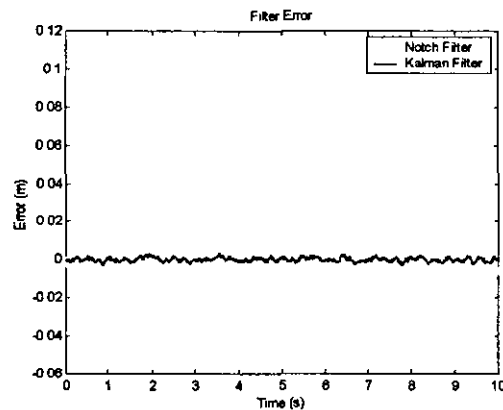
Figure 7- Two Mass Model Results

If the differences between phase lag for the notch filter and the Kalman filter are compared, it can be seen that again the Kalman filter provides an improvement

	0 5 Hz	1 Hz	1 5 Hz	2 Hz	2 5 Hz	3Hz
Notch	0 126	0 195	0 276	0 380	0 610	1 054
Kalman	-0 002	0 007	0 004	-0 027	-0 031	0 028

Table 1 Phase lag shown in degrees

One of the other important issues of interest is the robustness of the filtering technique to errors in the model   In this work, the error robustness has been assessed by altering the size of the smaller mass from half to twice the size that the Kalman filter (or notch filter) is expecting   The peak error (between filter output and actual large mass position) is shown below for each filter
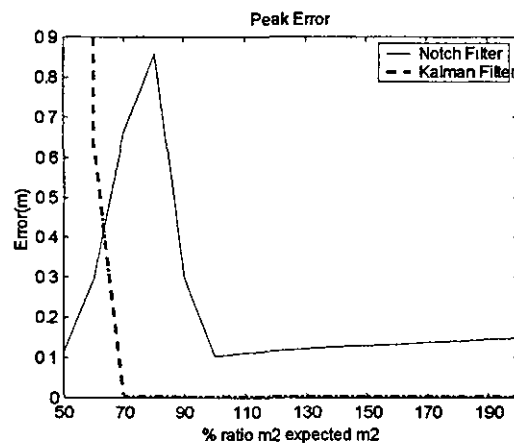
Figure 8- Two Mass Model Robustness Results

As can be seen, the Kalman filter provides a lower estimation error across the majority of the specified range It does however become unstable when the small mass is less than 70% of the expected size This loss of stability can be improved by tuning the Q matrix

5. FLEXIBLE BEAM ANALYSIS

A beam has been used as a next stage towards a more representative aircraft model The beam model consists of both rigid body and flexible body modes, enabling the effects of the flexible modes on the measurements used by the control system to be assessed

The method used here to model the flexibility is based on Bernoulli-Euler theory, and this is described in detail in [6]

For small deflections (v) of the beam, the motion perpendicular to the longitudinal axis (x) of the undeflected beam is described by the closed form of the Bernoulli-Euler equation

$$\frac{\partial^2 v}{\partial t^2} + \frac{EI}{A\rho} \frac{\partial^4 v}{\partial x^4} = 0$$

The solution is non-trivial but can be conveniently expressed in the following form,

$$v = \alpha_{xh} F e^{i\omega t}$$

where α_{xh} is called the receptance between a point of application of the force at a distance x along the beam, and h the point of measurement

$$\alpha_{xh} = \sum_{n=1}^{\infty} \frac{\Phi_n(x)\Phi_n(h)}{M(\omega_n^2 - \omega^2)}$$

The characteristic function $\Phi_r(x)$ represents the effect of a force applied at a point x along the beam of length l, and $\Phi_r(h)$ represents the measurement of the effect of that force at a point h along the beam, both for the nth mode or frequency
The receptance model for each flexible mode can be transformed into a state space representation as follows
Defining a generalised co-ordinate q_r for the nth mode

$$\ddot{q} = \frac{F}{M}\Phi_n(x) - q_n \omega_n^2 - 2\varsigma \dot{q}_n \omega_n$$

$$y(h) = q_n(t)\Phi_n(h)$$

In addition, this can be written in state space form as

$$\begin{bmatrix} q_n \\ \dot{q}_n \end{bmatrix} = \begin{bmatrix} 0 & 1 \\ -\omega_n^2 & -2\varsigma\omega_n \end{bmatrix} \begin{bmatrix} q_n \\ q_n \end{bmatrix} + \begin{bmatrix} 0 \\ \frac{\Phi_n(x)}{M} \end{bmatrix} F$$

The output or measurement equation is defined as

$$[z_n] = \begin{bmatrix} -\Phi_n(h)\omega_n^2 & -\Phi_n(h) 2\varsigma \omega_n \end{bmatrix} \begin{bmatrix} q_n \\ q_n \end{bmatrix} + \begin{bmatrix} \frac{\Phi_n(h)\Phi_n(x)}{M} \end{bmatrix} F$$

Where z_n is beam deflection at the measurement point due to the nth flexible mode

It is straightforward to include extra input terms to allow for moments exciting the beam's flexible modes, and also to include extra output terms which enable the slope of the beam to be calculated at a given measurement point

Kalman Filter Formulation
In the first stage, the three IMUs are spaced out along a simple beam The beam has been constrained to have only two degrees of freedom, one rotational and one translational In addition to this, simple sensor models have been used, although the fidelity of the sensor models and the beam model itself will be increased as the study progresses Figure 9 shows a representation of the simple beam model
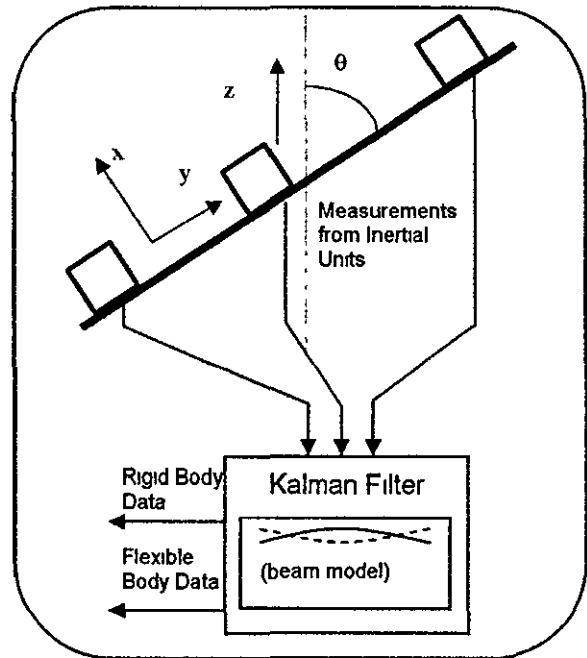
Figure 9 Beam Model

A discrete state-space representation of the beam that can be used in the Kalman filter is

$$\begin{bmatrix} x \\ y \\ \delta\theta \\ \theta \\ \theta \end{bmatrix}_{k+1} = \begin{bmatrix} 1 & 0 & 0 & 0 & 0 \\ 0 & 1 & 0 & 0 & 0 \\ 0 & 0 & 1 & 0 & 0 \\ 0 & 0 & 0 & 1 & T \\ 0 & 0 & 0 & 0 & 1 \end{bmatrix} \begin{bmatrix} x \\ y \\ \delta\theta \\ \theta \\ \theta \end{bmatrix}_k + \begin{bmatrix} w_{\ddot{x}} \\ w_{\ddot{y}} \\ w_{\delta\theta} \\ w_\theta \\ w_{\dot{\theta}} \end{bmatrix}$$

The states have been chosen to be the acceleration perpendicular (x-axis) to the beam's longitudinal axis (y-axis), the acceleration along the y-axis (not used in the results reported here), the incremental change in the rotation angle, the rotational rate and the rotational acceleration Associated with each state is some process uncertainty and this is represented by the inclusion of white Gaussian noise in the state space model

The measurements are from the three accelerometers and three gyros distributed along the beam (and associated with each sensor is measurement noise)

$$
\begin{bmatrix} a_1 \\ a_2 \\ a_3 \\ g_1 \\ g_2 \\ g_3 \end{bmatrix}_k = \begin{bmatrix} 1 & 0 & 0 & 0 & h_1 \\ 1 & 0 & 0 & 0 & h_2 \\ 1 & 0 & 0 & 0 & h_3 \\ 0 & 0 & 0 & 1 & 0 \\ 0 & 0 & 0 & 1 & 0 \\ 0 & 0 & 0 & 1 & 0 \end{bmatrix} \begin{bmatrix} \ddot{x} \\ \ddot{y} \\ \delta\theta \\ \theta \\ \ddot{\theta} \end{bmatrix}_k + \begin{bmatrix} v_{a1} \\ v_{a2} \\ v_{a3} \\ v_{g1} \\ v_{g2} \\ v_{g3} \end{bmatrix}
$$

Where h1, h2 and h3 are the respective distances of the three IMUs from the beam's centre of gravity

The above equations can be re-expressed as

$$
x^r_{k+1} = \begin{bmatrix} A^r \end{bmatrix} x^r_k + w^r
$$

$$
y^r = \begin{bmatrix} C^r \end{bmatrix} x^r_k + v
$$

where the superscript r denotes rigid body dynamics, w the process uncertainty and v the measurement noise If the structural coupling problem is to be dealt with by the Kalman filter then the flexible body modes need to be modelled and included The flexible mode model described previously needs to be transformed to a discrete state space representation and then it can be appended to the model defined above

The flexible dynamics model is defined by

$$
x^f_{k+1} = \begin{bmatrix} A^f \end{bmatrix} x^f_k + \begin{bmatrix} B^f \end{bmatrix} u + w^f
$$

$$
y^f = \begin{bmatrix} C^f \end{bmatrix} x^f_k + \begin{bmatrix} D^f \end{bmatrix} u
$$

The inputs to the flexible dynamics are forces and moments (or linear and rotational accelerations) acting on the beam, and these are estimated by the Kalman filter, i e

$$
\begin{bmatrix} x \\ \dot{\theta} \end{bmatrix}_k = \begin{bmatrix} 1 & 0 & 0 & 0 & 0 \\ 0 & 0 & 0 & 0 & 1 \end{bmatrix} \begin{bmatrix} x \\ y \\ \delta\theta \\ \theta \\ \theta \end{bmatrix}_k
$$

this can be re-expressed as

$$
u = \begin{bmatrix} C^c \end{bmatrix} x^r_k
$$

The combined state space model is then

$$
\begin{bmatrix} x^r_{k+1} \\ x^f_{k+1} \end{bmatrix} = \begin{bmatrix} A^r & 0 \\ B^f C^c & A^f \end{bmatrix} \begin{bmatrix} x^r_k \\ x^f_k \end{bmatrix} + \begin{bmatrix} w^r \\ w^f \end{bmatrix}
$$

$$
y = y^r + y^f = \begin{bmatrix} C^r + D^f C^c & C^f \end{bmatrix} \begin{bmatrix} x^r_k \\ x^f_k \end{bmatrix} + v
$$

Clearly, the number of flexible modes included in the model determines the total number of states in the above equations How many modes are to be included can only be answered by the use of more complex and representative models

Simulation Results
A rotary actuator is used to control the rotational velocity of the beam The rationale for this is to mimic a pitch control loop within an aircraft's flight control system Outputs from the notch filter or from the Kalman filter are fed through a controller which generates an actuator demand signal

Figure 10 shows the open loop frequency response for the beam model, with the Notch filter (dashed) and Kalman filter (solid) The input is the demanded angular beam rate, and the output is the system feedback signal (angular rate)

Figure 10 Beam model frequency response
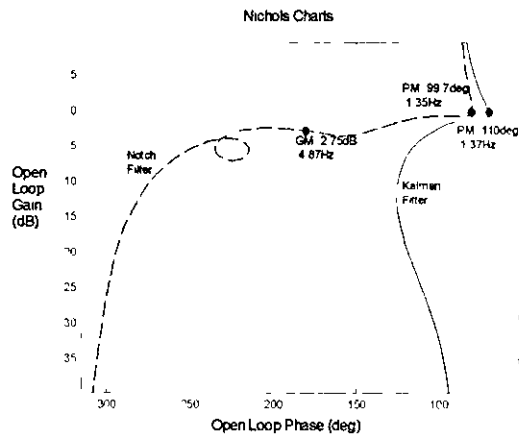
As can be seen from the Nichols plot, using the Kalman filter has increased the phase margin (by about 10deg) and with the Kalman filter the gain margin becomes infinite

Figure 11 shows the estimation error (error between sensor reading and filter output) Both approaches result in a similar level of estimation error, the Kalman filter providing marginally lower levels transiently

Figure 12 shows the estimated angular rate generated by the notch filter and by the Kalman filter Clearly the Kalman filter has removed the effects of the flexible modes from the control loop The notch filter reduces the effects of the flexible modes, but does not manage to eliminate them entirely
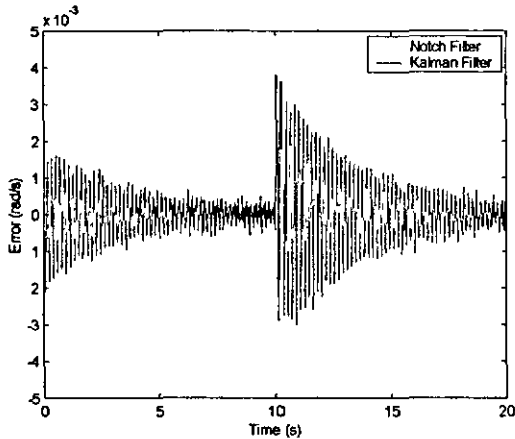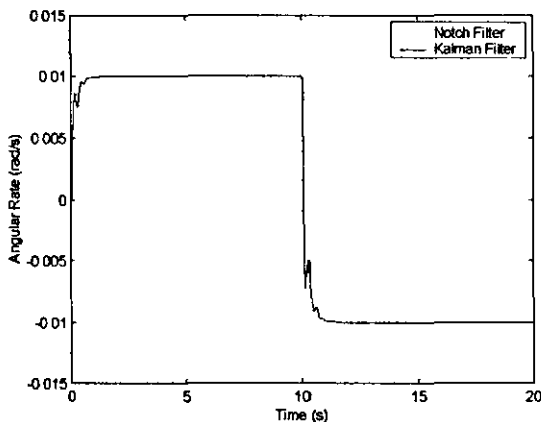

Figure 11 Beam model estimation errors

Figure 12 Beam model feedback signals

6. CONCLUSION

Initial indications are that a Kalman Filter based approach can be used to estimate flexible modes, without introducing significantly worse levels of phase lag at low frequencies than a notch filter

Currently a more complex model which represents the aircraft structural problem more closely is being developed in conjunction which British Aerospace Military Aircraft and Aerostructures Future research involves a practical rig-testing phase, which will aim to validate the algorithms developed in the simulation analyses

REFERENCES

1) Pratt, R W, Taylor, R., Caldwell, B D, Aeroservoelasticity **Key issues affecting the design of flight control systems** IEE International Conference on Control, Control 94, Conference Publication Number 389, pp1522-1527, March1994

2) Taylor, R , Pratt, R W , Caldwell, B D , **Effect of Actuator Non-linearities on Aeroservoelasticity,** Journal of Guidance, Control, and Dynamics, pp309-315, vol 19, March 1996

3) Caldwell, B D , **Flight Control/Structural Coupling – BAE Warton Experience in Aeroservoelasticity** Institute of Mechanical Engineers, Aerotech 92, UK, 1992

4) Caldwell, B D., **FCS Design for Structural Coupling Stability,** The Aeronautical Journal, pp507-519, vol 100, Dec 1996

5) Kalman, R E , **A New approach to Linear Filtering and Prediction Problems,** Transactions of the ASME – Journal of Basic Engineering, pp35-45, March 1960

6) Bishop, R E D and Johnson, D C., **The Mechanics of Vibration,** Cambridge University Press 1960

REDUCING STRUCTURAL COUPLING ON A FLEXIBLE BEAM USING KALMAN FILTERS

S.A.Halsey[*], R.M.Goodall[*], J.T.Pearson[*], B.D.Caldwell[+]

[*]*Systems and Control Research Group, Loughborough University, Loughborough, LEICS, LE11 3TU, UK. Email s a halsey@lboro ac uk, r m goodall@lboro ac uk, j t pearson@lboro ac uk*

[+]*BAE Systems, Warton Aerodrome, Preston, LANCS, PR4 1AX, UK. Email brian caldwell@baesystems com*

Abstract Structural coupling is the disturbance to the aircraft's inertial sensors caused by the flexibility in the airframe, and is particularly problematic for modern combat aircraft The current solution uses a series of notch filters to remove the structural frequencies, but these introduce significant phase delays into the control loop This paper presents some experimental and theoretical results from a flexible beam, and the use of Kalman filters to reduce the effects of structural coupling This work is part of an ongoing project in conjunction with BAE Systems *Copyright © 2002 IFAC*

Keywords Structural Coupling, Aerospace, Flight Control, and Kalman Filtering

1 INTRODUCTION

Structural Coupling is a phenomena caused by interactions between the Flight Control System (FCS) of an aircraft, and the structural dynamics and aerodynamics of its airframe Structural coupling can cause high frequency oscillations of the control surfaces due to propagation of signals (inertial sensors) caused by the flexibility of the airframe, through the IMU and the flight control laws

Instability of this feedback loop could result in degradation of the structure though fatigue, and/or degradation of the performance of the FCS through saturation of the control surface actuators Both of these effects have serious safety implications for the aircraft

2 STABILITY MARGIN LIMITS

Prevention or limitation of structural coupling is an integral part of the design of the FCS Frequency domain methods based upon the Nyquist stability criterion in conjunction with Bode and Nichols charts are commonly used in the design process

System design stability and clearance requirements are given in the form of gain and phase margins, and exclusion regions on the Nichols chart (Caldwell

1996) These regions follow the 5dB line on the closed loop Nichols chart axes Around the -180° 0dB point, this limit is bounded by +35°, -90°, and –6dB Around the -540° 0dB point, it is bounded by ±90° These two regions are shown in Figure 1

It is the objective of the FCS designer to ensure that the frequency response of the open loop control system does not encroach on these exclusion regions under all expected flight conditions
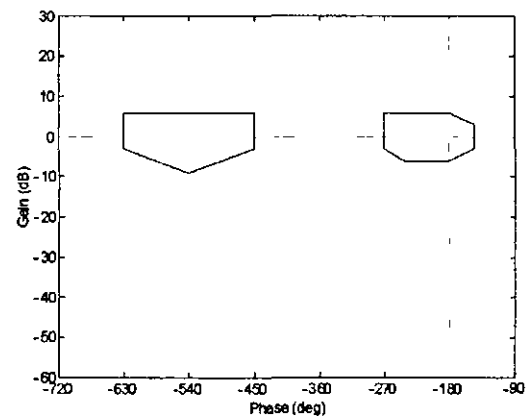

Figure 1 Stability Margin Exclusion Regions

3   CURRENT TECHNIQUES

At present, notch filters are used to attenuate the effects of structural coupling The filters are placed in the control system feedback paths, and provide the FCS with a signal where the components of the feedback caused by the flexibility of the airframe have been attenuated, in the sensor output paths, reducing the structural frequency components in the sensor signals to the control loop, in the actuator demand paths, minimising the forward propagation of the high frequency signals   Figure 2 shows the placement of these filters

Whilst the filters can achieve the desired goal of minimizing the structural coupling effects, they introduce phase lag into the control system at low frequencies The summation of the phase lag from all the filters can lead to significant total delay, which may impinge upon the stability margins of the control loop, which must be maintained, or effectively reduce the bandwidth of the actuators, compromising the FCS performance

In general the notch filter solution arrived at will be unique to a specific aircraft The design requires data from aircraft models and also from ground and flight testing   In addition the mode frequencies can typically vary significantly, according to the aircraft configuration, a factor which also needs to be taken into account

In recent years, with the development of more sophisticated and aerodynamically unstable aircraft, so the complexity of the notch filter solution has increased   The Jaguar and Tornado aircraft both required 1 notch filter on each feedback axis   In comparison to these two aircraft, the EAP (Experimental Aircraft Programme) aircraft required 7 notch filters on the pitch axis alone

The design is an iterative process, involving a trade off between the desired filter attenuation and the phase lag introduced by the filters This process can become very time consuming, and any alterations to the aircraft specification can result in the need to redesign the whole system of filters
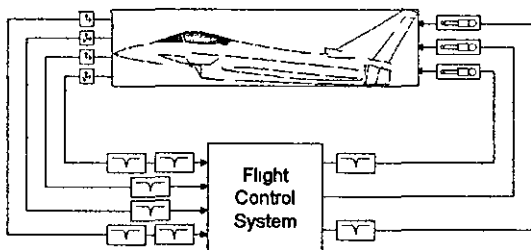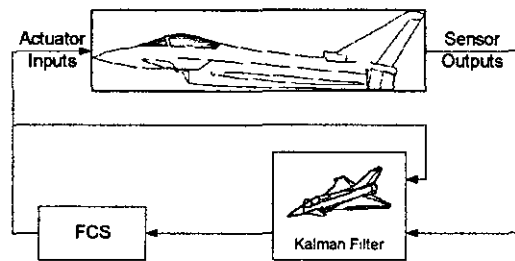

Figure 3 Kalman Filter FCS Loop

4   PROPOSED TECHNIQUE

As an alternative to the use of notch filters, it is proposed that a model-based approach could be used The Kalman filter provides a state estimate based upon a combination of information from system inputs and outputs, and a model of the system (Kalman 1960)

A modern FCS may provide command and/or stability augmentation functions based on measurements of the aircraft motion   The measurements available to the FCS (generally accelerometers and angular rate gyroscopes) contain both rigid and flexible modes The Kalman filter can use this information combined with a model of the aircraft to provide an estimate of the rigid motion of the aircraft, free from the corruption of the flexible modes Figure 3 shows this arrangement

This approach has a number of potential benefits These include
- a)   Reduced Phase Lag
- b)   Simpler design process
- c)   Greater robustness to configuration changes

These are explained in more detail below

4 1 Phase Lag Reduction

Since the Kalman filter approach uses information from the inputs as well as the outputs from the system, preliminary theoretical analysis and computer simulations have shown that this adds less phase lag into the system than a comparable notch filter design

4 2 Simpler Design Process

The Kalman filter uses a mathematical model of the aircraft in order to generate the estimate This model is part of the process that is used to design the notch filters

Since the mathematical equations of the Kalman filter remain unchanged from system to system, only the

Figure 2 Notch Filter FCS Loop

system parameters change The process to design the filter will therefore be much simpler, since it would involve developing the model of the aircraft and inserting this into the filter, as opposed to developing the model, and then designing the filters to accommodate the model

Simplicity largely arises out of increased robustness, fewer design cases are required It also extends to the design of the control laws, since a reduction in the phase lag introduced by the filters leads to easier clearance

4 3 Configuration Change Flexibility

The notch filters are fixed in the aircraft, and so need to be designed to cover all possible changes in frequency dependent upon the current aircraft configuration The Kalman filter approach could be used in two ways to overcome this need for flexibility

First the model in the Kalman filter could easily be updated at the start of each flight Alternatively, the uncertainty parameters in the Kalman filter can be adjusted to provide greater robustness to these changes

5 REPRESENTATIVE MODEL

Previously published work (Pearson, et al, 2000) examined the possibilities of using the proposed solution on a simple model with a single flexible mode – this showed that the concept could be used with success

This work has been extended to a more complicated model, which provides a better representation of an aircraft In addition the model has been designed on a scale that allows experimental validation of the work through the use of a test rig with similar parameters (Section 6)

The beam model is based upon Benoulli-Euler theory (Bishop and Johnson, 1960) This allows an unlimited number of flexible modes to be developed, though only two flexible modes have been modelled in this work

The beam is provided with a pair of spring / damper mechanisms offering rigid 'pitch' and 'heave' modes The gyroscope, controller and actuator configuration provide closed loop pitch rate control which emulates the aerodynamics effects that apply to aircraft control in the longitudinal axis The flexibility of the beam introduces flexible mode components into the sensor feedback signal, and provides the potential for
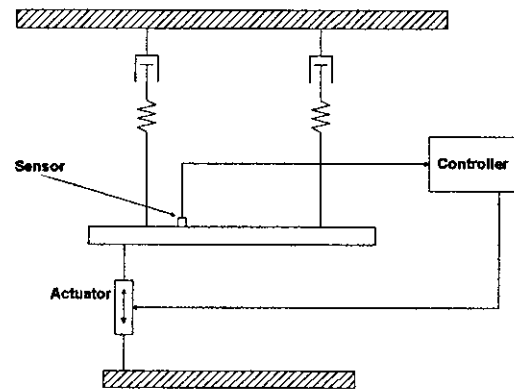

Figure 4 Beam Model

structural coupling The arrangement of this model is shown in Figure 4

The dimensions of the beam and the values of the springs and dampers have been selected to provide rigid and flexible mode frequencies that are representative of those found on an aircraft These are shown in Table 1

Table 1 Beam Mode Frequencies

	Frequency	Damping
Rigid	3 09Hz	47 4%
1st Flexible	5 44Hz	0 8%
2nd Flexible	15 01Hz	0 8%

5 1 Filter Design

As can be seen from Figure 5, whilst the first stability margins of the beam response are adequate, the effects of the flexible modes cause the frequency response of the beam model to encroach into the exclusion regions In fact there is instability due to the response at around 15Hz, because the gain at 540° is close to unity

In order to satisfy the restrictions imposed by the exclusion regions, some filtering is required to attenuate the effects of the flexible modes
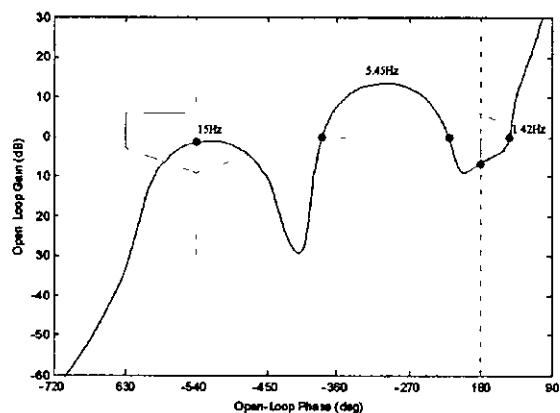

Figure 5 Unfiltered Response

The traditional notch filter approach requires two filters to be added into the system. Table 2 shows the parameters chosen for these filters

Table 2 Notch Filter Parameters

	Notch Frequency	Numerator Damping	Denominator Damping
Filter 1	5 44Hz	3 5%	35 3%
Filter 2	15 0Hz	2 4%	25 6%

These filters alter the frequency response of the system to that shown in Figure 6

The filters have improved the response, however this is at the cost of additional phase lag to the system, leading to degradation of stability margin in the 'rigid' frequency region and encroachment into the exclusion region

The alternative approach uses a continuous Kalman-Bucy filter instead of the notch filters. This uses the same basic model of the beam, although the output from the filter uses only the rigid states of the model. The parameters of the Kalman filter have been developed from the variance of the system states (in response to a step input), and the variance of the sensor noise

The frequency response of the system including the Kalman filter is shown in Figure 7

The Kalman filter has removed the effects of the flexible modes from the system, and remains clear of the exclusion region. This represents an ideal solution, since the Kalman filter and the plant have identical models

5 2 Effects of Errors in Model

As discussed in Section 3, the filter design process in an aircraft system has to account for some variation in the frequencies over which the filters are effective
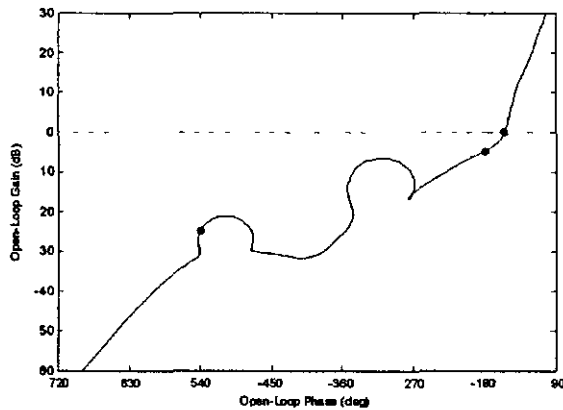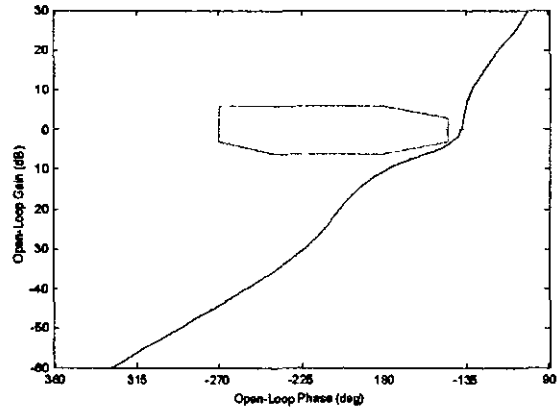

Figure 7 Kalman Filter Response

The notch filter parameters given in Table 2 were chosen to take this into account, in particular the relatively high denominator damping that broadens the range of attenuated frequencies, but also of course increases the phase lag at lower frequencies

In order to compare the effectiveness of the filters when the flexible frequencies change, the stiffness of the beam has been varied by ±15%, which results in a frequency variation of ±7 5%

For both filter types, the filters remain unchanged, expecting no errors in the model

Figure 8 shows the frequency response for the notch-filtered system at the two extremes and also the nominal system

The notch filter is effective except for large positive errors, when there is further encroachment into the first exclusion region

Figure 9 shows the response of the Kalman filter to the same range of frequency variation

Although the flexible modes can be seen when there are errors in the model, the Kalman filter successfully manages to keep the frequency responses outside the exclusion regions
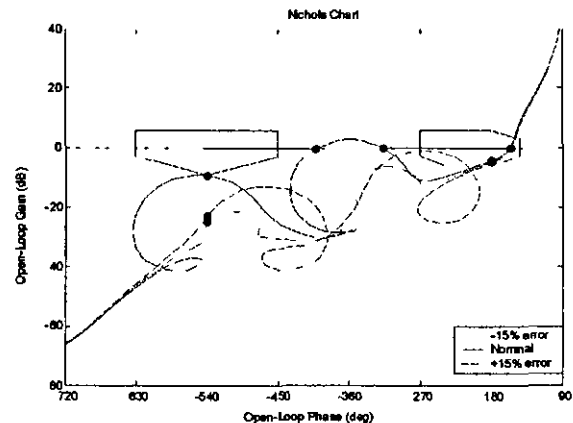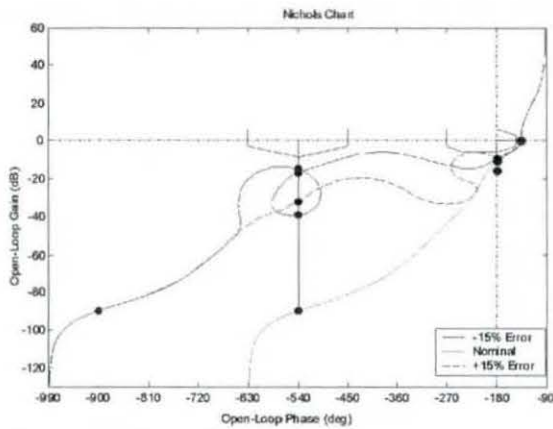

Figure 6 Notch Filtered Response

Figure 8 Notch Filter Error Response

Figure 9. Kalman Filter Error Response

Figure 11. Photo of Experimental Rig

6. EXPERIMENTAL RIG

The beam model was developed with the intention of producing an experimental rig, which will allow the results obtained through modelling to be validated in a practical environment.

The rig has been designed to operate in the horizontal plane, which isolates the flexible modes from the effects of gravity. The beam is suspended on long wires, which allow it freedom of movement. Figure 10 shows a representation of the rig, and Figure 11 shows a photograph of the implementation.

Since the beam is very lightweight, friction in the system is a key consideration; both the actuator and the dampers have been selected to minimize friction. The control input to the beam is provided from a linear electro magnetic actuator. The control system emulating the aircraft pitch loop uses the actuator (representing the control surfaces) to control the angular velocity of the beam about the vertical axis, measured with a solid state gyro.
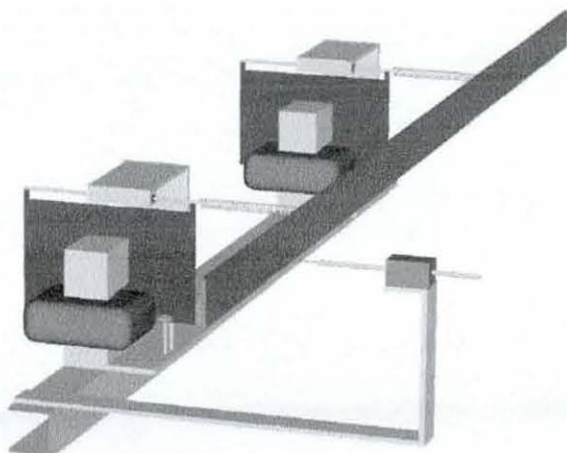
The dampers are also based upon electro magnetism. The movement of a copper sheet (supported on linear bearings) is damped by a magnetic field. A number of accelerometers provide information for data logging purposes.

To date the experimental work has measured the open-loop frequency response of the system (i.e. form actuator force to angular velocity) and this can be seen in Figure 12 together with the theoretical response from the model as described in Section 5. Broadly the responses are similar, although there are significant variations at low frequencies, which relate to the effects of the suspension of the experimental beam.

7. CONCLUSIONS

Computer simulations have show that a Kalman filter based approach has the potential to successfully estimate flexible modes without introducing worse levels of phase lag at low frequencies than a notch filter.

Figure 10. Drawing of Experimental Rig
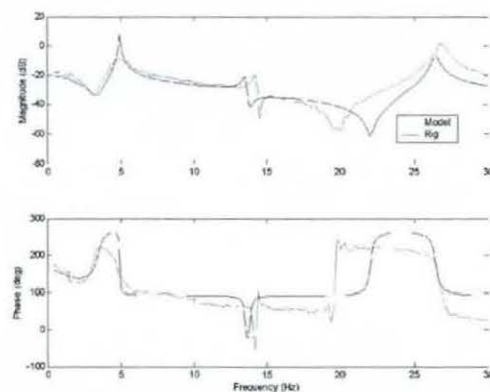
Figure 12. Comparison of Model and Rig Frequency Responses

Preliminary experimental work has validated the basic concept, and investigations are continuing to asses the robustness properties of the notch filter and Kalman filter solutions in a comprehensive manner

Future work will include applying the ideas to a more complex model, developed in conjunction with BAE Systems, which will more closely represent the structural coupling problem

ACKNOWLEDGEMENTS

REFERENCES

Bishop, R E D And Johnson, D C (1960), *The Mechanics of Vibration*, Cambridge University Press, London

Caldwell, B D, (1996) FCS Design for Structural Coupling, *The Aeronautical Journal*, 100, pp506-519

Kalman, R.E, (1960), A New Approach to Linear Filtering and Prediction Problems, *Trans ASME Journal of Basic Engineering*, 82, pp35-45

Pearson, J T, Goodall, R.M, Halsey, S A, Caldwell, B D (2000), Kalman Filters for Reducing the Effects of Structural Coupling, *Control 2000*

Appendix C - Two Mass Simulink Model

This appendix includes the Simulink model used to simulate the two mass model system, and the Matlab m-file which set up the model.
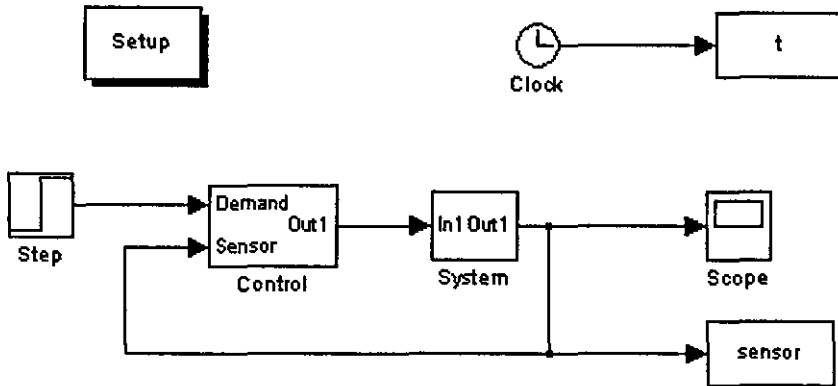
Figure C-1. Top Level Window

Figure C-1 shows the top level of the Simulink model 'Step' creates the input signal which is used to create the model 'Clock' generates an incremental timing signal which can be used during the analysis of the simulation 'Scope' provides a real time graphical representation of the system output
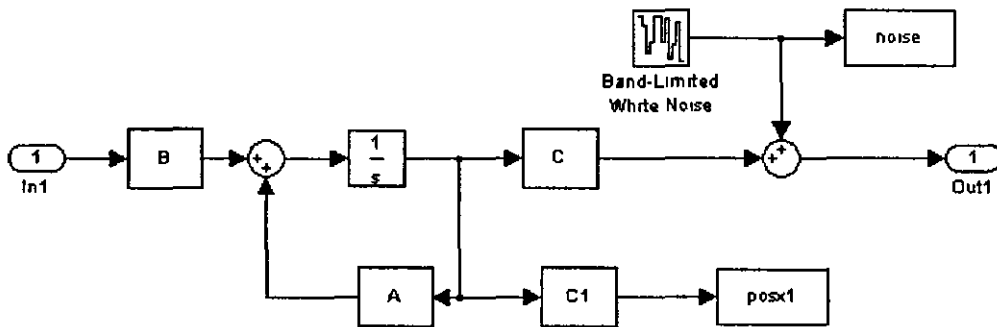
Figure C-2. System Window

Figure C-2 shows the state space system, along with the state space model, noise is added to the output from the system The position of the larger mass (x1) is also recorded, to allow comparison with the Kalman filter estimation
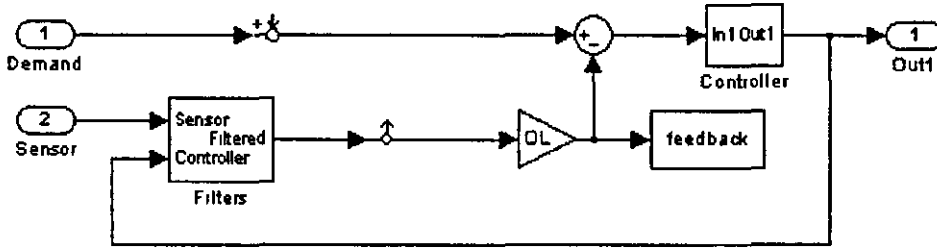
Figure C-3. Simulink Control Window

Figure A-3 includes the components which make up the control aspect of the simulation, i e the controller and the filters
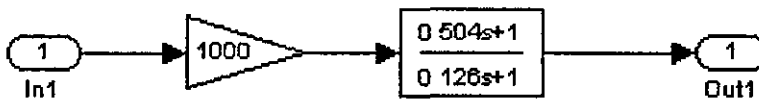
Figure C-4. Controller Window

The controller representation is shown in Figure C-4
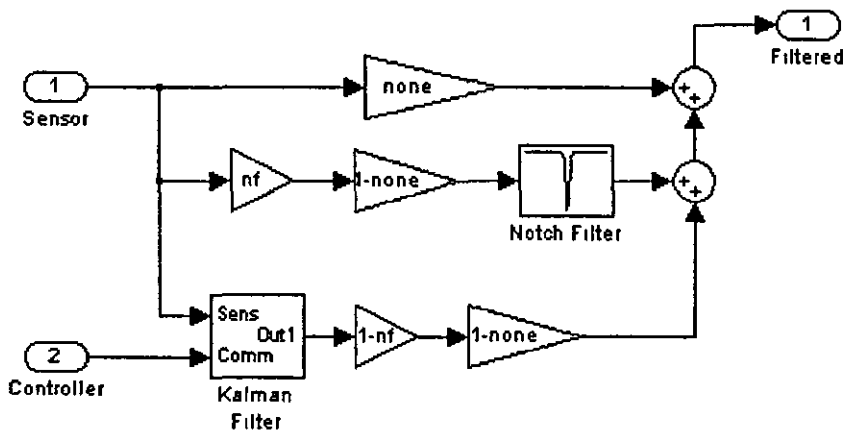
Figure C-5. Filters Window

Figure C-5 shows the filters used in the model and the constants used to allow select the desired filtering option (no filtering, notch filter, or Kalman filter)
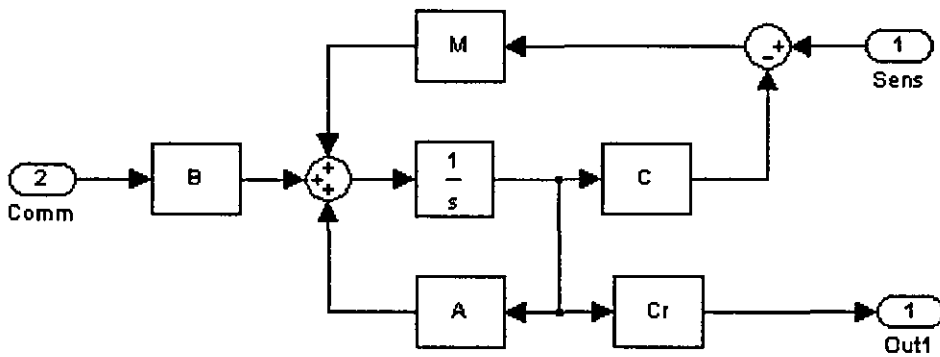
Figure C-6. Kalman Filter Window

The Kalman filter is shown in Figure C-6

```
%basicdata m

%file to initialise original 2 mass model

%Initialise model parameters
m1=50;      %large mass (kg)
m2=25;      %small mass (kg)
k=20000;       %spring constant (N/m)
c=3;        %damping constant (Ns/m)

%Initialise A matrix
A=[ 0      0      1      0;
    0      0      0      1;
   -k/m1   k/m1  -c/m1   c/m1;
    k/m2  -k/m2   c/m2  -c/m2];

%Initialise B matrix
B=[ 0 ; 0 ; 1/m1 ; 0];

%Initialise C matrix (position of M2)
C=[0 1 0 0];

%Initialise 'rigid' C matrix (position of M1)
Cr=[1 0 0 0];

%Initialise D matrix
D=0;

%Initialise Kalman Filter Parameters
G=eye(4);      % 'Process noise' state influence matrix
R=0.01;        % sensor variance matrix
Q=G;           % process noise variance matrix
Q(1,1)=0.001; % x1 variance
Q(2,2)=0.001; % x2 variance
Q(3,3)=0.1;      % x1dot variance
Q(4,4)=0.01;  % x2dot variance

%Get Kalman Filter Gain Matrix
[K P E]=lqe(A,G,C,Q,R);
```

Appendix D- Beam Model Matlab Files

This appendix outlines the Simulink model and Matlab m-files used to simulate the beam model
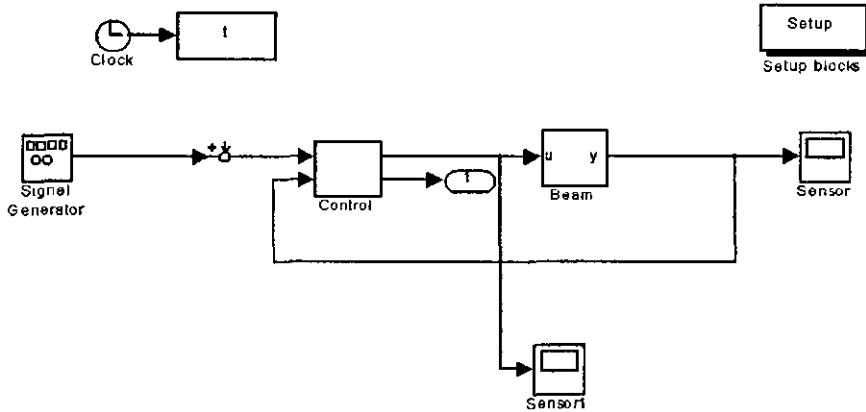
Figure D-1. Top Level of Simulink Model

The top level of the beam Simulink model is shown in Figure D-1 The Beam block contains components related to the beam (e g beam and actuator) Control contains those aspects of the system which are added to the beam (e g Notch or Kalman filter and controller)
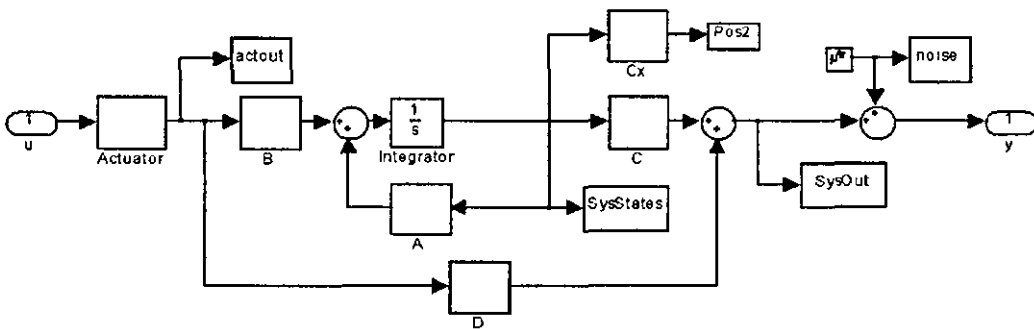
Figure D-2. Beam Block

Figure D-2 shows the arrangement of the state space model of the beam A number of blocks record elements of the system (System states, position of the beam, etc) White noise is added to the output of the beam system It includes the actuator block shown in Figure D-3
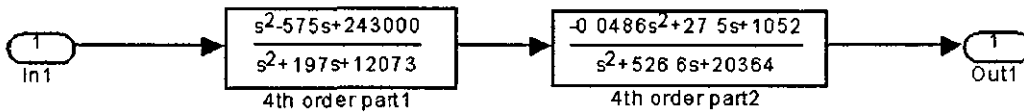
Figure D-3. Actuator Block
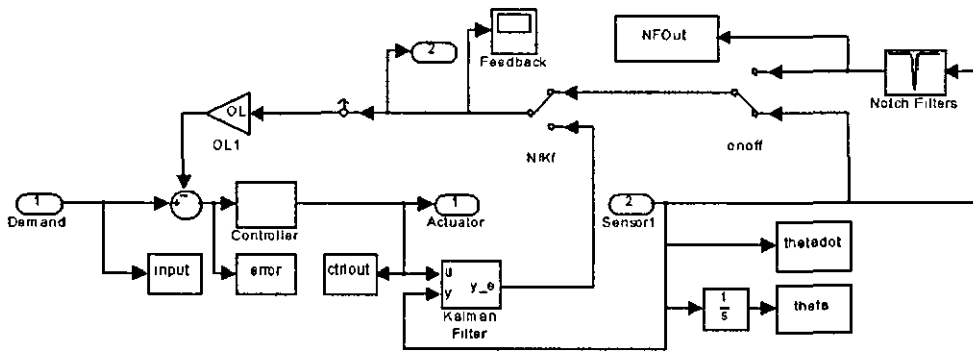
Figure D-4. Control Block

Figure D-4 shows the links between the different blocks which make up the control modules of the system Included are a number of blocks which record data from simulations, as well as the filter blocks and the controller, which is shown in Figure D-5
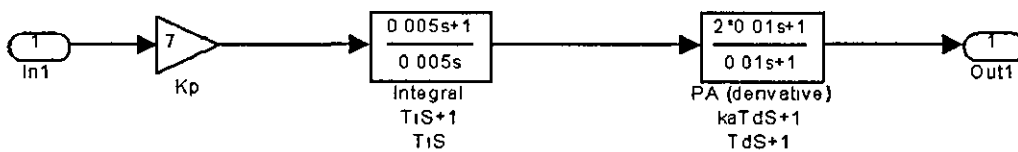
Figure D-5. Controller Block
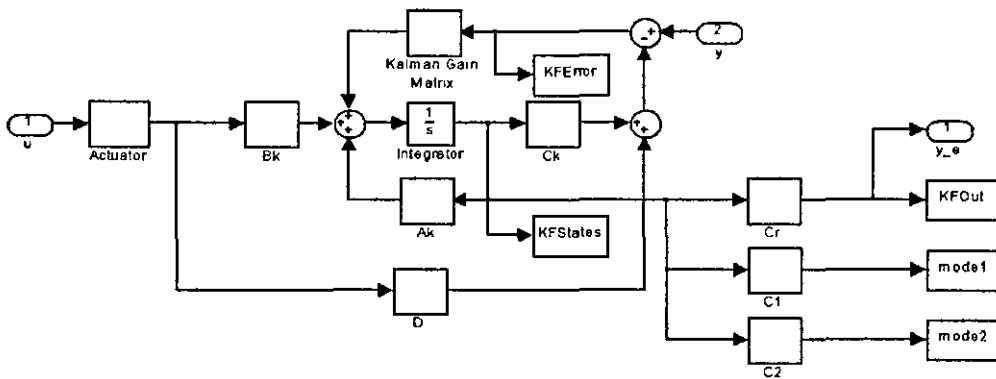
Figure D-6. Kalman Filter Block

The Kalman filter is shown in Figure D-6 It includes an actuator block, which is identical to that shown in Figure D-3 Along with the filter output and state estimation error, the component of each of the modes (both rigid and flexible) is recorded
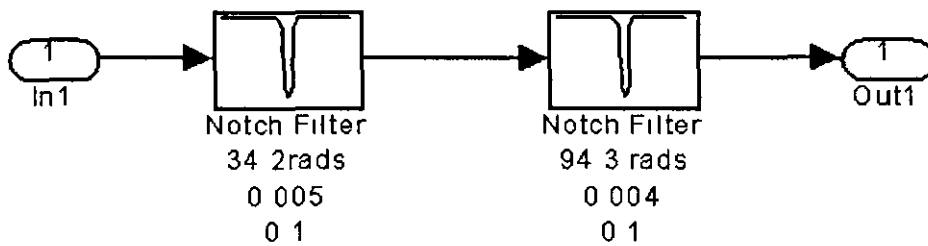
Figure D-7. Notch Filter Block

Figure D-7 shows the notch filter block

```
%%%%%%%%%%%%%%%%%%%%%%%%%%%%%%%%%%%%%%%%%%
% basicdata.m                           %
%  file to set up beam parameters %
%  for basic beam model                  %
%%%%%%%%%%%%%%%%%%%%%%%%%%%%%%%%%%%%%%%%%%
clear;

% beam dimensions etc
l=3.1;          % length of beam in m
w=0.10;         % width of beam in  m
h=0.01;         % height of beam in m
A=w*h;          % cross sectional area of beam
p=2700;         % mass density of beam - Aluminum
m=1*A*p;        % mass of beam
E=70e9;         % Young's modulus - Aluminum
I=(h^3*w)/12;   % moment of inertia of beam
EI=E*I;         % flexural rigidity of beam
zeta=0.008;          % structural damping of beam


lambda=[4.73004 7.85320 10.9956 14.1372 17.2788]/l;


% Set up beam with 2 flexible modes
% for single actuator + springs

N=2;                    % number of modes
k1=3000;        % spring stiffness
c=167;          % damping constant
ns=1.05e-9;         % noise power
Ts=0.01;        % Sample time

for n=1:N,
%calculate beam natural frequencies
omegw(n)=((lambda(n)^4*EI/(A*p))^0.5);
        freq(n)=omegw(n)/(2*pi);

    %calculate characteristic functions
    %measurement points every 1/8 of beam
        a00(n)=frefre(lambda(n),0,l);
        a12(n)=frefre(lambda(n),1*l/8,l);
        a25(n)=frefre(lambda(n),2*l/8,l);
        a37(n)=frefre(lambda(n),3*l/8,l);
        a50(n)=frefre(lambda(n),4*l/8,l);
        a62(n)=frefre(lambda(n),5*l/8,l);
        a75(n)=frefre(lambda(n),6*l/8,l);
        a87(n)=frefre(lambda(n),7*l/8,l);
    a01(n)=frefre(lambda(n),l,l);

        b00(n)=frefrel(lambda(n),0,l);
        b12(n)=frefrel(lambda(n),1*l/8,l);
        b25(n)=frefrel(lambda(n),2*l/8,l);
        b37(n)=frefrel(lambda(n),3*l/8,l);
        b50(n)=frefrel(lambda(n),4*l/8,l);
        b62(n)=frefrel(lambda(n),5*l/8,l);
        b75(n)=frefrel(lambda(n),6*l/8,l);
        b87(n)=frefrel(lambda(n),7*l/8,l);
        b01(n)=frefrel(lambda(n),l,l);
end

Af1=[0 1 ; -omegw(1)^2 -2*zeta*omegw(1)];
Af2=[0 1 ; -omegw(2)^2 -2*zeta*omegw(2)];
```

```
Ar=[0     1   0;
    -k1/m  0   k1/m;
    k1/c  0  -k1/c];

A0=zeros(2,2);
A1=zeros(3,2);
A2=zeros(3,3);

A=[Af1 A0   A1'  A1';
   A0   Af2 A1'  A1';
   A1   A1  Ar   A2;
   A1   A1  A2   Ar];

B1f1=[ 0 ; (a12(1)-1.25*a25(1)+0.25*a75(1))/m ];
B1f2=[ 0 ; (a12(2)-1.25*a25(2)+0.25*a75(2))/m ];
Br1 =[ 0 ; 1.25/m  ; 0 ];
Br2 =[ 0 ; -0.25/m , 0 ];

B=[B1f1;B1f2;Br1;Br2];

s1=0.25;

Cr1=[0 2/l 0];
Cr2=[0 -2/l 0];

%thetadot output matrix
C=[ 0 b37(1) 0  b37(2) Cr1 Cr2 ];


%Position of beam output
Cx=[a00(1) 0 a00(2) 0 1+2*s1       0 0 -2*s1       0 0
    a12(1) 0 a12(2) 0 1+2*(s1-1/8) 0 0 -2*(s1-1/8) 0 0
    a25(1) 0 a25(2) 0 1+2*(s1-2/8) 0 0 -2*(s1-2/8) 0 0
    a37(1) 0 a37(2) 0 1+2*(s1-3/8) 0 0 -2*(s1-3/8) 0 0
    a50(1) 0 a50(2) 0 1+2*(s1-4/8) 0 0 -2*(s1-4/8) 0 0
    a62(1) 0 a62(2) 0 1+2*(s1-5/8) 0 0 -2*(s1-5/8) 0 0
    a75(1) 0 a75(2) 0 1+2*(s1-6/8) 0 0 -2*(s1-6/8) 0 0
    a87(1) 0 a87(2) 0 1+2*(s1-7/8) 0 0 -2*(s1-7/8) 0 0
    a01(1) 0 a01(2) 0 1+2*(s1-1)   0 0 -2*(s1-1)   0 0];

% kalman filter modes
C1=[0 b37(1) 0 0 0 0 0 0];
C2=[0 0 0 b37(2) 0 0 0 0];


D=[0];
Dr=D;

%KF state space model:
[Ark,Brk1,Crk1,Dk]=ssdata(minreal(ss(Ar,Br1,Cr1,D)));
[Ark,Brk2,Crk2,Dk]=ssdata(minreal(ss(Ar,Br2,Cr2,D)));

Ak=[Af1 A0   A0   A0;
    A0   Af2 A0   A0;
    A0   A0  Ark A0;
    A0   A0  A0   Ark];

Bk=[B1f1;B1f2;Brk1;Brk2];

Ck=[ 0 b37(1) 0  b37(2) Crk1 Crk2 ];
```

```
Cr=[0 0 0 0 Crk1 Crk2];

Dk=D;

%covariance Matricies:
G=eye(8);

R=1.1316e-7;

Q=zeros(8,8);
%var(SysState) settings
Q(1,1)  =  5.0440e-004; %fleximode 1 state 1
Q(2,2)  =  3.7758e-004; %fleximode 1 state 2
Q(3,3)  =  2.7377e-005; %fleximode 2 state 1
Q(4,4)  =  1.5922e-005; %fleximode 2 state 2
Q(5,5)  =  2.4900e+000; %rigid mode 1 state 1
Q(6,6)  =  2.9509e-004; %rigid mode 1 state 2
Q(7,7)  =  9.9605e-002; %rigid mode 2 state 1
Q(8,8)  =  1.1805e-005; %rigid mode 2 state 2

[kest,K,P]=kalman(ss(Ak,[Bk G],Ck,Dk),Q,R);
```

Functions to calculate receptance data

```
function u=frefre1(l,x,L)
  frefre
% frefre(lamda,sensor position,beam length)
% function calculates phi values for given beam data for
   Displacement data

s =(cosh(l*L) - cos(l*L))/(sinh(l*L)-sin(l*L));

u =cosh(l*x)+ cos(l*x) - s*(sinh(l*x+sin(l*x));


function u=frefre1(l,x,L)
% frefre
% frefre(lamda,sensor position,beam length)
% function calculates phi values for given beam data for
   Slope data

s =(cosh(l*L) - cos(l*L))/(sinh(l*L)-sin(l*L));

u = sinh(l*x) - sin(l*x) - s*(cosh(l*x)+cos(l*x));
```

Appendix E – Actuator Data Sheet

Electric linear/rotary moving coil actuators

The ability to perform work and verify its accuracy at the same time.
Controllable speed, force and position.

High Speed: 0.005~ 1000 mm/s

• For electronic component insertion, 10 cycles per second are required. A profile of typical performance is shown in the figure.
• These kind of applications can be achieved using SMAC actuators.

SMC

SMAC
Moving coil actuator
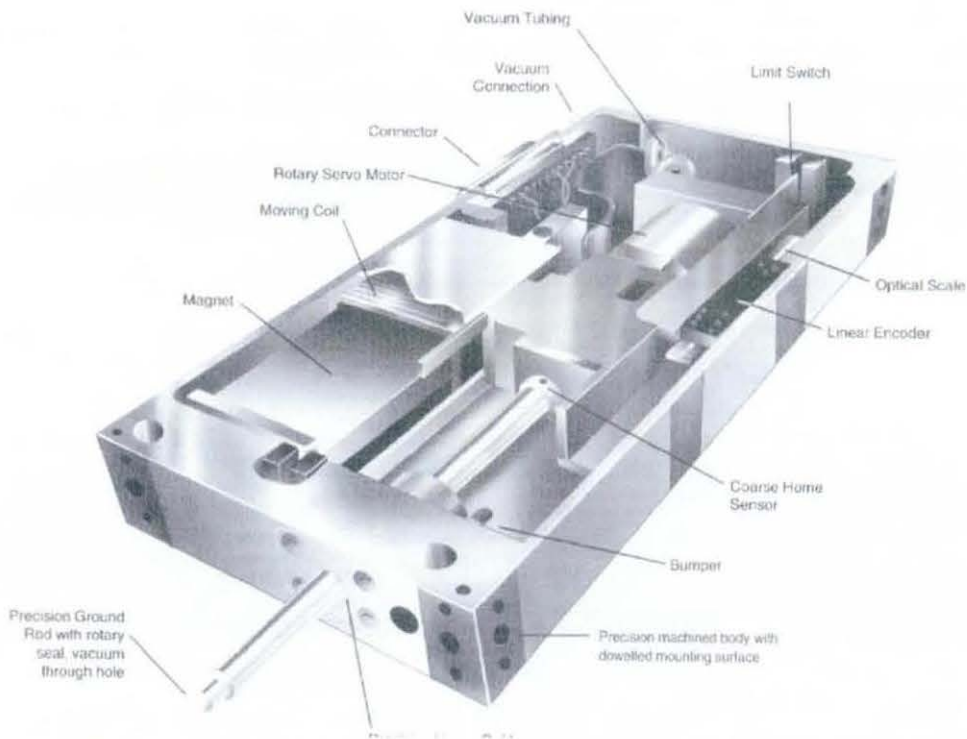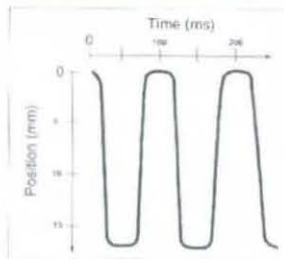
High resolution

- Linear Movement: $5\mu, 1\mu, 0.5\mu, 0.1\mu$
- Rotary Movement: $0.074°$. Up to $0.0072°$, on request.

Long life

Assembly machines are expected to work 24 hours a day at a frequency of 10 cycles per second. In a motion profile of 15 mm, the actuator would cover 10,000 km in one at SMAC actuators use high quality guides to satisfy these requirements.

10000 Km

Tokyo

Controllable Forces

Forces used in linear movement can be programmed at any time of the stroke.

Maximum forces
The mass of the inner moving elements is 400 g (standard actuator). To obtain an acceleration of 10 G, a 40 N force is required. Nowadays, the actuators can generate 280 N.

| 40 newtons | → | 400 g | → 10 G |
| 280 newtons | → | 400 g | → 70 G |
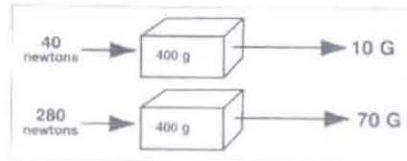
Minimum Forces
Friction represents the lower limit of the net forces applied to the part. The use of low friction guides can control forces to as low as 50 millinewtons.

Applied Force — Weight

Friction

Load Cell

0.05 N

Typical Applications

Common Pick and Place applications.
- Light forces to contact and pick up part.
- High forces to place part.

Force
500 — Press
10 — Contact
0
Time

![SMC logo]
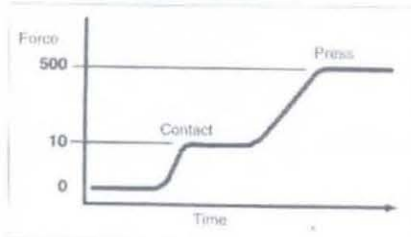
Moving coil technology

The most common application of this technology is in loudspeakers. A speaker coil moves in a magnetic circuit and drives a loudspeaker cone to generate sound waves. Tweeters operate up to 30,000 cycles per second. Amplifiers convert audio signals into an alternating current, which circulates through the coil. The sound intensity is proportional to this current.

These moving coils can be very useful in industrial applications. The small moving mass (200 g), combined with the actuation force (10 N) produce high accelerations (5-G). The only limitation is the stroke, which is too short to be useful.

This technology has been developed by SMAC using high intensity magnets. The result has been a moving coil in a broad range of strokes to be used for industrial applications.

Operating Principle

The magnetic circuit produces a uniform magnetic field. The coil wound around the central pole conducts current perpendicular to the flux lines and generates a force parallel to the direction of travel. Force increases if the current, number of turns or flux strength is increased.
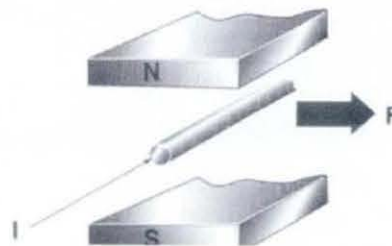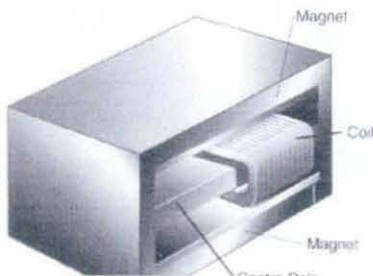
Linear Movement

The coil is mounted on a carriage. An accurate linear guide provides rigidity to the system. Thereby, the force generated by electrical current, which circulates through the coil, is converted into motion. An optical encoder controls the coil position, speed and acceleration.

Fixed Linear Glass Scale
Optical Reader Head
Rod
Coil
Linear Guide
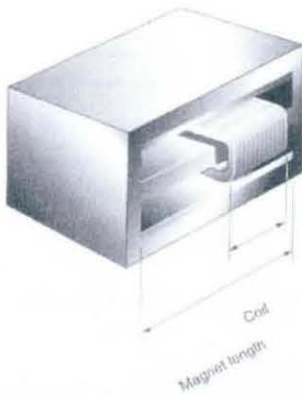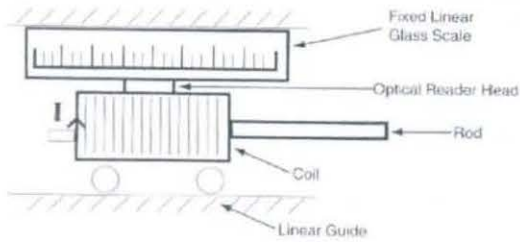
Stroke

The stroke of the linear movement is determined by the magnet length and the coil width.

Stroke= Magnet length - Coil width

Coil
Magnet length

Rotary Movement

Rotary movement is produced when a motor and the rod are assembled. This motor group is formed by:
  - Rotary motor
  - Gear group
  - Optical encoder

With the development of new miniature motors, the following characteristics have been achieved:
  - Resolution: 0.0072°
  - Speed: rotary motion of 90° in 50ms with an accuracy of ±0.045°

Fixed Linear Glass Scale
Optical Reader Head
Motor
Rod
Coil
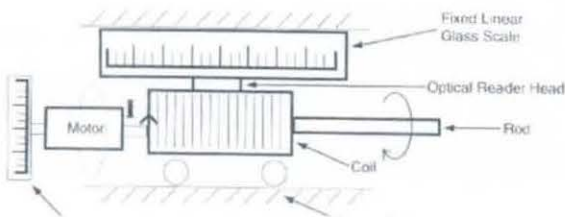
LAL-90

LAL-90
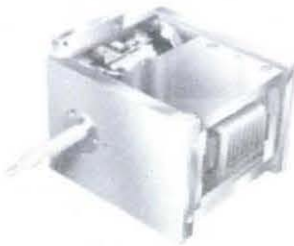
Mechanical Specifications

Stroke	15, 50 mm
Force	100 N (stroke 15mm), 60 N (stroke 50mm)
Payload	1 Kg
Moving Mass	0.25 Kg
Acceleration	15 G max.
Position Accuracy	±2 encoder counts
Rod Configuration	No thread, female or male thread

Electrical Specifications

Moving Coil	Supply*	48 VDC ±10%
	Resistance	12 Ω
	Inductance	7.5 mH
	Current*	2.5 A max.
Linear Encoder	Type	Incremental. Optical scale with index
	Resolution	5μ,1μ,0.5μ,0.1μ
	Supply*	5 VDC ±5%
	Output	TTL

* Provided by controller

General Specifications

Maximum operating time	40% maximum duty cycle
End-of-Stroke Limits	Opened Collector
Over-temperature protection	70°C with thermistor
Operating Ambient	0–50°C
LED's indicators	Green: Power on; Red: Fail
Body	Anodized Aluminum
Total Weight	2.1 Kg

How to order

LAL-90 - **015** - 53 **1** **D** **B**

Stroke
015	15 mm
050	50 mm

Encoder Resolution
0	0.5 μ (non contact)
1	1μ (non contact)
2	0.1μ (non contact)
5	5 μ (non contact)

Rod Configuration
B	No thread
F	Female thread
M	Male thread

Encoder Output
D	Differential (non contact encoder)

Note) For special requests (low friction, return spring, special rod, etc...), please, contact SMC.

LAL-90-015 dimensions

(mm)
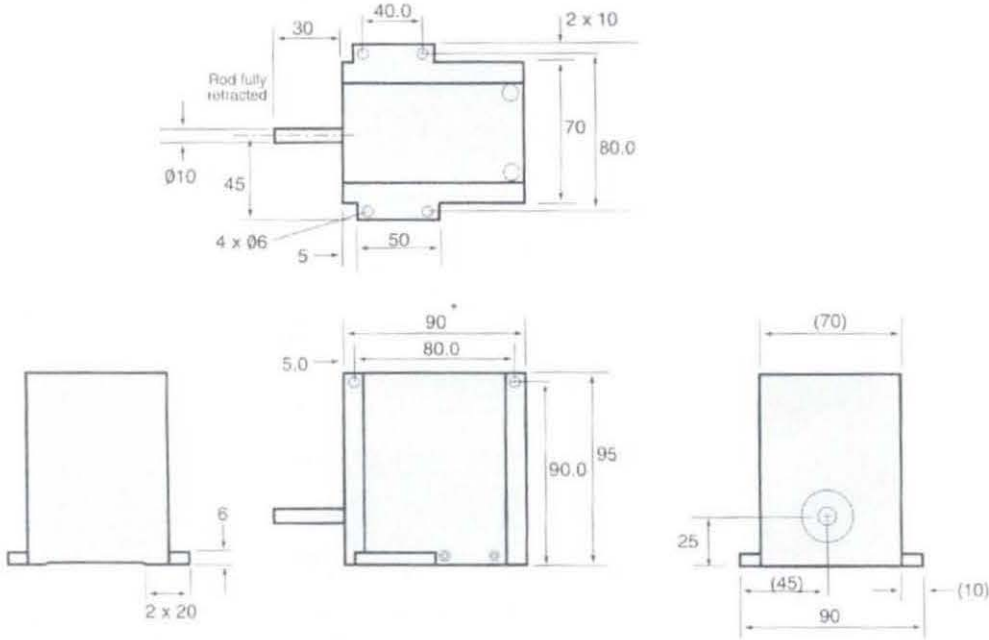
* For 50 mm stroke(LAL90-050), the height is 147 mm.

X = ± 0.50
X.X = ± 0.20

Rod Configuration Options

Type B (No thread)
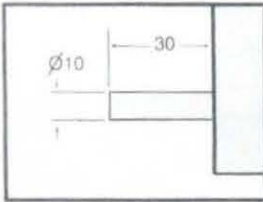
Type F (Female thread)

Type M (Male thread)

㉒
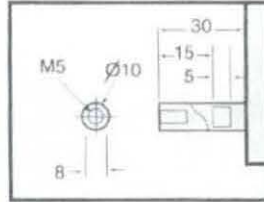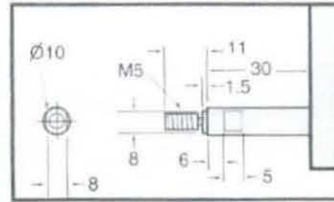
Appendix F – Sensor Sheet

SINGLE-AXIS RATE GYRO
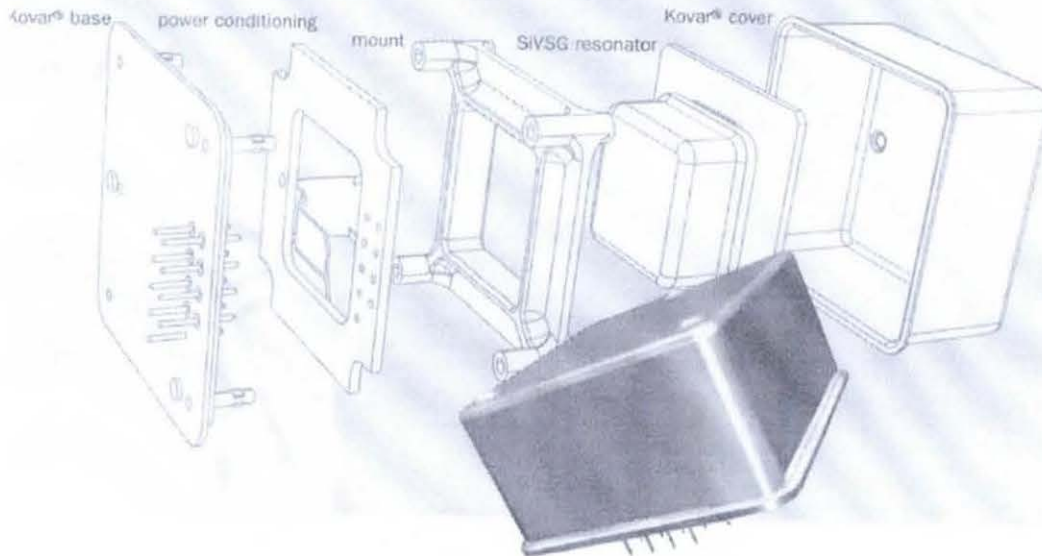
SiVSG - the world's first silicon micro-machined ring gyroscope technology, represents a breakthrough for systems designers who are under relentless pressure to provide solutions that are "smaller, better and cheaper". The fundamental characteristics of SiVSG provide low cost, size, weight and power benefits with unsurpassed reliability and robustness. This has enabled development of next generation systems such as gun-launched guided munitions.

is ideally suited for a wide range of commercial, aerospace and military applications.

The SiRRS is underpinned by BAE SYSTEMS' commitment to the technical backup and long-term support necessary for major procurement programmes.

The SiRRS angular rate sensor has evolved from the highly successful Vibrating Structure Gyroscope developed by BAE SYSTEMS, which has been in service since 1990. This MEMS implementation, which uses our new SiVSG technology, offers continued advancement in miniaturisation and reliability.

Designed to provide high performance operation under harsh environmental conditions, the SiRRS

- Micro-machined silicon (MEMS) technology
- Affordable, robust and rugged design
- Hermetically sealed
- Excellent shock and vibration performance
- Long life and exceptional reliability
- Comprehensive Built In Test
- Integrated temperature sensor
- Compact and lightweight
- Low power consumption
- Sensor modelling data available

BAE SYSTEMS

SPECIFICATION (typical data)

Rate Range	+/ 110°/s
other rate ranges available	
Scale Factor	
Nominal	18 2 mV/°/s
Linearity	+/ 1% of full scale
Variation with Temperature	+/ 3%
Repeatability	+/- 0 1% 1σ
Bias	
Setting (@20°C)	+/ 0 3°/s
Variation with Temperature	+/ 2°/s
Stability	3°/hr
Repeatability	0 1°/s 1σ
Angular Random Walk	0 2°/√hr
g Sensitivity	7°/hr/g
g² Sensitivity	2°/hr/g²
Bandwidth (-90° phase shift)	50 Hz
other bandwidths available	
Noise (in band)	0 25°/s rms
Environment	
Operating Temperature	40°C to +75°C
Humidity	100% RH
Vibration (operational)	10 g rms (20 Hz to 2 kHz)
Shock (operational)	60 g (30 ms, 1/2 sine)
Mass	<35 grams
Electrical	
Supply Voltage +/ Vs	+/ 5V DC
Supply Current	50 mA
General	
Built in Test	Command BIT
Start up Time	300 ms
Temperature Output	16 9 mV/°C (0V at 25°C)
MTBF	300 000 hrs

PLAN VIEW

END VIEW

SIDE VIEW

SIRRS01 Pinouts
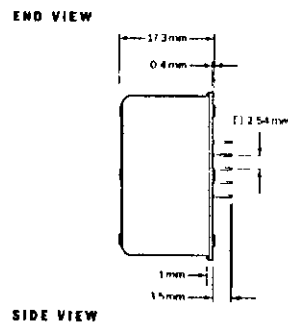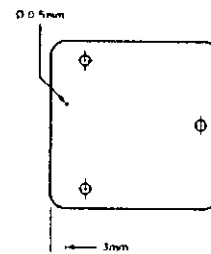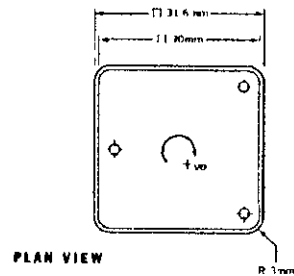
		9	Case Ground
Vs	4	8	Rate Reference
Command BIT	3	7	Rate Output
Alarm BIT	2	6	0V
+Vs	1	5	Temperature

FOR MORE INFORMATION CONTACT

Sales and Marketing
Silicon Sensors
T +44 (0) 1752 722068
- +44 (0) 1752 695927
- sales silicon@baesystems com

BAE SYSTEMS Clittaford Road Southway Plymouth Devon PL6 6DE United Kingdom
Telephone +44 (0) 1752 695695 Fax +44 (0) 1752 695500 www.baesystems com

Silicon 110 °/s RRS Sensor Test Results

Part No   .   RRS01-01-0100   Date ·   08/07/01

Serial No   D238   Tester   T ASPLAND-JUPI

+20°C	+5V Supply Current	mA		:	49.10
+20°C	-5V Supply Current	mA		:	47.70

+20°C	Warm-Up Bias Drift	°/s, 1 Sigma	:	0 005
+20°C	Switch On Bias Repeatability	°/s, 1 Sigma	:	0 021

-40°C	Zero Rate Offset	°/s		-1 05
-20°C	Zero Rate Offset	°/s	·	-0 78
0°C	Zero Rate Offset	°/s	:	-0 53
+20°C	Zero Rate Offset	°/s	:	-0 20
+40°C	Zero Rate Offset	°/s	:	0 22
+60°C	Zero Rate Offset	°/s		0.74
+75°C	Zero Rate Offset	°/s	.	1 18

-40°C	Scale Factor	mV/°/s	:	18 24
-20°C	Scale Factor	mV/°/s		18 21
+0°C	Scale Factor	mV/°/s		18.18
+20°C	Scale Factor	mV/°/s	·	18 09
+40°C	Scale Factor	mV/°/s		17 95
+60°C	Scale Factor	mV/°/s		17.75
+75°C	Scale Factor	mV/°/s	.	17 55

+20°C	Bandwidth (-90°)	Hz		61 00

+20°C	Rate Noise	°/s r m s	.	0 17

+20°C	CBIT Rate Offset	°/s	.	0 66

Appendix G - Electromagnetic Damper Design

There are two main stages to the design of an electro magnetic damper, firstly the magnetic field strength which is required to generate the desired level of damping must be calculated. From the field strength, the size of the core, the number of coils, and the current that is passed through the coils can be calculated

Required Field Strength

The first stage in designing the electromagnetic damper is to calculate the strength of the magnetic field that is required   A full description of the calculations is given in [Schieber – 1975][27]   The force (Fb) required to produce the desired damping is the product of the damping constant (D) and the velocity (u) of the sheet

$$Fb = D \cdot u \qquad (G\ 1)$$

The braking force can be calculated using the equation

$$Fb = \frac{\sigma \cdot \delta \cdot B_z^2}{\mu_0} \cdot u \cdot 4 \cdot h^4 \cdot l \qquad (G.1)$$

where σ is the conductivity of the sheet, δ is the thickness of the sheet, μ_0 is the permeability of vacuum, h is half the width of the core, and l is the inductivity per unit length, which is given by.

$$l = \frac{2}{\pi} \mu_0 \sum_{n=0}^{\infty} \frac{\sin^2\left[(2n+1)\frac{\pi}{2}\frac{h}{A}\right]}{\left[(2n+1)\frac{\pi}{2}\frac{h}{A}\right]^2} \cdot \frac{1 - \exp\left[-(2n+1)\pi\frac{b}{A}\right]}{(2n+1)} \qquad (G\ 1)$$

where A is half the width of the sheet, and b is half the depth of the core   These parameters are shown in Figure G-1
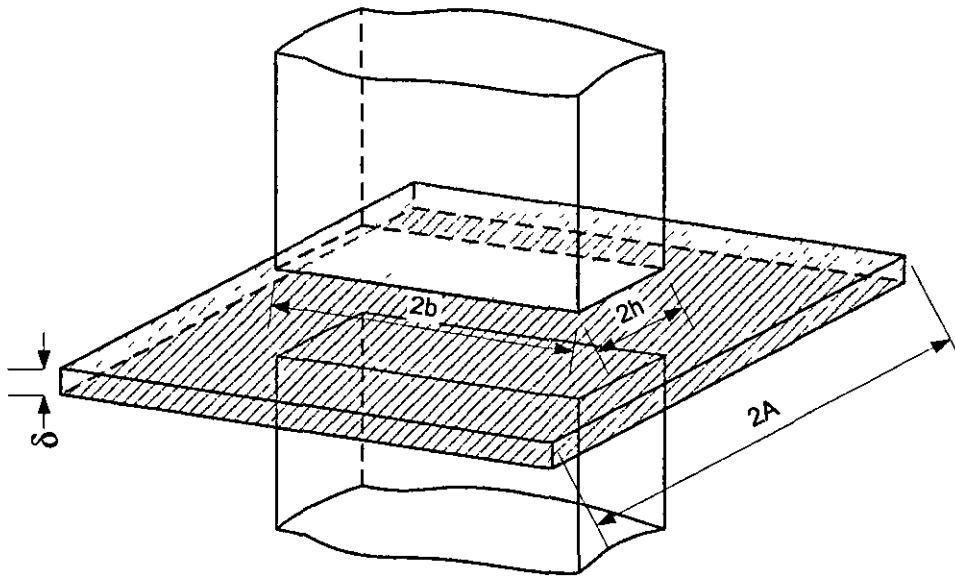
Figure G-1. Electromagnetic Damper Pole Dimensions

Substitution of equation (G 1) into equation (G 2), and rearranging, allows calculation of the magnetic flux density (B_z) required, given the dimensions of the magnet pole and the sheet

$$B_z = \sqrt{\frac{D \cdot \mu_0}{4 \cdot \sigma \cdot \delta \cdot h^4 \cdot l}}$$ (G 4)

Coil Requirements

The flux density calculated in equation (G 4) is used in the design of the coil for the electromagnet   From the flux density requirements, the remaining dimensions of the core, the number of turns on the coil, and the current in the coil can be calculated   The flux density can be described by

$$B = \mu_r \cdot \mu_0 \cdot H$$ (G 5)

Where μ_r is the relative permeability of the core, and H is the magnetic field intensity, given by the equation

$$H = \frac{N \cdot I}{l}$$ (G 6)

Where N is the number of turns on the coil, I is the current in the coil, and l is the length of the typical B-line in the core Figure G-2 shows these parameters
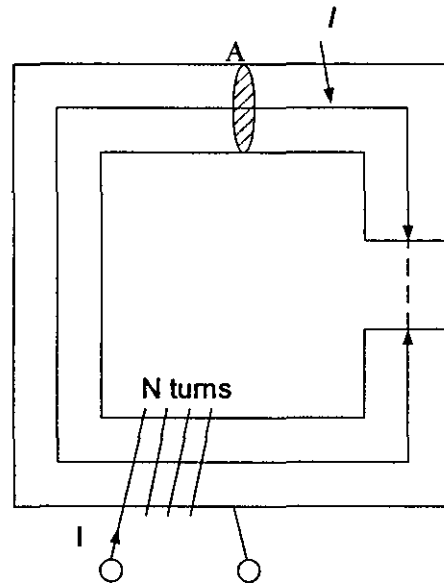
Figure G-2. Parameters of the Electromagnetic Damper Core

Substitution of equation (G 6) into equation (G 5), allows calculation of the magnetic flux density in terms of the parameters of the core

$$B = \frac{\mu_r \cdot \mu_0 \cdot N \cdot I}{l} \tag{G 7}$$

Equation (G 7) can then be used to design the core, in conjunction with equation (G 4).

Design of Dampers for Rig

The modelling of the beam (Chapter 4) used a damping constant of 167 Nsm^{-1}, and the dampers for the experimental stage have been designed to closely match this

Using equation (G 4) with the desired damping value, a 3mm thick and 25cm wide copper sheet, and selecting the poles of the electromagnet to be 5cm x 5cm, the parameters to calculate the flux density are

Half pole width (h)	-	0 025m
Half pole depth (b)	-	0 025m

Half sheet width (a)   -   0 145m

Sheet thickness (δ)   -   0 0032m

Conductivity of sheet (σ)   - $5 \times 10^8 \, \Omega^{-1}\mathrm{m}^{-1}$

Permeability of vacuum (μ0) - $4\pi \times 10^{-7} \, \mathrm{Hm}^{-1}$

From these parameters, flux density B_z is equal to 0 451T

Since the conservation of flux demands that for any region of a core, the product of flux density and cross sectional area of core must remain constant, i e

$$B_1 A_1 = B_2 A_2 = B_3 A_3 \qquad (G\ 8)$$

The flux density which the coil needs to set up can be halved by doubling the cross sectional area of the core, at the point where the coils are   At the poles, the cross section area of the core is 625mm². By doubling the depth of the core to 10cm, the area becomes 1250mm², this reduces the required flux density to 0 225T

If each of the coils is made with 1400 turns, and a current of 1A is passed through the coil, then using equation (5 8), if an iron core (relative permeability (μ_r) equals 500) is used, the length of the typical B line l can be calculated   This is equal to 0 845m Figure G-3 shows a cross section through the core of the damper (perpendicular to movement of copper sheet)
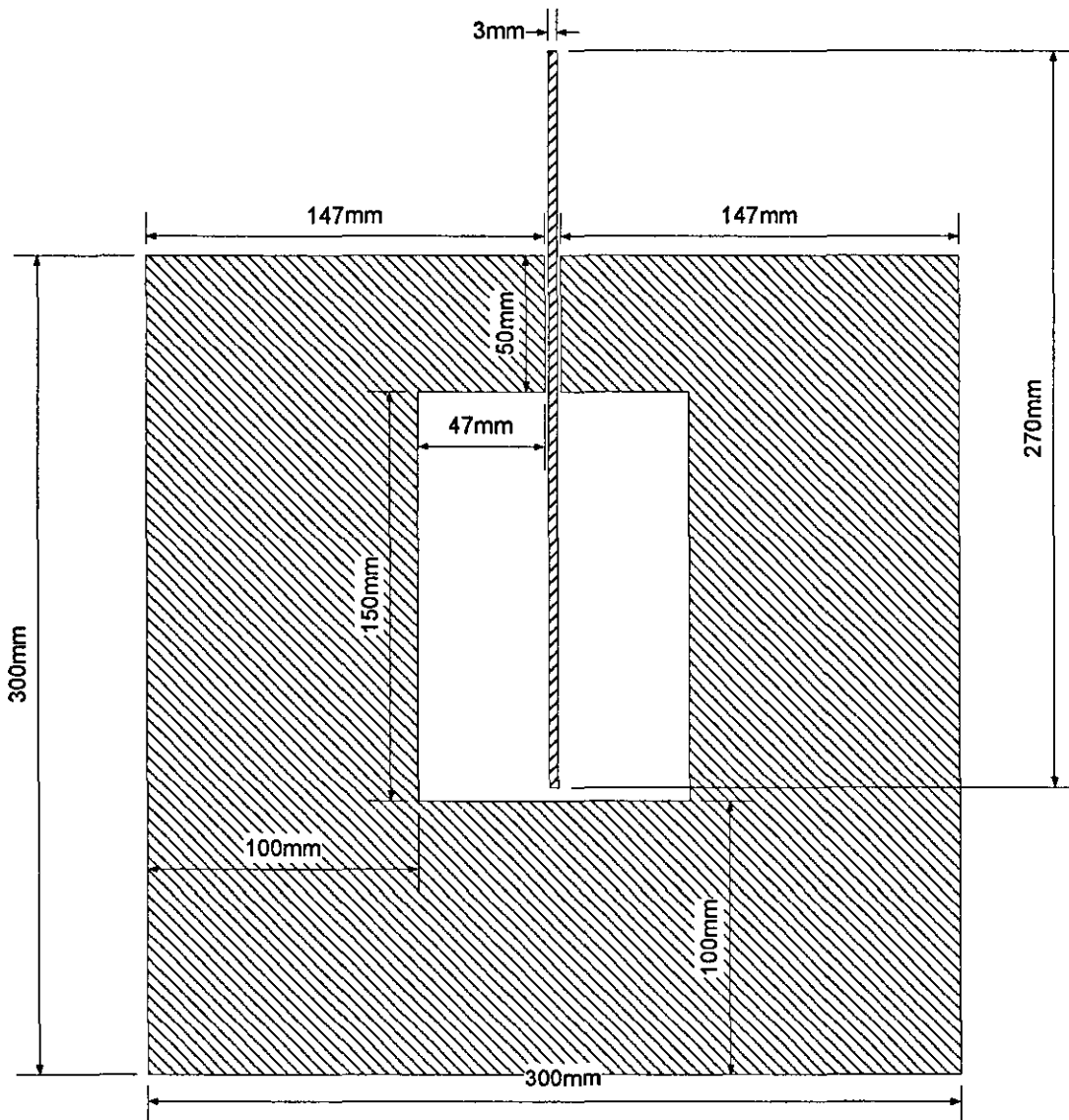
Figure G-3. Cross Section of Damper

The copper sheet is attached to a 9 5mm diameter shaft, supported on a pair of linear bearings, which allows the copper sheet to move with very little friction

Appendix H- Aircraft Model Matlab Files

This appendix outlines the Simulink model and Matlab m-files used to simulate the aircraft model

Figure H-1. Aircraft Model Top Level

Figure H-1 shows the top level of the Simulink aircraft model   The shadowed blocks allow quick changing of the initialisation of the model (control surface stimulation, filter type, etc)

Figure H-1. Aircraft State Space Model

The state space model has two outputs, the sensor data and the control surface positions   This block is shown in Figure H-1.

Figure H-3. Control Block

Figure H-3 shows the block labelled 'control' in the top level diagram   This block allows selection of input from either the sensors or the Kalman filter. It also combines two of the sensors to produce the angle of attack data (alpha)

Figure H-4. FCS Block

Figure H-4 shows the block containing all of the components of the FCS
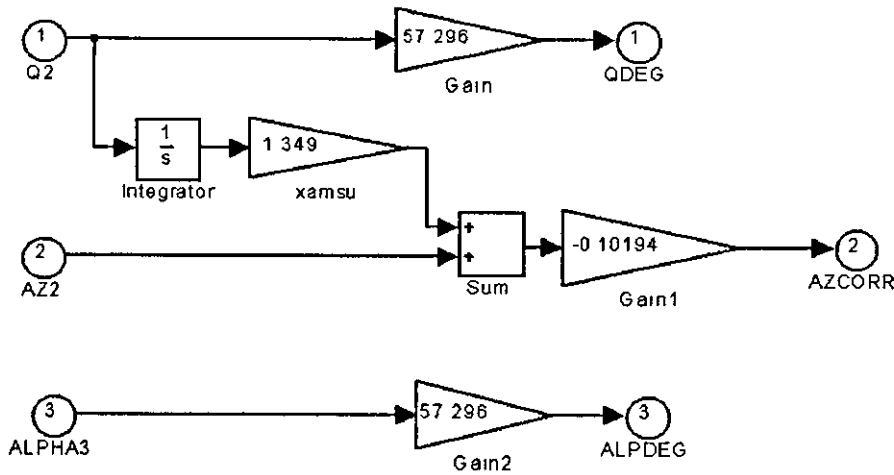
Figure H-5. Sensor Definitions

Figure H-5 shows the calculations made to convert the aircraft model sensors into the form used by the FCS (e g from radians to degrees)
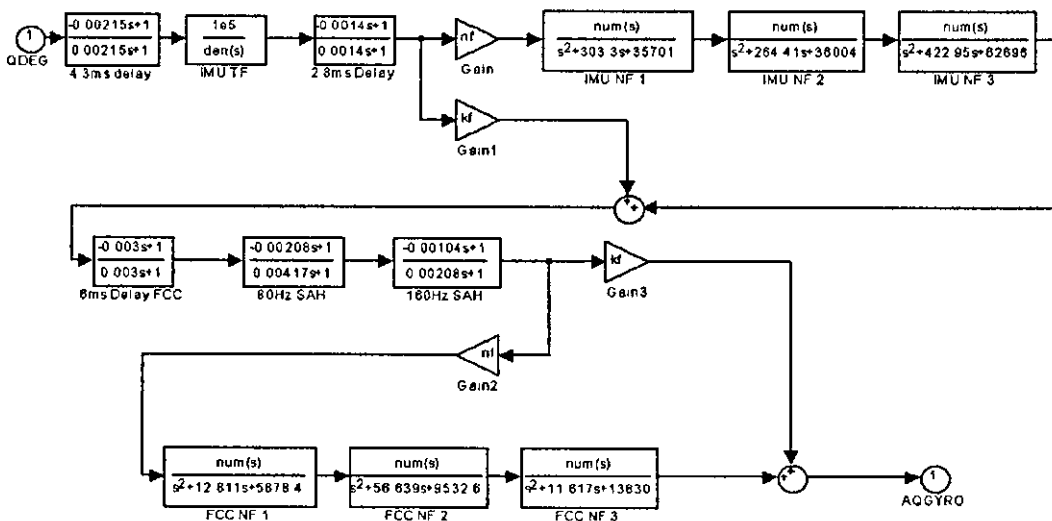
Figure H-6. Pitch Rate (Q) Path

Figure H-6 includes the filters and delays introduced in the pitch rate path It also shows some of the notch filters (which can be deselected if required)
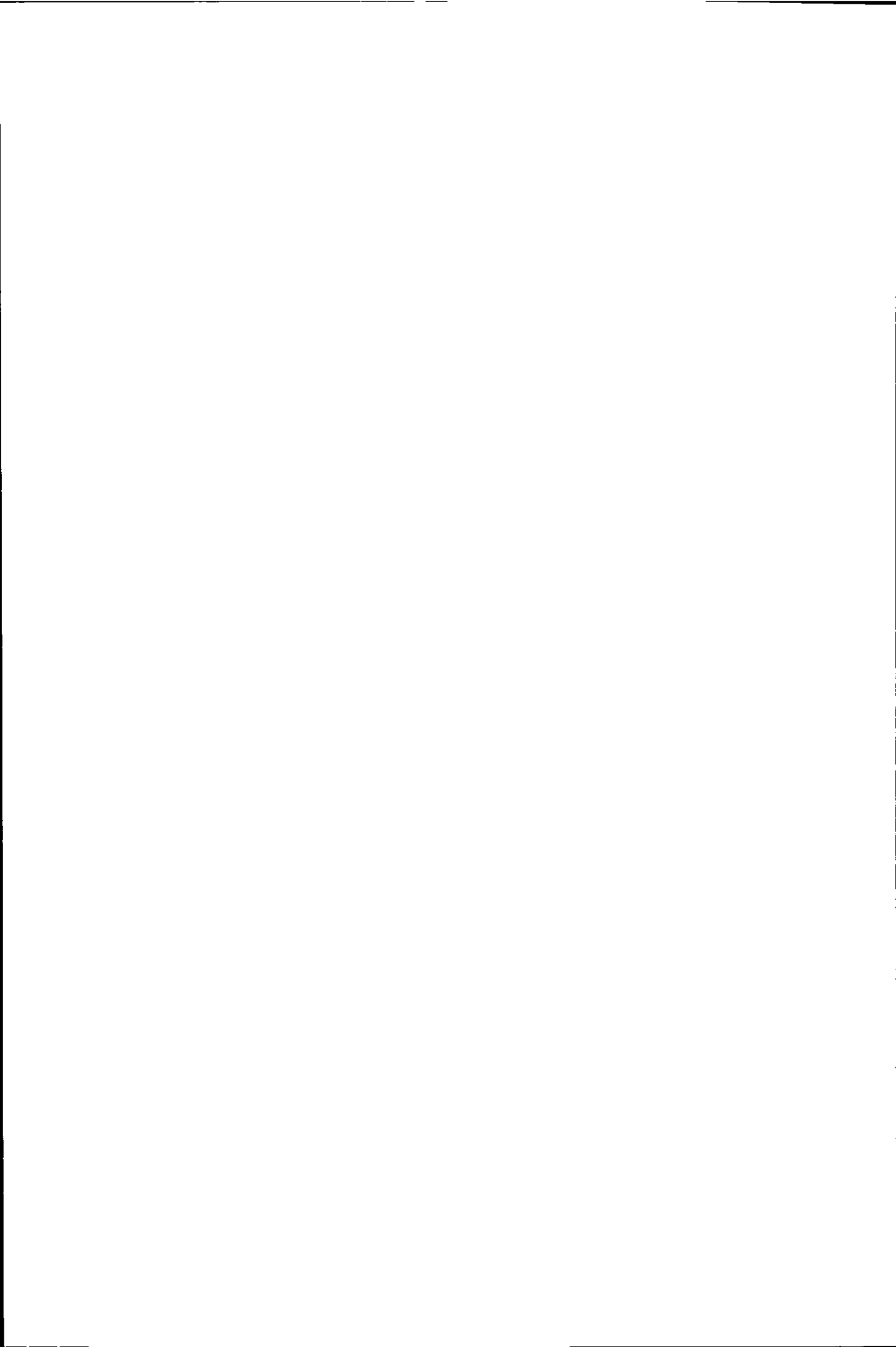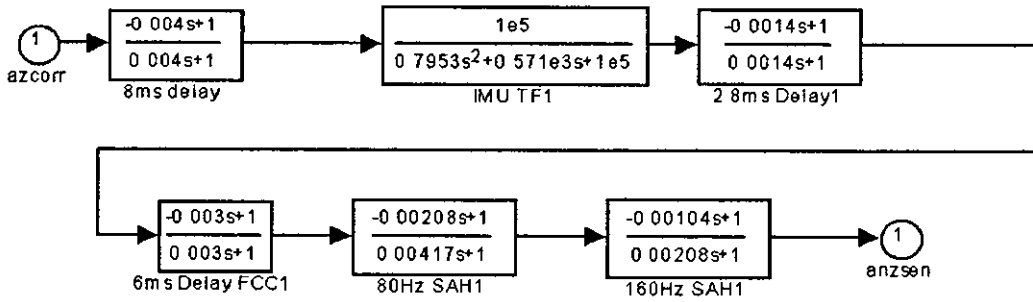
Figure H-7. AZ Path
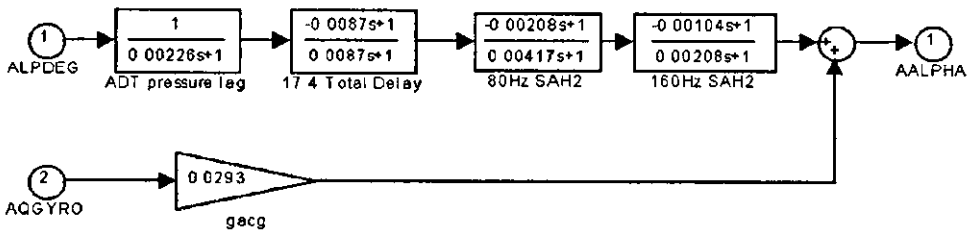
Figure H-8. Alpha Path

Figure H-7 and Figure H-8 show the transfer function paths for the vertical velocity and angle of attack paths respectively
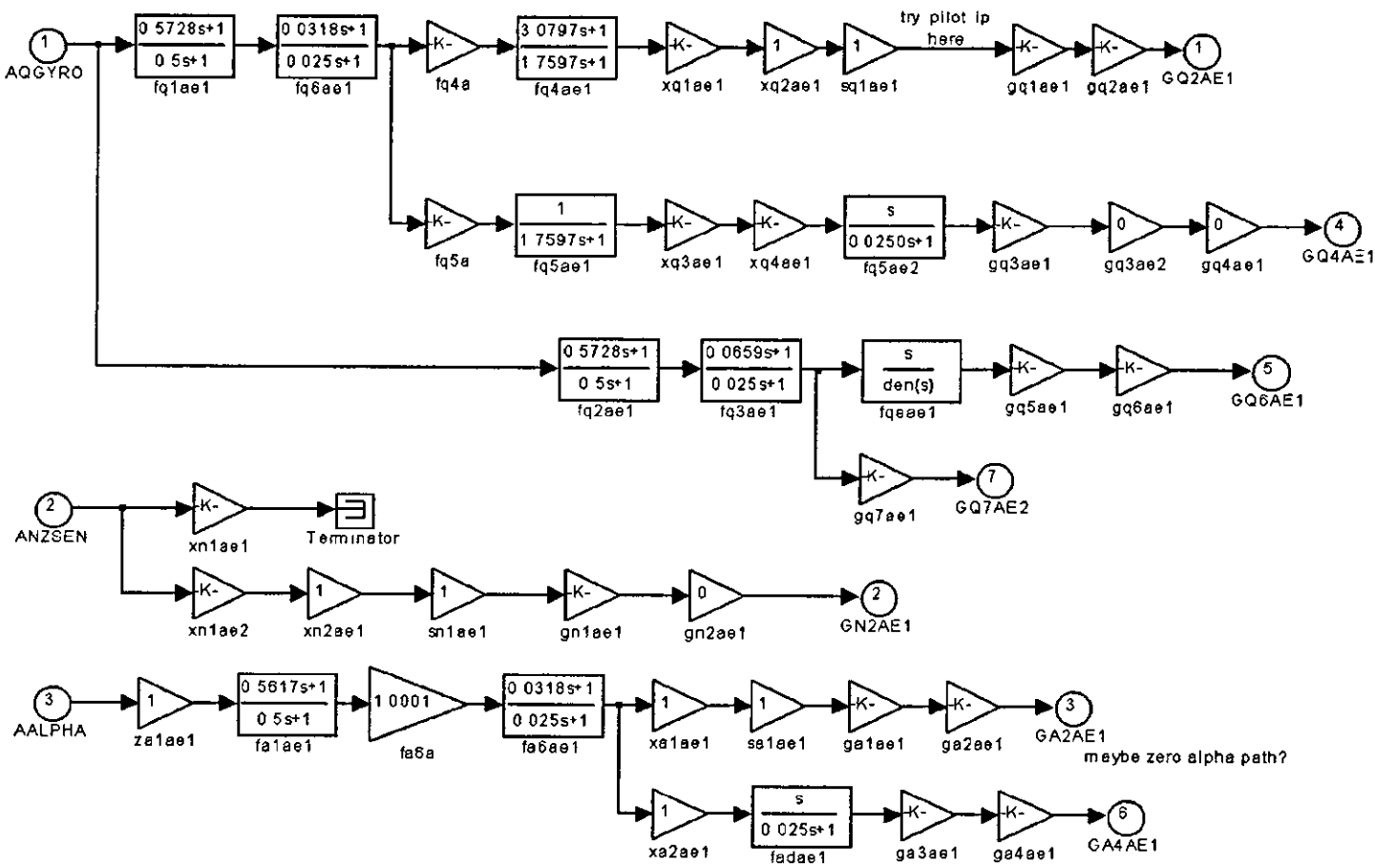
Figure H-9. Control Laws

Figure H-9 shows the transfer functions which make up the control laws for the FCS
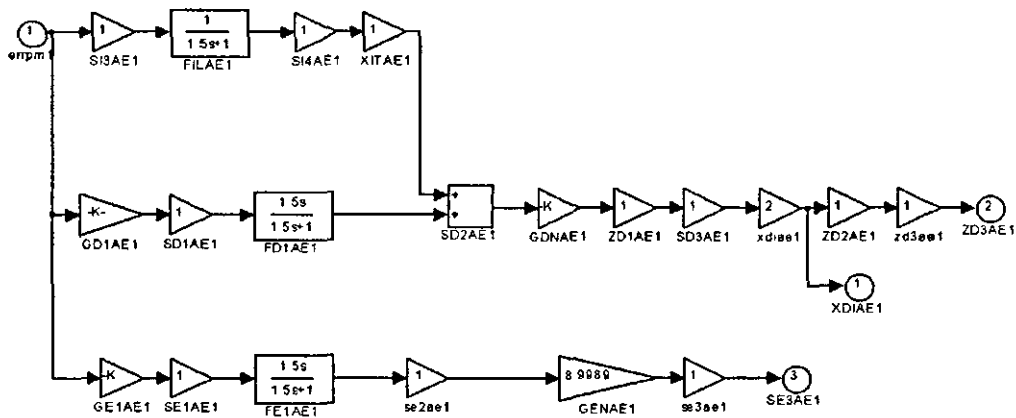
Figure H-10. Actuator Distribution Paths

The distribution of the control laws to the different actuators is shown in Figure H-10.
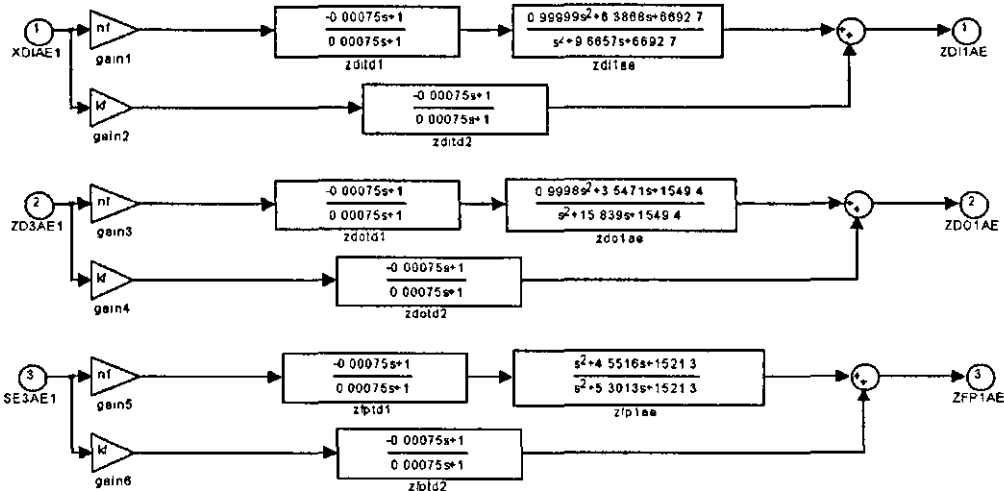
Figure H-11. Input Path FCC Notch Filters

The FCC input path notch filters are shown in Figure H-11   As with the pitch rate path, these filters can be deselected if desired
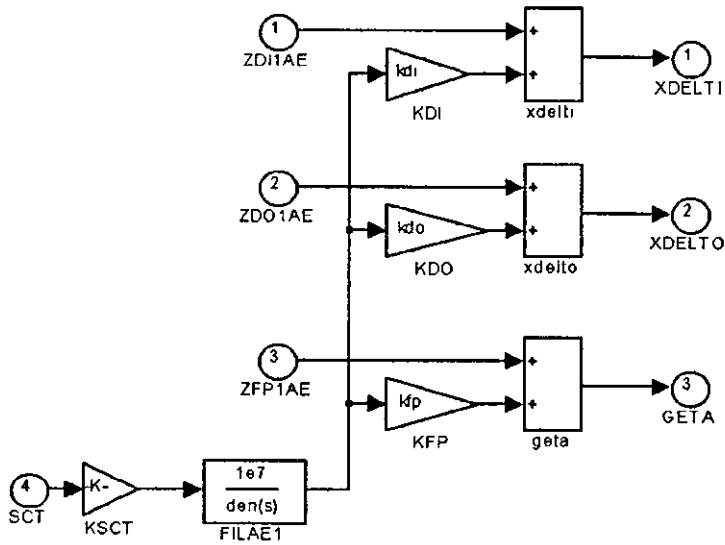
Figure H-12. Control Surface Stimulation Input

Figure H-12 allows stimuli to be applied to the control surfaces. The input is added to the output of the actuator distribution path

Figure H-13 the 3 paths (for the control surfaces) which take the FCS output and accounting for the effect of the actuator, convert them into actual demanded control surface moments
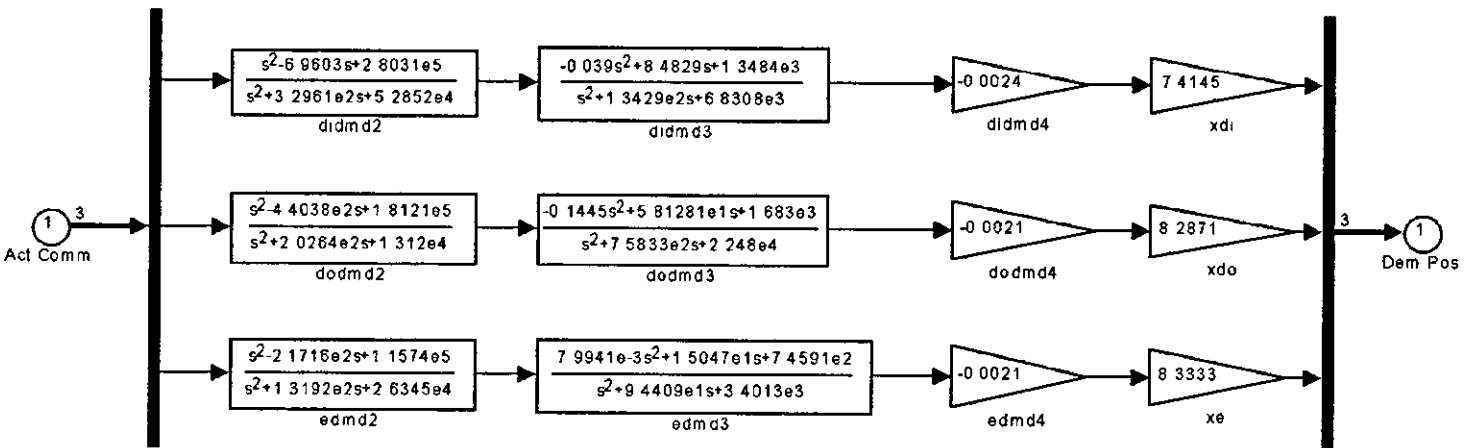
Figure H-13. Actuator Transfer Functions

Act Comm

$$\frac{s^2 - 6\ 9603s + 2\ 8031e5}{s^2 + 3\ 2961e2s + 5\ 2852e4}$$
dldmd2

$$\frac{-0\ 039s^2 + 8\ 4829s + 1\ 3484e3}{s^2 + 1\ 3429e2s + 6\ 8308e3}$$
dldmd3

-0 0024
dldmd4

7 4145
xdi

$$\frac{s^2 - 4\ 4038e2s + 1\ 8121e5}{s^2 + 2\ 0264e2s + 1\ 312e4}$$
dodmd2

$$\frac{-0\ 1445s^2 + 5\ 81281e1s + 1\ 683e3}{s^2 + 7\ 5833e2s + 2\ 248e4}$$
dodmd3

-0 0021
dodmd4

8 2871
xdo

Dem Pos

$$\frac{s^2 - 2\ 1716e2s + 1\ 1574e5}{s^2 + 1\ 3192e2s + 2\ 6345e4}$$
edmd2

$$\frac{7\ 9941e-3s^2 + 1\ 5047e1s + 7\ 4591e2}{s^2 + 9\ 4409e1s + 3\ 4013e3}$$
edmd3

-0 0021
edmd4

8 3333
xe

Figure H-14. Hinge Moments

The hinge moments, which are supplied to the aircraft model and Kalman filter, are calculated from the difference between the actual and demanded position of the control surfaces These calculations are shown in Figure H-14
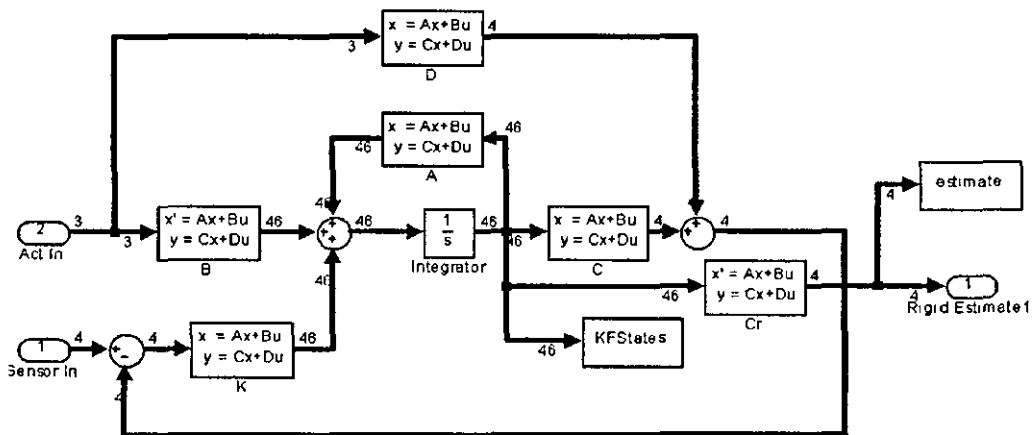
Figure H-15. Kalman Filter Block

Figure H-15 shows the Kalman filter

Original Kalman Filter m-file

```
% ********************************************
% * complex1.mdl                             *
% ********************************************
% * S.A.Halsey May 2002                      *
% ********************************************
% * File to run ac model at 20 modes         *
% *   with KF at 20 modes                     *
% ********************************************

clear

% read in matricies
A=dlmread('mata2',',');
B=dlmread('matb2',',');
C=dlmread('matc2',',');
D=dlmread('matd2',',');
E=dlmread('mate2',',');
Z=dlmread('matz2',',');

%set up constants
ALT=35000;  %(35000)
T=288.16-ALT*1.9812e-3;
rho=1.225571*(T/288.16)^4.254293;
sigma=rho/1.225571;
v=0.8*(20.051268*sqrt(T));

%add control mode values - ommited from model'
E(75,75)=3213769;
E(76,76)=2226065;
E(77,77)=1137600;

%reduce size of matricies to 14NM plus control & rigid
% reduce A
A1=A(1:20,1:20);
A1(15:20,15:20)=A(75:80,75:80);
A1(1:14,15:20)=A(1:14,75:80);  %[A(1:14,75:77) zeros(14,3)];  %
A1(15:20,1:14)=A(75:80,1:14);  %[A(75:77,1:14);zeros(3,14)];  %

% reduce B
B1=B(1:20,1:20);
B1(15:20,15:20)=B(75:80,75:80);
B1(1:14,15:20)=B(1:14,75:80);  %[B(1:14,75:77) zeros(14,3)];  %
B1(15:20,1:14)=B(75:80,1:14);  %[B(75:77,1:14);zeros(3,14)];  %

% reduce C
C1=C(1:20,1:20);
C1(15:20,15:20)=C(75:80,75:80);
C1(1:14,15:20)=C(1:14,75:80);  %[C(1:14,75:77) zeros(14,3)];  %
C1(15:20,1:14)=C(75:80,1:14);  %[C(75:77,1:14);zeros(3,14)];  %

% reduce D
D1=D(1:20,1:20);
D1(15:20,15:20)=D(75:80,75:80);
D1(1:14,15:20)=D(1:14,75:80);  %[D(1:14,75:77) zeros(14,3)];  %
D1(15:20,1:14)=D(75:80,1:14);  %[D(75:77,1:14);zeros(3,14)];  %

% reduce E
E1=E(1:20,1:20);
```
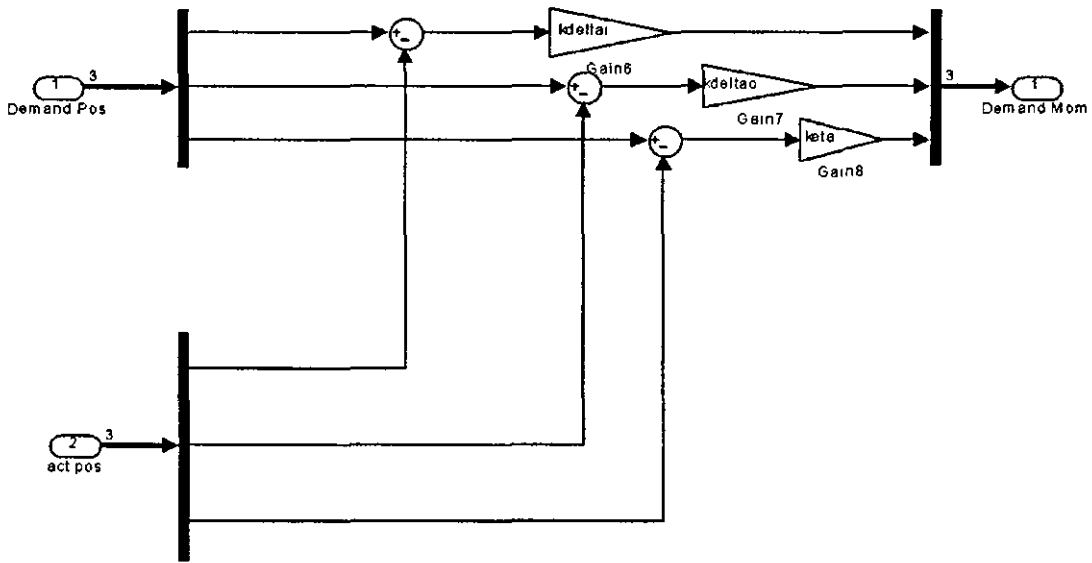
```
E1(15:20,15:20)=E(75:80,75:80);
E1(1:14,15:20)=E(1:14,75·80); %[E(1:14,75:77) zeros(14,3)]; %
E1(15:20,1:14)=E(75:80,1:14); %[E(75:77,1:14);zeros(3,14)]; %

% reduce Z
Z1=Z(:,1:20);
Z1(:,15:20)=Z(:,75:80);

% Check A is square & equal in size to other matrices
sizea=size(A1);
sizeb=size(B1);
sizec=size(C1);
sized=size(D1);
sizee=size(E1);

if sizea(1)~=sizea(2)
   error('Input A matrix is not square - Program cannot run');
elseif sizea~=sizeb
   error('A is not same size as B - Program Terminating');
elseif sizea~=sizec
   error('A is not same size as C - Program Terminating');
elseif sizea~=sized
   error('A is not same size as D - Program Terminating');
elseif sizea~=sizee
   error('A is not same size as E - Program Terminating');
end

% Convert matricies to ss form
a1=zeros(20,20);
a2=eye(20);
a3=-inv(A1)*(sigma*v^2*C1+E1);
%a3=-inv(A)*E1;
a4=-inv(A1)*(sigma*v*B1+D1);
%a4=-inv(A)*D1;

a=[a1 a2;a3 a4];

ip20=zeros(20,3);
ip20(15:17,:)=E1(15:17,15:17);

b20=inv(A1)*ip20;

b=[zeros(20,3) ; b20];

%output matrices
ctrl=[15:17];

%model
c=zeros(7,40);
c(1,21:40)=Z1(27,:); %27
c(2,21:40)=Z1(26,:); %26
c(3,1:20)=Z1(51,:);
c(4,21:40)=Z1(50,:);
c(5:7,ctrl)=eye(3);

%kalman filter
ak=a;
bk=b;

ck=zeros(4,40);
```

```
ck(1,21:40)=[Z1(27,1:20)];
ck(2,21:40)=[Z1(26,1:20)];
ck(3,1:20) =[Z1(51,1:20)];
ck(4,21:40)=[Z1(50,1:20)];

%rigid only (output)
cr=zeros(4,40);
cr(1,21:40)=[zeros(1,14) Z1(27,15:20)];
cr(2,21:40)=[zeros(1,14) Z1(26,15:20)];
cr(3,1:20) =[zeros(1,14) Z1(51,15:20)];
cr(4,21:40)=[zeros(1,14) Z1(50,15:20)];

d=zeros(7,3);
dk=zeros(4,43);

'calculate eigenvalues
[vec,val]=eig(inv(A)*(sigma*v^2*C+E));
val=diag(sqrt(val))/(2*pi);
val=sort(val);
disp('System Eigenvalues:');
val(4:17)

?Kalman filter variances
R=1.1316e-7*eye(4);
G=eye(40);
load var;
Q=diag(Q);

[est,K,p]=kalman(ss(a,[b G],ck(1:4,:),dk),Q,R);

control;
```

control m

```
%control data for Aircraft model

keta=1137600;
kdeltai=3213769;
kdeltao=2226065;

ilfp=8.3333;
ilflpi=7.4145;
ilflpo=8.2871;

gy=0;
ksct=0;
kstk=1;
kdi=0;
kdo=0;
kfp=0;

disp('stim to stk');

ts=0.01;
```

Original Kalman Filter Gain Matrix **K** =

```
-2.1601e+3  -2.2981e+3  -1.2174e+3   1.2468e+3
-3.2142e+1  -4.8957e+1   1.7919e+0   2.8979e+1
 1.1995e+1   2.0785e+1   5.0092e+0  -1.1867e+1
-4.6038e+0   1.5773e+0  -7.0200e+0  -4.3832e+0
 1.4648e+2   1.2892e+2  -1.0560e+1  -4.3566e+1
-1.0167e+1  -7.4486e+0  -3.4614e+0  -5.2093e+0
-7.4293e+0  -4.0474e+0   1.8655e+0  -2.5223e+0
-1.9028e+1  -1.0705e+1  -2.6880e-1   3.8019e+1
-3.5200e+2  -2.5402e+2  -5.4062e+1  -3.9052e+2
-1.4320e+2   1.6274e+2   1.4600e+1   5.7237e+2
 1.4780e+2   5.6333e+1   1.4236e+1   1.1366e+2
 9.0610e+1  -2.1861e+2  -8.7622e+0   2.3676e+2
 3.7089e+1  -8.1673e+1  -2.8725e-1   4.7108e+1
 8.8310e+1   2.1652e+1  -1.2055e+0   2.8164e+2
 1.4663e+2  -2.1643e+3  -1.5209e+1   1.2727e+3
-1.5010e+3  -5.1057e+2  -1.4844e+1   3.5910e+2
-9.6190e+2  -2.6469e+2  -8.6032e+0  -1.3810e+3
 4.0732e+3  -4.7181e+4  -9.3467e+3  -2.8175e+3
 5.4076e+2   1.6611e+2   2.2720e+2  -1.2144e+3
-1.0179e+1  -3.5846e+0   4.3319e+1  -3.2244e+0
 7.4221e+4   4.0723e+3  -1.6551e+4   3.7746e+4
 4.4857e+3   1.0751e+3  -1.6572e+3  -1.0308e+3
 7.6226e+3   1.5577e+3   7.3399e+2   1.4321e+2
-1.3127e+4  -5.7139e+3  -2.0174e+2  -2.5882e+3
-8.5257e+4  -2.6638e+4   2.8090e+3  -2.3717e+4
-2.2507e+3  -6.8519e+2  -3.2852e+2   2.2127e+3
 1.3432e+4   4.1088e+3  -1.0295e+2   2.0594e+3
 2.7761e+4   1.3873e+4  -2.1421e+2   1.1496e+4
 1.9387e+5   5.1698e+3  -8.9262e+3   7.9020e+4
 6.9199e+3   3.8883e+4  -1.6205e+3   2.3323e+4
-2.0900e+5  -3.2002e+4   2.8154e+3  -7.2242e+4
 3.9310e+4   5.2733e+4  -2.3497e+2   3.5302e+4
-3.5488e+4   1.6344e+4   4.5826e+2  -2.3555e+3
-1.0821e+5  -5.5632e+3   1.2560e+3  -5.2098e+4
 4.8971e+5   7.3382e+5  -2.0023e+4   3.9354e+5
 1.8241e+6   1.0016e+5  -3.5419e+4   1.9907e+5
 5.0871e+5  -8.7404e+4  -2.2438e+4   1.3700e+5
-1.7937e+2  -5.1889e+3  -1.2822e+3   1.0656e+3
 2.5094e+3   4.7549e+3   6.2100e+2   8.6409e+2
 1.1927e+3   2.4160e+2   1.2044e+2  -1.0441e+3
```

Modified Kalman Filter m-file

```
% ***************************************
% * complex1.mdl                        *
% ***************************************
% * S.A.Halsey May 2002                 *
% ***************************************
% * File to run ac model at 80 modes    *
% *   with KF at 20 modes               *
% ***************************************

clear

% read in matricies
A=dlmread('mata2',',');
B=dlmread('matb2',',');
C=dlmread('matc2',',');
D=dlmread('matd2',',');
E=dlmread('mate2',',');
Z=dlmread('matz2',',');

%set up constants
ALT=35000; %(35000)
T=288.16-ALT*1.9812e-3;
rho=1.225571*(T/288.16)^4.254293;
sigma=rho/1.225571;
v=0.8*(20.051268*sqrt(T));

%add control mode values - ommited from model'
E(75,75)=3213769;
E(76,76)=2226065;
E(77,77)=1137600;

%reduce size of matricies to 14NM plus control & rigid
% normal model
% reduce A
A1=A(1:20,1:20);
A1(15:20,15:20)=A(75:80,75:80);
A1(1:14,15:20)=A(1:14,75:80); %[A(1:14,75:77) zeros(14,3)]; %
A1(15:20,1:14)=A(75:80,1:14); %[A(75:77,1:14);zeros(3,14)]; %

% decoupled model
% reduce A
A2=A(1:20,1:20);
A2(15:20,15:20)=A(75:80,75:80);
A2(1:14,15:20)=[A(1:14,75:77) zeros(14,3)]; %A(1:14,78:80)]; %
A2(15:20,1:14)=[A(75:77,1:14);zeros(3,14)]; %A(78:80,1:14)]; %

% reduce B
B2=B(1:20,1:20);
B2(15:20,15:20)=B(75:80,75·80);
B2(1:14,15:20)=B(1:14,75:80); %[B(1:14,75:77) zeros(14,3)]; %
B2(15:20,1:14)=B(75:80,1:14); %[B(75:77,1:14);zeros(3,14]); %

% reduce C
C2=C(1:20,1:20);
C2(15:20,15:20)=C(75:80,75:80);
C2(1:14,15:20)=C(1:14,75:80); %[C(1:14,75:77) zeros(14,3)]; %
C2(15:20,1:14)=C(75:80,1:14); %[C(75:77,1:14);zeros(3,14)]; %
```

```
% reduce D
D2=D(1:20,1:20);
D2(15:20,15:20)=D(75:80,75:80);
D2(1:14,15:20)=D(1:14,75:80);  %[D(1:14,75:77) zeros(14,3)];  %
D2(15:20,1:14)=D(75:80,1:14);  %[D(75:77,1:14);zeros(3,14)];  %

^ reduce E
E2=E(1:20,1:20);
E2(15:20,15:20)=E(75:80,75:80);
E2(1:14,15:20)=E(1:14,75:80);  %[E(1:14,75:77) zeros(14,3)];  %
E2(15:20,1:14)=E(75:80,1:14);  %[E(75:77,1:14);zeros(3,14)];  %

% reduce Z
Z1=Z(:,1:20);
Z1(:,15:20)=Z(:,75:80);

% Check A is square & equal in size to other matrices
sizea=size(A2);
sizeb=size(B2);
sizec=size(C2);
sized=size(D2);
sizee=size(E2);

if sizea(1)~=sizea(2)
   error('Input A matrix is not square - Program cannot run');
elseif sizea~=sizeb
   error('A is not same size as B - Program Terminating');
elseif sizea~=sizec
   error('A is not same size as C - Program Terminating');
elseif sizea~=sized
   error('A is not same size as D - Program Terminating');
elseif sizea~=sizee
   error('A is not same size as E - Program Terminating');
end

% Convert matricies to ss form
% model
a1=zeros(20,20);
a2=eye(20);
a3=-inv(A1)*(sigma*v^2*C2+E2);
%a3=-inv(A)*E1;
a4=-inv(A1)*(sigma*v*B2+D2);
%a4=-inv(A)*D1;

a=[a1 a2;a3 a4];

ip20=zeros(20,3);
ip20(15:17,:)=E2(15:17,15:17);

b20=inv(A1)*ip20;

b=[zeros(20,3)  ; b20];

% kalman filter
   coupled
a1=zeros(sizea);
a2=eye(sizea(1));
a3=-inv(A1)*(sigma*v^2*C2+E2);
%a3=-inv(A1)*E2;
```

```
a4=-inv(A1)*(sigma*v*B2+D2);
%a4=-inv(A1)*D2;

%decoupled
a3d=-inv(A2)*(sigma*v^2*C2+E2);
a4d=-inv(A2)*(sigma*v*B2+D2);

ad=[a1 a2;a3 a4];
ad1=[a1 a2;a3d a4d];

%kalman filter amalgamation of coupled and decoupled
% X=[f,rc,c,rd]
ak=[ad(1:20,1:20)    zeros(20,3) ad(1:20,21:40)    zeros(20,3);
    ad1(18:20,1:20) zeros(3,3)  ad1(18:20,21:40) zeros(3,3);
    ad(21:40,1:20)   zeros(20,3) ad(21:40,21:40) zeros(20,3);
    ad1(38:40,1:20) zeros(3,3)   ad1(38:40,21:40) zeros(3,3)];

b20=inv(A1)*ip20;
bd=[zeros(20,3) ; b20];

ip20(15:17,:)=E2(15:17,15:17);
b20d=inv(A2)*ip20;
bd1=[zeros(20,3) ; b20d];

bk=[bd(1:20,:);
    bd1(18:20,:); %zeros(3,3);
    bd(21:40,:);
    bd1(38:40,:) ]; %zeros(3,3)]; %bd(38:40,:)


%output matrices
ctrl=[15:17];

%model
c=zeros(7,40);
c(1,21:40)=Z1(27,:); %27
c(2,21:40)=Z1(26,:); %26
c(3,1:20)=Z1(51,:);
c(4,21:40)=Z1(50,:);
c(5:7,ctrl)=eye(3);

%kalman filter (coupled)
ck=zeros(4,46);
ck(1,24:46)=[Z1(27,:) zeros(1,3)]; %Z1(21,18:20)]; %
ck(2,24:46)=[Z1(26,:) zeros(1,3)]; %Z1(20,18:20)]; %
ck(3,1:23) =[Z1(51,:) zeros(1,3)]; %Z1(39,18:20)]; %
ck(4,24:46)=[Z1(50,:) zeros(1,3)]; %Z1(38,18:20)]; %

%rigid only
ckd=zeros(4,40);
ckd(1,21:40)=[zeros(1,14) Z1(27,15:20)]; %[Z1(21,1:17)
  Z1(21,18:20)]; %
ckd(2,21:40)=[zeros(1,14) Z1(26,15:20)]; %[Z1(20,1:17)
  Z1(20,18:20)]; %
ckd(3,1:20) =[zeros(1,14) Z1(51,15:20)]; %[Z1(39,1:17)
  Z1(39,18:20)]; %
ckd(4,21:40)=[zeros(1,14) Z1(50,15:20)]; %[Z1(38,1:17)
  Z1(38,18:20)]; %
```

```
%external decoupled
cr=[ckd(:,1:17) zeros(4,3) ckd(:,18:37) zeros(4,3)
  ckd(:,38:40)];
ck(:,41:43)];


d=zeros(7,3);
dk=zeros(4,49);

 calculate eigenvalues
[vec,val]=eig(inv(A)*(sigma*v^2*C+E));
val=diag(sqrt(val))/(2*pi);
val=sort(val);
disp('System Eigenvalues:');
val(4:17)

%model constants
states=46;

%Kalman filter variances
R=1.1316e-7*eye(4);
load var1;
G=eye(46);

Q=diag(Q);
Q=Q*100;
sys=ss(a,b,c,d);

[est,K,p]=kalman(ss(ak,[bk G],ck(1:4,:),dk),Q,R);

control;
```

Modified Kalman Filter Gain Matrix **K** =

```
-2.6086e+2  -2.1274e+2  -1.4086e+1   1.3571e+2
-1.6522e+1  -4.3094e+0  -1.2867e+0  -1.2247e+0
 4.5466e+0   1.6749e+0   5.7423e-1  -5.9122e-1
 3.4318e+0   6.7471e+0  -1.1228e+0  -5.4833e+0
 5.7598e+1   5.1133e+1  -6.6453e-1  -2.8486e+1
-1.6422e+0  -1.9772e+0  -1.1213e+0  -9.9738e-1
-3.0768e+0  -2.7107e+0   2.1054e-1   5.5479e-1
 1.8631e+0  -1.1355e+1  -1.2201e+0   2.1590e+1
-5.0360e+1  -5.6285e+1  -5.5316e+0  -1.1254e+2
-4.9413e+1   1.0330e+1  -9.9434e+0   2.2023e+2
-2.2148e+1   1.8102e+1   2.9578e+0   1.8249e+0
 6.5325e+1  -9.6885e+1  -1.1357e+0   1.1676e+2
 1.0078e+1  -2.5946e+1  -5.3436e-1   1.8782e+1
-7.3789e+0  -7.7520e+0  -1.1162e+0   9.2672e+1
 1.5737e+2  -8.7657e+2  -7.6200e-1   7.4199e+2
-2.6448e+2  -2.6848e+2  -2.5663e-2   3.0999e+2
-2.3085e+2  -3.1786e+0  -3.3014e-2  -5.1648e+2
-7.3748e+3  -4.5474e+4  -1.2724e+3  -2.9357e+3
 6.5979e+3  -2.1811e+3   9.9035e+0  -1.1227e+4
-2.2862e+0  -2.8170e+0   1.5931e+2  -1.8718e+0
-9.9372e+3  -4.5875e+4  -1.3099e+3   1.1353e+3
 9.3878e+2  -3.0431e+2   2.1024e+0  -1.6312e+3
 1.1538e+1  -7.1673e+0  -2.6669e-2  -1.7721e+1
 1.9894e+4   3.6406e+3  -1.6679e+2   6.3366e+3
 3.2300e+3   7.2756e+2  -2.7451e+2   1.1598e+3
 3.2275e+3   2.1948e+1   1.5264e+2   9.0104e+2
-4.3458e+3  -2.4496e+3  -1.8386e+2  -1.4127e+3
-3.6468e+4  -1.1787e+4  -4.2894e+2  -1.5175e+4
-3.9214e+2  -8.2557e+2  -1.6657e+2   1.1584e+3
 5.1802e+3   1.7137e+3   3.4667e+1   1.8797e+3
 9.1521e+3   6.8625e+3  -4.8619e+1   5.2465e+3
 1.0286e+5  -2.2426e+4  -4.3066e+2   6.5112e+4
-2.6777e+4   5.2133e+4  -2.1842e+3  -1.8034e+4
-8.8829e+4  -7.6946e+2   1.1245e+2  -5.1297e+4
 8.5558e+1   2.3270e+4   4.0075e+2   7.9828e+3
-1.8706e+4   5.8886e+3   1.5189e+2  -5.6983e+3
-5.6922e+4   1.9934e+4  -2.4061e+2  -4.1477e+4
 4.9526e+4   3.1616e+5   1.9909e+3   1.1670e+5
 7.7753e+5   8.2819e+4  -6.5840e+2   2.1721e+5
 3.1110e+5  -1.3849e+5  -1.2522e+3   2.0125e+5
-4.0614e+3  -1.3390e+4  -4.3741e+2   2.1172e+3
 9.8093e+2   4.3562e+3   7.4115e+1   1.3833e+3
 6.1767e+2   1.7815e+2   1.4248e+1  -7.5005e+2
-9.3545e+2  -5.0594e+2  -6.2156e+1   1.0517e+3
 1.3890e+2   3.6364e+3   4.1299e+1   4.9148e+1
 2.3948e+2   9.3602e+1   1.5449e+1  -6.7027e+2
```